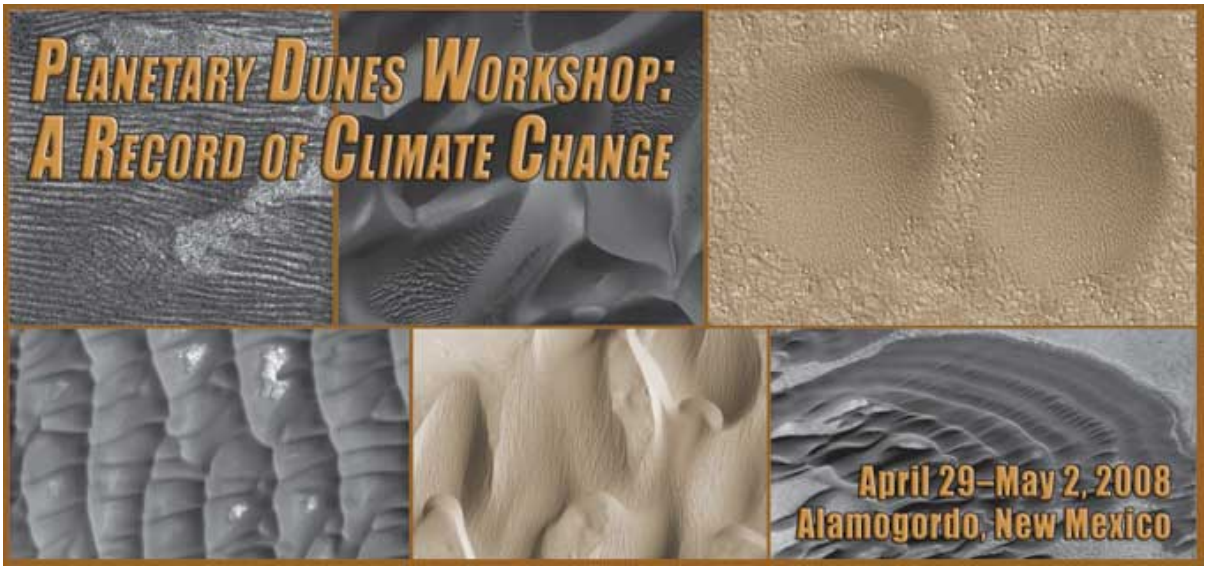

PROGRAM AND ABSTRACTS

LUNAR AND PLANETARY INSTITUTE

LPI Contribution No. 1403

PLANETARY DUNES WORKSHOP: A RECORD OF CLIMATE CHANGE

April 29 – May 2, 2008 • Alamogordo, New Mexico

Sponsors

Lunar and Planetary Institute

National Aeronautics and Space Administration

NASA Mars Exploration Program

Scientific Organizing Committee

Timothy Titus
U. S. Geological Survey

Rose Hayward
U. S. Geological Survey

Mary Bourke
Planetary Science Institute

Nick Lancaster
Desert Research Institute

Lori Fenton
Carl Sagan Center

Lunar and Planetary Institute 3600 Bay Area Boulevard Houston TX 77058-1113

LPI Contribution No. 1403

Compiled in 2008 by
LUNAR AND PLANETARY INSTITUTE

Abstracts in this volume may be cited as

Author A. B. (2008) Title of abstract. In *Planetary Dunes Workshop: A Record of Climate Change*, p. XX. LPI Contribution No. 1403, Lunar and Planetary Institute, Houston.

This volume is distributed by

ORDER DEPARTMENT
Lunar and Planetary Institute
3600 Bay Area Boulevard
Houston TX 77058-1113, USA
Phone: 281-486-2172
Fax: 281-486-2186
E-mail: order@lpi.usra.edu

Mail orders requestors will be invoiced for the cost of shipping and handling.

ISSN No. 0161-5297

Preface

This volume contains abstracts that have been accepted for presentation at the Planetary Dunes Workshop: A Record of Climate Change, April 29–May 2, 2008, Alamogordo, New Mexico.

Administration and publications support for this meeting were provided by the staff of the Publications and Program Services Department at the Lunar and Planetary Institute.

Contents

Program

Tuesday, April 29, 2008
TITAN: AN OILER'S DREAM
8:30 a.m. Auditorium

Chairs: N. Lancaster
S. Sutton

8:30 a.m. *WELCOME AND INTRODUCTION*

8:45 a.m. Zimbelman J. R. *
Planetary Dune Fields: Examples of Performance Under Pressure **[#7005]**

9:30 a.m. Lorenz R. D. * Radebaugh J. Cassini RADAR Team
The Sand Seas of Titan: Discovery and Implications for Methane Climatology and Wind Patterns **[#7034]**

10:00 a.m. Radebaugh J. * Lorenz R. D. Spencer C. Cassini RADAR Team
Terrestrial Analogues of Longitudinal Dunes on Titan **[#7037]**

10:30 a.m. BREAK

10:45 a.m. Reffet E. * Courrech du Pont S. Hersen P. Douady S. Fulchignoni M.
Longitudinal Dunes on Titan: A Laboratory Approach **[#7018]**

11:15 a.m. Barnes J. W. *
Imaging and Spectroscopy of Titan's Dunes in the Near-Infrared **[#7020]**

11:45 a.m. DISCUSSION

12:15 p.m. POSTER INTRODUCTIONS

12:30 p.m. LUNCH and POSTERS

* *Denotes Speaker*

Tuesday, April 29, 2008
POSTER SESSION I: EARTH, TITAN, INSTRUMENTS
12:15 p.m. Auditorium

Ewing R. C. Kocurek G. Peyret A. P. B. Mohrig D.
Three-Dimensional Characterization and Morphological Dynamics of Gypsum Sand Dunes at White Sands National Monument Using Airborne LiDAR **[#7031]**

Bristow C. S. Jol H. M.
GPR Surveys of the Jurassic Navajo Sandstone: A Potential Analogue to the Burns Formation, Meridiani Planum, Mars **[#7003]**

Goudie A. S. Bourke M. C.
Varieties of Barchan Form in the Namib Desert and on Mars **[#7023]**

Sutton S. L. F. McKenna Neuman C. Nickling W.
The Role of Reptation in Dune Slipface Dynamics **[#7028]**

Bourke M. C. Ewing R. Finnegan D. McGowan H. A.
Migration Rates of Niveo-Aeolian Dunes in Antarctica: Implications for Martian Dunes **[#7040]**

Tuesday, April 29, 2008
EARTH — A NICE PLACE TO VISIT BUT I WOULDN'T WANT TO LIVE THERE
1:30 p.m. Auditorium

Chairs: M. C. Bourke
B. Thomson

1:30 p.m. Lancaster N. *
Aeolian Sand Transport Systems — A Terrestrial Perspective **[#7014]**

2:15 p.m. Bishop M. A. *
Comparative Point Pattern Analysis of Hyperboreae Undae, Mars, and the Rub' al Khali Sand Sea, Earth **[#7021]**

2:45 p.m. Szynkiewicz A. * Pratt L. M. Glamoclija M. Moore C. H. Singer E. Bustos D.
White Sands Gypsum Dunes — A Terrestrial Analog to North Polar Dunes on Mars? **[#7011]**

3:15 p.m. BREAK

3:30 p.m. Bristow C. S. * Jol H. M. Augustinus P. Wallis I.
GPR Surveys of Sand Dunes in Antarctica as Analogs for Dunes on Mars **[#7004]**

4:00 p.m. Lepper K. *
In-Situ Geochronology for Martian Dunes: A Review of Optical Dating Concepts and Experiments with Analog Materials **[#7027]**

4:30 p.m. DISCUSSION

5:15 p.m. FIELD TRIP INFORMATION

Wednesday, May 1, 2008
FIELD TRIP
8:30 a.m. Auditorium

8:30 a.m. David Bustos and Gary Kocurek
Field Trip Introduction

9:30 a.m. Buses Depart for White Sands National Monument

Thursday, May 1, 2008
MARS — FOURTH ROCK FROM THE SUN
8:30 a.m. Auditorium

Chairs: T. N. Titus
T. I. Michaels

8:30 a.m. Gillies J. A. * Nickling W. G. King J. Lancaster N.
Modeling Aeolian Sediment Transport Thresholds on Mars: A Shear Stress Partitioning Approach **[#7007]**

9:15 a.m. Tanaka K. L. * Hayward R. K.
Mars' North Circum-Polar Dunes: Distribution, Sources, and Migration History **[#7012]**

9:45 a.m. Putzig N. E. * Mellon M. T. Herkenhoff K. E. Phillips R. J.
Thermophysical Analysis of the North Polar Erg on Mars **[#7032]**

10:15 a.m. BREAK

10:30 a.m. Horgan B. H. N. * Bell J. F. III Thomas P. C. Noe Dobrea E. Z.
Hydrated Minerals in the North Polar Chasmata and Circum-Polar Erg **[#7035]**

11:00 a.m. Silvestro S. * Ori G. G.
Interconnected Ergs in East Thaumasia Region: Sediment Transport Pathways and Possible Source Areas **[#7019]**

11:30 a.m. Tirsch D. * Jaumann R.
Mars: Dark Intra-Crater Dunes on a Regional Scale **[#7006]**

12:00 noon DISCUSSION

12:30 p.m. POSTER INTRODUCTIONS

12:45 p.m. LUNCH and POSTERS

Thursday, May 1, 2008
POSTER SESSION II: MARS
12:30 p.m. Auditorium

Wheeler A. J. Bishop M. A.
Comparative Study of Higher-Order Neighbour Statistics and Dune Field Self Organization for the Hyperboreae Undae and Olympia Undae Ergs, Mars **[#7033]**

Titus T. N.
Thermal Inertia Characterization of Olympia Undae **[#7025]**

Feldman W. C. Bourke M. C.
Estimate and Expression of Water Ice in Polar Sand Dunes **[#7029]**

Cushing G. E. Titus T. N. Hayward R. K.
Thermophysical Properties of Proctor Dune Field, Mars **[#7038]**

Bourke M. C. Balme M.
Megabarchans on Mars **[#7036]**

Hayward R. K. Mullins K. F. Fenton L. K. Titus T. N. Tanaka K. L. Bourke M. C. Colaprete A. Hare T. M. Christensen P. R.
Mars Global Digital Dune Database (MGD^3): User's Guide **[#7013]**

Scheidt S. Ramsey M. S. Lancaster N.
Thermal Remote Sensing of Sand Transport Systems **[#7041]**

Thursday, May 1, 2008
MARS — FOURTH ROCK FROM THE SUN (CONTINUED)
1:45 p.m. Auditorium

Chairs: R. K. Hayward
G. E. Cushing

1:45 p.m. Balme M. R. * Berman D. C. Bourke M. C. Rafkin S. Zimbelman J. R.
Transverse Aeolian Ridges on Mars **[#7017]**

2:15 p.m. Zimbelman J. R. *
Transverse Aeolian Ridges on Mars: Results Obtained from Analysis of HiRISE Images **[#7010]**

2:45 p.m. Fenton L. K. * Hayward R. K.
Southern Hemisphere Dunes of Mars: Morphology Trends and Climate Change **[#7030]**

3:15 p.m. Gardin E. * Quantin C. Allemand P.
Dune Fields on Mars: Markers of Climatic Changes? **[#7022]**

3:45 p.m. BREAK

4:00 p.m. Bourke M. C. *
Barchan Dune Asymmetry: Observations from Mars **[#7024]**

4:30 p.m. Tsoar H. *
Linear Dunes on Earth and Mars — Similarity and Dissimilarity **[#7001]**

5:00 p.m. Di Achille G. * Silvestro S. Ori G. G.
Defrosting Processes on Dark Dunes: New Insights from HiRISE Images at Noachis and Aonia Terrae, Mars **[#7026]**

5:30 p.m. DISCUSSION

Friday, May 2, 2008
MODELING — WHAT WE DON'T UNDERSTAND, WE JUST MAKE UP
8:45 a.m. Auditorium

Chairs: L. K. Fenton
R. C. Ewing

8:45 a.m. Claudin P. * Andreotti B.
Dunes on Mars, 'Venus', Earth, and Subaqueous Ripples: A Scaling Law for Their Elementary Size **[#7009]**

9:30 a.m. Yizhaq H. * Isenberg O. Wenkrat R. Tsoar H.
Aeolian Megaripples as a Self-Organization Phenomenon: Mathematical Modeling, Field Studies and Implications to Martian Megaripples. **[#7015]**

10:00 a.m. Diniega S. * Glasner K.
Modeling 2-D Dune Interactions **[#7016]**

10:30 a.m. Michaels T. I. *
Unlocking the Environmental Conditions Recorded by Aeolian Bedforms with the Aid of High-Resolution Atmospheric Modeling **[#7039]**

11:00 a.m. DISCUSSION

11:30 a.m. ADJOURN

TRANSVERSE AEOLIAN RIDGES ON MARS. M. R. Balme[1], D. C. Berman[1], M. C. Bourke[1], S. Rafkin[2], and J. R. Zimbelman[3], [1]Planetary Science Institute, 1700 E. Ft. Lowell Rd., Suite 106, Tucson, AZ, 85719, mbalme@psi.edu; [2]SouthWest Research Institute, 1050 Walnut St, Suite 300 Boulder, CO 80302; [3]Center for Earth and Planetary Studies, National Air and Space Museum, Smithsonian Institution, PO Box 37012, MRC 315, Washington, DC 20013-7012.

Introduction: The martian surface hosts a range of aeolian bedforms; two types been observed from orbit: Large Dark Dunes (LDDs) and Transverse Aeolian Ridges (TARs [1]). Unlike LDDs, TARs are generally brighter than their surrounding terrain, are about an order of magnitude smaller and have simple ripple-like forms. LDDs occur mainly in circumpolar ergs and in intra-crater dune-fields, but the global distribution of TARs is not well constrained. The aim of this work is to explore when and how TARs formed and how they are related to LDDs.

Method: We have conducted a survey of ~10,000 high-resolution Mars Orbiter Camera narrow angle images (MOCNA) in a pole-to-pole swath between 0 and 45° E longitude to identify, classify, and map the distributions and orientations of TARs.

Distribution: The geographic distribution of TARs in the study swath is significantly non-random. TARs are more numerous in the southern hemisphere than the northern but are particularly common in the Terra Meridiani region (Figure 1). The lack of TARs in the northern lowlands and southern mid- to high-latitudes correlates with the lack of steep slopes in these regions. Locally, TARs are found on crater floors and in regions containing mesas and layered outcrops.

The Meridiani area is unique not only for the abundance of TARs, but also for their morphology: many have a distinctive barchan-like form, rarely seen in other locations. Where they are not topographically controlled, TAR orientations are regionally consistent, suggesting they are shaped by regional winds.

Association with LDDs: Although globally there is no spatial association of TARs with LDDs, throughout the southern mid-latitudes TARs most frequently occur close to large LDD fields in impact craters (figure 2). These TARs are almost always south or southwest of the LDDs and form within a few tens of kilometers of them. Interestingly, this spatial trend matches the climate model data [2] of wind directions, suggesting that TARs are found consistently upwind of LDDs. This suggests that in this region TARs and LDDs are genetically related. Moreover, our studies [3] have shown that, where they occur together and a superposition relation can be established, TARs are generally older than LDDs, consistent with the ~ 0-2 Ma impact crater retention ages for TARs [4] and the lack of even small impact craters seen on LDDs.

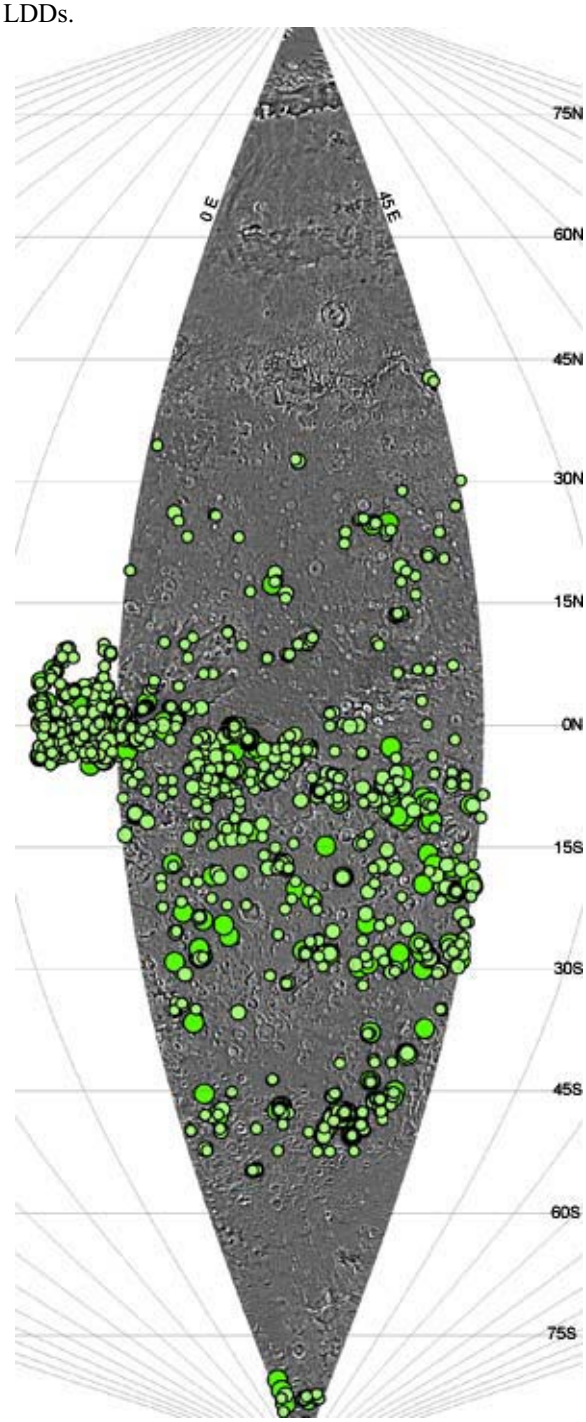

Figure 1. Location of MOC NA images that have >25% areal coverage of TARs. Largest circles repre-

sent >75% cover; smaller circles represent >25% or >50% cover. Background: USGS Viking MDIM 2.1.

Discussion: The spatial distribution of TARs seems closely linked to the presence of steep slopes and/or layered terrains. Thus the sediment source seems most consistent with formation from mass-wasting or denudation products. This suggests that sources are local and that TARs do not travel great distances. In Terra Meridiani the widespread outcrops of sedimentary terrains provide an abundant source of particulates, explaining why so many TARs are present here. The distinctive form of TARs in Meridiani suggests a control of their morphology by either the source lithlogy, or the rate of sediment supply. Given that we currently have only a poor understanding of local meterology, investigating this link with higher resolution climate models is a priority for our future studies

That TARs and LDDs are genetically related in the southern mid-latitudes provides new information on aeolian processes on Mars. If LDD materials here are indeed related to upwind TARs, this suggests that 1) They formed from the same source lithology, and 2) that TARs are a lag deposit from the least mobile part of the sediments and that LDDs form from the most mobile. This observation seems consistent with estimates of particle sizes equivalent to medium to coarse sand for LDDs [5] and with observations of TAR-like form in Meridiani that appear composed of finer grade material armored by a coarser lag [6].

References: [1] Bourke, M.C. *et al.*, LPSC XXXIII [CDROM], Abstr. # 2090, 2003. [2] Hayward, R.K. *et al.*, U.S. Geological Survey Open-File Report 2007-1158. http://pubs.usgs.gov/of/2007/1158/. [3] Balme, M.R. *et al.*, Geomorphology, accepted pending corrections, 2008. [4] Reiss, D., S. *et al.*, J. Geophy. Res., 109 (E06), 2004. [5] Fenton, L.K. *et al.*, J. Geophys. Res. 108 (E12), 5129, doi:10.1029/2002JE002015, 2003 [6] Sullivan, R. *et al.*, Nature, 436, 58-81, 2005

Figure 2. (below) Southern mid-latitude association of TARs with LDDs. Images with TARs are shown as green circles (as for figure 1 except images with <5% TARs are also shown as black dots) and mapped dune fields (from [2]) are shown in red. Climate model results for this region (also from [2]) are shown by blue lines that point in the direction of the winds. The modeled winds are broadly from the southwest, consistent with the spatial association of TARs and LDDs. Background: MOLA topography (warmer colors = higher elevations) draped over a MOC wide angle mosaic.

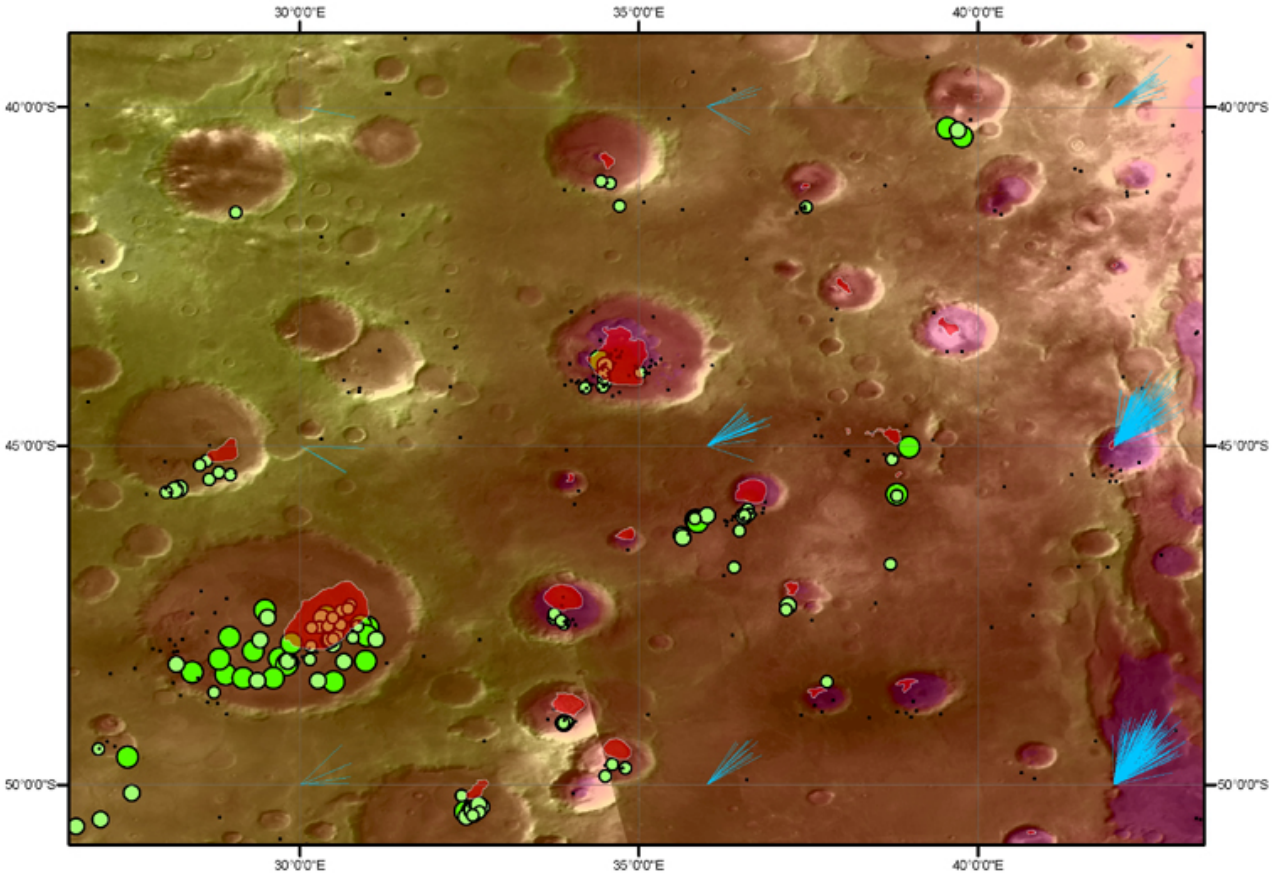

IMAGING AND SPECTROSCOPY OF TITAN'S DUNES IN THE NEAR-INFRARED. Jason W. Barnes, *NASA Ames Research Center, M/S 244-30, Moffett Field, CA 94034-1000, USA, (Jason.W.Barnes@nasa.gov).*

Abstract:

Cassini's Visual and Infrared Mapping Spectrometer (VIMS) instrument is able using infrared light to see through the haze that envelops Saturn's moon Titan within 8 spectral windows. The 64 VIMS spectral channels that show some surface expression form a hyperspectral imaging system capable of spatial resolution as fine as 250 meters per pixel (though in practice the best yet achieved is 500 meters/pixel). VIMS has studied Titan's clouds [1], surface composition [2], and spectral variability [3, 4, 5]. It has also made important contributions regarding Titan's craters [6], mountains [7], erosion [8], channels [7], and candidate extrusive features [9, 10].

Cassini's RADAR revealed Titan to be the fourth planetary body known to have sand dunes on its surface [11]. The dunes are longitudinal, like most of Earth's, but not most of Venus' or Mars'. [12] showed that areas where RADAR sees dunes are correlated with areas that VIMS sees as "dark brown" within its spectral windows (showing low albedo with a shallow red slope relative to the rest of Titan). Based on this correlation, a whopping 20% of Titan's surface area is covered by dunes. All of the dunes lie within Titan's tropics, within 30 degrees of the equator (Figure 1).

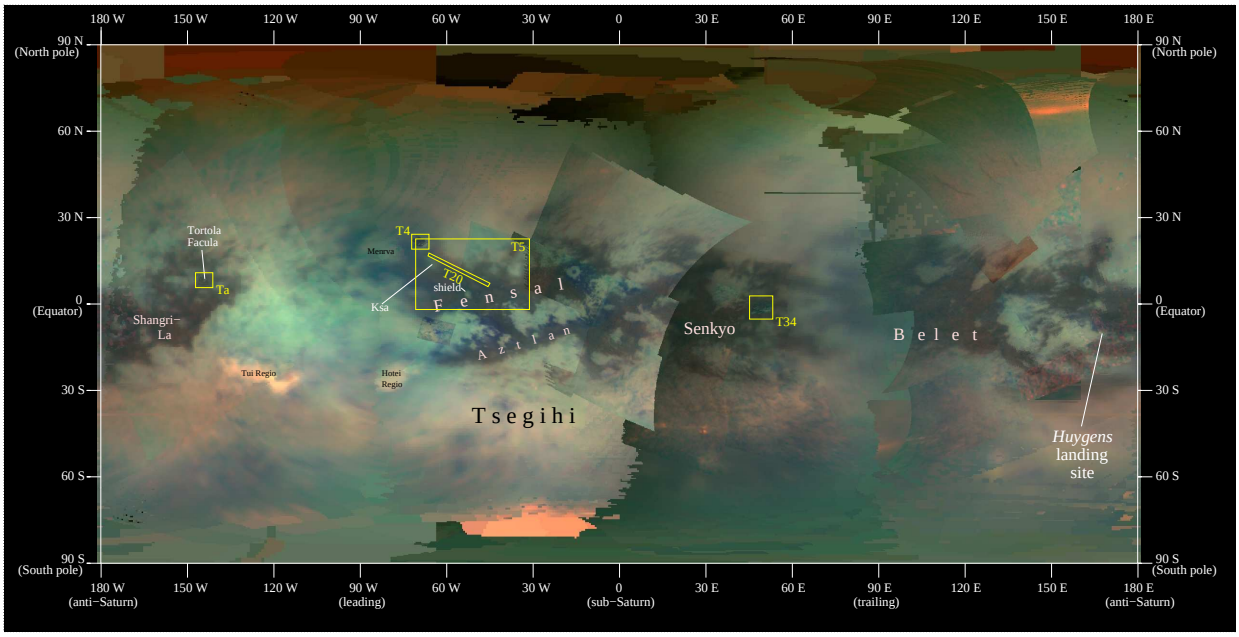

Figure 1: Simple cylindrical global map of Titan in infrared color from *Cassini*/VIMS. Sand seas appear dark brown in this color scheme, and lie entirely girding the moon's equator.

VIMS was first able to resolve Titan's dunes in retrospect during the fourth close flyby of Titan made by *Cassini*, T4 [4]. Photoclinometry of the T4 observation revealed the dunes' heights to be between 30 and 70 meters [13]. The dunes' separations as measured by VIMS are between 1 and 3 km, consistent with the values measured with the RADAR [14].

Very fine spatial resolution from the T20 flyby (2006 October 25) revealed that some of Titan's dunes are separated by sand-free interdune regions [13] (Figure 2). The spectrum of these interdunes corresponds to the dunes' substrate unit. Generalizing to coarser spatial resolution data, these unresolved spectra must consist of a linear mixture of dune and interdune spectra, which will allow global mapping of the dunes' substrate. The fact that these interdunes remain sand-free in Titan's actively eroding environment implies that they are either presently active or were so in the geologically recent past.

Spatially resolving the sand dunes allows us to more precisely constrain their composition. Surprisingly the dunes' sand does not appear to be composed of water-ice, as might be expected from liquid methane erosion of Titan's icy crust. Instead the spectra are consistent with that of solid hydrocarbons. The ultimate source of the dune material might therefore be reasonably expected to be the atmospheric haze particles raining down over time. However, the mechanism by which to create sand-sized particles from the tiny ($\sim$ 1 micron) haze particles has not yet been established.

Near-infrared imaging of the dunes, with complementing RADAR observations, hold the promise to help us understand Titan's sand cycle and to thereby allow us to use something that we think we understand somewhat, Titan's dunes, to help us understand those parts of Titan that we know that we don't understand: everything else.

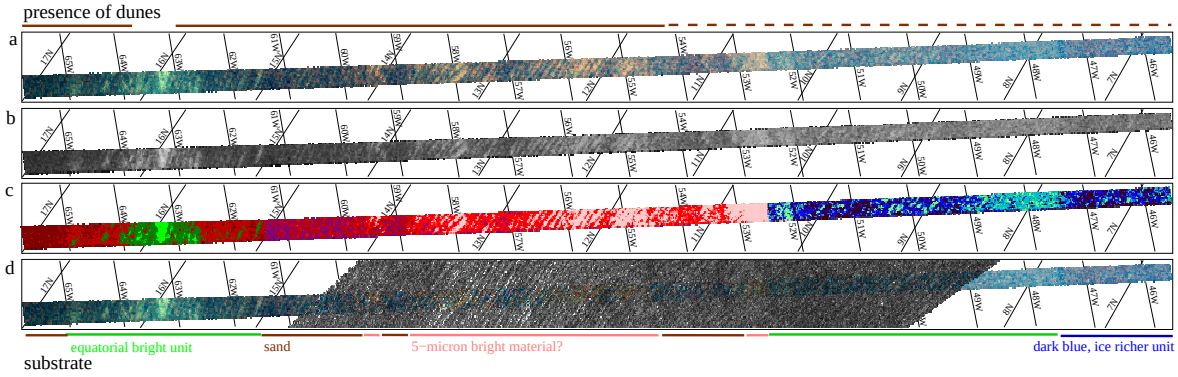

Figure 2: 500 meter per pixel strip showing both dunes and sand-free interdunes on Titan.

References

[1] Griffith C.A., Penteado P., Baines K., Drossart P., et al. (2005) *Science*, *310* 474–477.

[2] McCord T.B., Hansen G.B., Buratti B.J., Clark R.N., et al. (2006) *Planet. Space Sci.*, *54* 1524–1539.

[3] Barnes J.W., Brown R.H., Turtle E.P., McEwen A.S., et al. (2005) *Science*, *310* 92–95.

[4] Barnes J.W., Brown R.H., Soderblom L., Buratti B.J., et al. (2007) *Icarus*, *186* 242–258.

[5] McCord T.B., Hayne P., Combe J.P., Hansen G.B., et al. (2007) *Icarus* accepted.

[6] Le Mouèlic S., Paillou P., Janssen M.A., Barnes J.W., et al. (2007) *JGR* submitted.

[7] Barnes J.W., Radebaugh J., Brown R.H., Wall S., et al. (2007) *JGR* accepted.

[8] Jaumann R., Brown R.H., Stephan K., Soderblom L.A., et al. (2007) *Icarus* submitted.

[9] Sotin C., Jaumann R., Buratti B.J., Brown R.H., et al. (2005) *Nature*, *435* 786–789.

[10] Barnes J.W., Brown R.H., Radebaugh J., Buratti B.J., et al. (2006) *Geophys. Res. Lett.*, *33* 16,204–+.

[11] Lorenz R.D., Wall S., Radebaugh J., Boubin G., et al. (2006) *Science*, *312* 724–727.

[12] Soderblom L., Kirk R.L., Lunine J.I., Anderson J.A., et al. (2007) *Planet. Space Sci.* Published online 2007 April 27.

[13] Barnes J.W., Brown R.H., Soderblom L., Sotin C., et al. (2007) *Icarus* submitted; `http://www.barnesos.net/vims/dunes.pdf`.

[14] Radebaugh J., Lorenz R.D., Lunine J.I., Wall S.D., et al. (2007) *Icarus* accepted.

COMPARATIVE POINT PATTTERN ANALYSIS OF HYPERBOREAE UNDAE, MARS, AND THE RUB' AL KHALI SAND SEA, EARTH. M. A. Bishop[1,2], [1]Planetary Science Institute, 1700 East Fort Lowell Road, Tucson, AZ 85719, USA, [2]School of Natural and Built Environments, University of South Australia, Adelaide, SA 5095, Australia (bishop@psi.edu)

Introduction: The geographic signature of dune distribution and self-organization as measured by the *R*-statistic offers a viewpoint on the geography of crescentic eolian systems and proposes an index from which to determine the degree of self-organization across a variety of spatial scales. Fields of simple dunes (dome, barchan, barchan-seif) are comparatively less regular in distribution than are those fields, or part thereof, that consist of compound (barchanoid) morphologies whose patterns are more highly regular [1]. This analog study examines and compares the geography of crescentic dune patterns for the Martian north polar erg, Hyperboreae Undae, and the Rub' al Khali sand sea of the Arabian Peninsula, Earth.

Methods: Data points representing the point of maximum crest-line curvature for both barchan and barchanoid crescentic dunes were derived by on-screen ('heads-up') digitization using the software ArcView 3.3 and ArcGIS 9.2. Nine georeferenced and sinusoidal projected narrow angle Mars Orbiter Camera (MOC NA) images produced some 2800 data points for Hyperboreae Undae. Similarly, 3400 data points projected to WGS 84 UTM Zone 39N were derived from a 3-sec (90 m) SRTM (Shuttle Radar Topography Mission) DEM tile for the Rub' al Khali dunes.

Synopsis of statistical calculations: Commonplace in the analysis of point pattern is nearest neighbour analysis (NNA). The nearest neighbour distance for an event in a point pattern, is the distance from that event to the nearest event, also in the point pattern. NNA calculates the dimensionless statistic *R*, which is the ratio of the observed average distance between nearest neighbors of a point distribution (r_o) and the expected average distance (r_e) between nearest neighbors as determined by a theoretical pattern; the Poisson probability distribution. For each point, the shortest distance among all neighbors becomes the nearest distance which is then averaged using all points. In its simplest form the nearest neighbor statistic, *R*, compares the observed, r_o, with the expected, r_e, (random) nearest neighbor distances and identifies whether points are random ($R \cong 1$), completely clustered ($R = 0.0$, in which all points lie on top of each other) or dispersed ($R = 2.00$ in which points distribute in a square lattice, or $R = 2.149$, which is the theoretical value for the most dispersed pattern, being that of a triangular lattice). If $Z_R > 1.96$ or < -1.96 it can be expressed that the difference is statistically significant at $\alpha < 0.05$. Alternatively, if $-1.96 < Z_R < 1.96$ the pattern is not statistically different from a random pattern; although recent work by Baloga et al., [2] has shown that according to sample size, the range for statistical significance may require adjustment.

With an ability to detect patterns, NNA has been extended to accommodate second, third and higher-order neighbor statistics to detect heterogeneous processes at different spatial scales. As with the nearest or first order neighbor, higher-ordered neighbor (H-ON) analysis (2nd, 3rd, 4th …etc) is based on comparing the observed average distances (spacing) between neighboring points and a known pattern, and evaluates the pattern at different spatial scales. Higher-order neighbor statistics reach beyond the local scale represented by the nearest neighbor measure, by offering greater insight into patterns over a more regional perspective.

Results and Discussion: H-ON statistics have shown that the patterns for fields of crescentic dunes within Hyperboreae Undae are one of statistically significant dispersion (Figure 1).

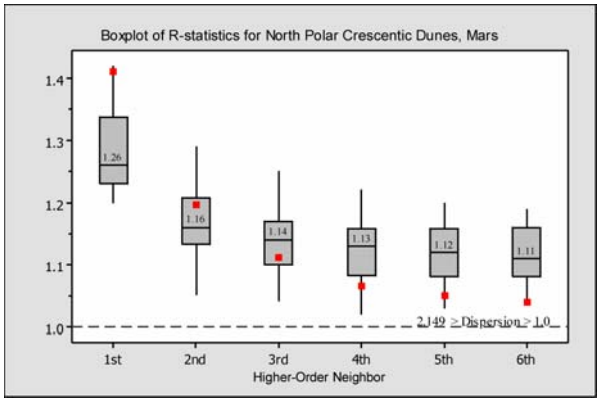

Figure 1. A boxplot of the distribution of the *R*-statistic for the ordered neighbors of crescentic dunes. Each boxplot represents a synopsis of the range of *R*-values determined for Hyperboreae Undae. The plots show: (a) that all *R*-statistics fall within the statistical field of dispersion (b) numerical median values (c) the absence of outliers (d) positive (right) skew of the data for the 1st, 2nd, 3rd, and 6th higher-order neighbors which indicates fewer data points having values above the median (e) a slightly negative skewed distribution for the 4th higher-order neighbor which shows more data demonstrating a greater degree of dispersion (f) a near-normal distribution of data points for the 5th higher-order neighbor. Comparatively, box symbols (red) show *R*-indices

from a sample of the Rub' al Khali barchanoid dunes for a single areal extent of 15,595 square km; n = 2,428 points (Table 1).

Similarly, pattern regularity (dispersion) is also characteristic of the mega-barchanoids of the Rub' al Khali (Empty Quarter) sand sea of the Arabian Peninsula (Figure 2). Spatial statistics for the prevailing northernmost dune field demonstrates close agreement with the geographic indices of compound crescentic (barchanoid) dunes of Hyperboreae Undae (Table 1).

Ordered Neighbor	*R-statistic*	Z_R	*Pattern*
1st	1.41	39.0531	Dispersed
2nd	1.20	26.4533	Dispersed
3rd	1.11	18.4745	Dispersed
4th	1.07	12.6199	Dispersed
5th	1.05	10.0091	Dispersed
6th	1.04	9.97432	Dispersed

Table 1. Ordered neighbor statistics for mega-barchanoid dunes, Rub' al Khali erg (Area of dune sample = 15,595 square km; n = 2,428 points, 3-sec SRTM data)

For an area of 15,595 square km and 2,428 data points, the nearest neighbor shows the highest degree of dispersion, R = 1.41, with successively lesser but highly significant patterns of regularity for all higher orders (Table 1; Figure 1). Several smaller intra-field comparisons were made for which the R-indices of the NN ranged between 1.39-1.47; results that characterize local variations in distribution.

Overall, both ergs demonstrate that the regularity of pattern is greatest for the 1st- and 2nd-order distances followed by a distribution that migrates towards randomness with each successive order. Dispersion or a spatial semblance of uniformity characterizes the geography of these sand seas. Furthermore, spatial homogeneity and its apparent relationship to morphology is a process that typifies the crescentic dunes of both the Hyperboreae Undae and Rub' al Khali sand seas. The repetitious compound morphology and substantial areal extent for the dunes of the Empty Quarter implies that a relationship exists between form and the degree of pattern uniformity. Such occurrences are found also for sequences of barchanoid morphology within Hyperboreae Undae. In both instances this implies that the evolution of crescentic dunes into compound fields identifies with the process of long term self-organization (and maturity) of the eolian system. Where domes, barchans, barchan-seif and short barchanoid 'chains' occur, the degree of self-organization is less than for those regions comprising compound forms. Therefore, it is plausible that spatial statistical indices may indicate a relative scale from which dune field maturity can be ascertained across a variety of scales. These results parallel the views of Wilkins and Ford [2] who suggest that eolian systems reflect, within different spatial regions of the field, the sum of changes that result in the spatially variable states of dune field organization.

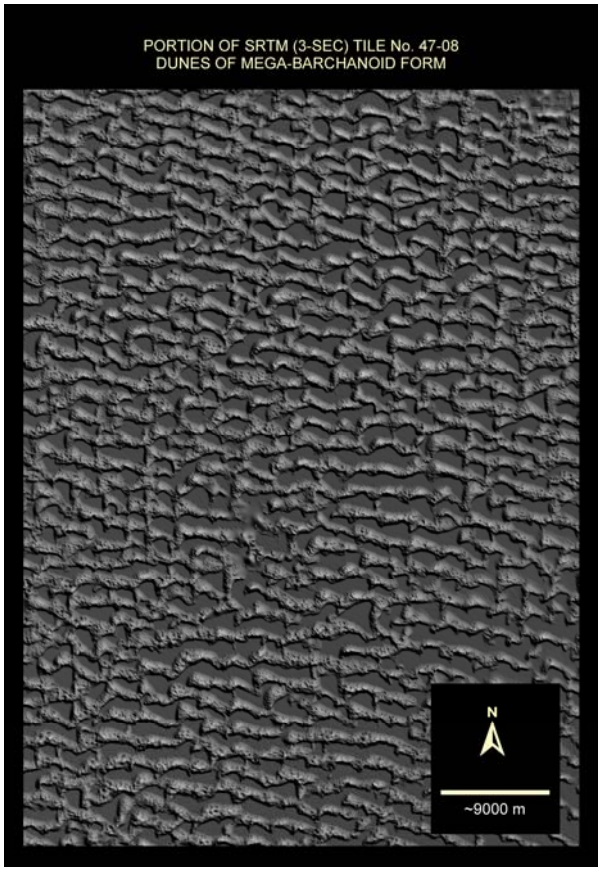

Figure 2. Radar part-image (image center ~54.183ºE, 22.278ºN) of the Rub' al Khali mega-barchanoids.

Summary: Ordered neighbor analysis of point patterns has shown that dune geography for high-latitude dune fields on Mars and the terrestrial erg Rub' al Khali is not a random process, but one that identifies with a geomorphic system that has evolved towards a pattern of uniformity and self-organization across a variety of spatial scales.

References: [1] Bishop M.A. (2007) *Icarus 191,* 151-157. [2] Baloga, S.M. et al., (2007) *Journal of Geophysical Research 112*, E03002. [3] Wilkins D.E. and Ford R.L. (2007) *Geomorphology 83,* 48-57.

BARCHAN DUNE ASYMMETRY: OBSERVATIONS FROM MARS. Mary C. Bourke, Planetary Science Institute, 1700 E. Ft. Lowell, #106, Tucson, Arizona 85719, USA
mbourke@psi.edu

Introduction: Barchan asymmetry refers to the preferential extension of one barchan limb downwind. It is found at many locations on Mars. Although several sites exhibit unidirectional limb orientations, others show that limbs may extend in multiple directions even leading to superimposition. Resultant dune field ridge patterns can be highly complex suggesting that there may be several causes of dune asymmetry on Mars.

On Earth, four triggers of dune asymmetry are identified: 1. bi-directional winds [1-7], 2. local topography [8, 9] 3. dune collision [11, 12] and 4. asymmetry in sediment supply [13, 14]. This paper describes limb morphology and uses this to infer triggers of barchan asymmetry on Mars.

Asymmetric limb morphology on Mars: Asymmetry is found on both barchan and barchanoid dunes. Associated limb morphologies are categorized as linear, beaded and kinked (Fig.1). Linear limbs are generally straight, but may have seif-like form. They can taper downwind or assume a more rounded end (Fig. 1a). Some have well developed crestlines and/or slipfaces on the inner side of the limb. Beaded limbs have broad, high sections that alternate with narrow, low sections and resemble a string of beads (Fig. 1 b). For some, the broadest section occurs at the tip of the limb and may produce small domes by calving [15]. Kinked limbs have distinct, often angular changes in downwind alignment followed by straight sections of variable length (Fig.1 c). The apex of the kink may have a well developed (remnant) slipface. Some limbs have several kinks resulting in a seif-like morphology.

Barchan asymmetry models: Bi-directional wind: In Bagnold's model [1, pg. 223] asymmetry is initiated by storm events that are oriented oblique to the dune. Asymmetry develops on the windward barchan limb and is sustained and enhanced by gentler winds that parallel the barchan form (Fig. 2 a). In Tsoar's model [7] there are important differences in the inferred wind direction and the limb that adjusts. The dune is oriented parallel to the stronger winds and modified by gentler winds that trend oblique to the barchan (Fig. 2b). The limb furthest from the approaching gentle wind is extended and the closest limb is eroded.

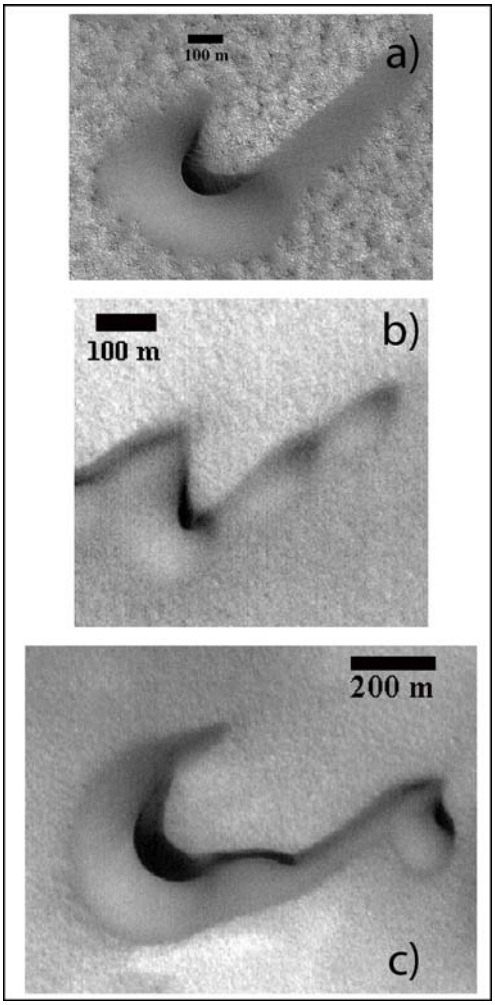

Figure 1: Asymmetric limb styles. a) Linear. HiRISE image PSP_001660_2570,76.7°N; 109.6°E, 50 cm/pixel. b) Beaded. MOC narrow angle image M0202629, 240.67°W; 76.70°N, 3.22 m/pixel. c) Kinked. M0204193, 239.61°W; 76.72°N, 3.22 m/pixel.

The morphology and placement of the asymmetric limb may enable a differentiation between these two models. In Bagnold's model (*sensu stricto*), the growing limb migrates across the front of the dune. Once it enters the sand stream from the opposite barchan limb, it grows

more rapidly than the connecting limb and a new dune (or bead) is formed. Resultant limb morphologies would therefore include: variable width, development of a lee side slip face and/or new dune formation coupled with an limb that crosses the path of the barchan dune. In Tsoar's model [7] the limb would have a seif form, variable width, and importantly, would extend away from the barchan (~ 120° angle) [examples are given in 16].

Unidirectional wind: *Dune collisions* distort dune morphology and can cause asymmetry. The collisions reported on here are assumed to occur in unidirectional winds that trend parallel to the dune orientation. It is noted that barchans can form in uni, bi- and multi-modal wind regimes.

Flume studies of two moving barchans under unidirectional flow show that absorption of the smaller impacting barchan by the larger barchan leads to asymmetry [10] (Fig. 1 c). This was also observed in Antarctic barchans [17].

The proximity of dunes, prior to collision, may also trigger asymmetry [18]. A second study [11] found that the back slope of the down-flow dune was eroded by the advancing smaller dune, triggering asymmetry (Fig. 1 d).

Asymmetry on Mars is associated with the lateral merging of smaller barchans and the direct collision of dunes on the windward slope. Dune and limb morphologies that suggest collision as the trigger for the development of asymmetry include a distinctive kink(s) in the asymmetric limb or the vestiges of the impactor dune on the windward slope. Dune collisions explain the asymmetric extension of different limbs within a given dune field [16].

Topography: Local topography (*e.g.*, gullies, bedrock exposures and inclined slopes) distort dune shape [8, 9]. On Mars asymmetric dunes occur on declining and inclining slopes and in locations of confining topography [examples are given in 16].

Conclusion: Barchan dune asymmetry is prevalent on Mars and is triggered in bi-directional wind regimes, in certain topographies and by dune collisions. Limb morphology may help differentiate between these triggers. Seif-like morphologies that trend across the barchan path or away from the barchan suggest bi-directional winds; distinctive kinks in the limb and vestiges of dunes on the windward slope suggest collision; finally topographic obstructions or clearly dipping underlying slopes may induce asymmetry, however the influence of bi-directional winds cannot be excluded.

Dune asymmetry on Mars represents a morphological adjustment to environmental changes such as variable wind direction, enhanced sediment supply through dune collision and variable local topography. There is potential to use asymmetry as a proxy for wind direction and relative strength. However, given the range of potential triggers, attention should be paid to morphological indices outlined here that will allow a more confidently assessment of the wind regime.

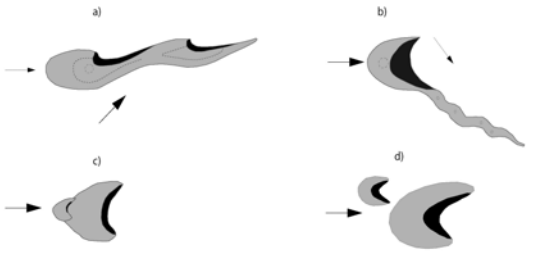

Figure 2: Schematic of models of dune asymmetry. a) Bagnold [1] b) Tsoar [7] c) dune collision (absorption) [10]. d) dune collision (impending) [11] . Arrow indicate wind direction, size indicates relative strengths.

Acknowledgement: This work is funded by NASA MDAP NNX07AV36G

References:[1] Bagnold, R. A., *The Physics of Blown Sand and Desert Dunes*. (Methuen, London, 1941), pp. 265. [2] King, W. H. J., *Geography Journal* **51**, 16-33 (1918). [3] Melton, F. A., *Journal of Geology* **48**, 113-174 (1940). [4] Holm, D. A., *Science* **132**, 1329-1379 (1960). [5] McKee, E. D., *Sedimentology* **7**, 1-60 (1966). [6] Norris, R. M., *Journal of Geology* **74**, 292-306 (1966). [7] Tsoar, H., *Zeitschrift fur Geomorphologie* **28**, 99-103 (1984). [8] Long, J. T. *et al.*, *Geological Society of America Bulletin* **75**, 149-156 (1964). [9] Finkel, H. J., *Journal of Geology* **67**, 614-647 (1959). [10] Endo, N. *et al.*, *Geophysical Research Letters* **31**, 12503 (2004). [11] Hersen, P. *et al.*, *Geophysical Research Letters* **32**, 1-5 (2005). [12] Close-Arceduc, A., Institut Geographique National, 1969. [13] Rim, M., *Bulletin of the Research Council of Israel* **7-G**, 123-137 (1958). [14] Lancaster, N., *Earth Surface Processes and Landforms* **7**, 575-587 (1982). [15] Bourke, M. C., *Geomorphology*, (submitted). [16] Bourke, M. C., *Icarus*, (submitted). [17] Bourke, M. C. *et al.*, *Permafrost and Periglacial Processes*, (submitted). [18] Shehata, W. *et al.*, *Journal of Arid Environments* **23**, 1-17 (1992).

MEGABARCHANS ON MARS. M. C. Bourke[1] and M. Balme[1] [1]Planetary Science Institute, Tucson, Arizona, 85719, USA, mbourke@psi.edu, mbalme@psi.edu

Introduction: Megabarchans are large dunes generally >500 m wide. The term has been applied to both transverse ridges and isolated crescentic dunes [1]. The latter are less common, but have been described in a few localities: *e.g.,* Peru [2], the southern end of the Algodones dunefield, and the Skeleton coast [3].

While most barchans range between 3 and 10 m high, isolated crescentic megabarchans are significantly higher (see below). On Earth the growth of these dunes to a larger size is also marked by a progression from simple to compound or complex [1].

Some of the largest barchans on Mars occur in the northern latitudes. In Viking images they were measured to be up to 1 km^2 and 150 m high [4]. Tsoar et al. [5] noted that they were often located at significant distances upwind of dunefields and created a 'frame' of merged large barchan dunes. This was attributed to a higher sediment supply.

Methodology: We conducted a survey of 350 Themis Visible images in the north polar region of Mars (between 70°N and 90°N). The selection criteria were for dunes to be ≥500 m wide, have a crescentic shape and be isolated from surrounding dunes. In order to avoid barchanoid dunes we deselected forms that had multiple slipfaces or crescentic segments. Our data base contains morphometric measurements (width, length and height) of 36 megabarchans. We used methods outlined in other publications [6, 7].

Morphometry: Megabarchans on Mars are on average 740 m wide, 245 m long and 65 m high (Table 1). Dune width, height and length are positively correlated, but the relationships are not statistically significant. Maximum values indicate that isolated megabarchans in the north polar region of Mars can attain widths of 1,340 m, lengths of 500 m and can be up to 130 m high (Table 1 and Fig 1).

There are few data on isolated crescentic megabarchans on Earth to compare the Martian data to. Horn-to-horn width on the Pur-Pur dune in Peru is between 750-850 m, and maximum height is 55 m. [2]. Isolated megabarchans on the margins of the Algones dunefield in Arizona measure between 800 and 1,600 m wide [8]. In the Rub' al Khali, Saudi Arabia, megabarchans are 2,760 wide and 3,000 m long (to base of slipface) [1] . Skeleton coast megabarchans are 25-30 m high [3]. These data suggests that megabarchan morphometry on Mars is similar to Earth. We note one example of a megabarchan that is a candidate for the largest barchan dune in our solar system. Kaiser Dune, in the southern hemisphere is ~500 m tall, 6.5 km wide and has an estimated volume of 2.5 km^3 [9].

Morphology: The majority of megabarchans in the north polar region tend to have a simple form, *i.e.* no superimposed smaller dunes at the available resolution (Fig. 2a). This suggests that simple barchans grow into simple megabarchans on Mars. Complex megabarchans do exist but are not frequently observed (Fig. 2c). Dune collision may be an additional important mechanism of megabarchan growth on Mars. The sinuous crestlines on some megabarchans suggest a former phase of dune collision and merging where smaller dunes have been almost completely absorbed (Fig. 2b). If there is a reduction in collision frequency, the megabarchans evolve towards a more simple morphology. The sequence of evolution is illustrated by viewing figure 2c through 2a.

Based on a ratio of the length of the stoss slope to width, barchan dune shape has been categorized as Fat, Pudgy, Normal and Slim [10]. Megabarchans in the NPSS fall into the Slim to Normal class with a ratio of 0.35.

Location and Orientation: Megabarchans are located in chasma, on crater floors, along the margins of akle and rectilinear dune fields and both upwind and downwind of converging dune masses. While our findings support the observations of Tsoar et al. [5] for the location of frame dunes they show that megabarchans are not limited to those locations on Mars.

The majority of megabarchans sampled were oriented in a direction similar to other dunes in the area (Fig. 2a and c). These include significantly smaller barchans that are able to adjust to a change in wind regime at a faster rate than the megabarchans. The matching orientations suggest a consistent wind direction for millennia at these locations on Mars.

References: [1] Breed, C. S. *et al.*, in *A study of global sand seas,* E. D. McKee, Ed. (United States Geological Survey, Professional Paper, 1052, 1979), pp. 253-304. [2] Simons, F. S., *Journal of Geology* **64**, 517-521 (1956). [3] Lancaster, N., *Earth Surface Processes and Landforms* **7**, 575-587 (1982). [4] Breed, C. S. *et al.*, *Journal of Geophysical Research (Planets)* **84**, 8183-8204 (1979). [5] Tsoar, H. *et al.*, *Journal of Geophysical Research* **84**, 8167-8180 (1979). [6] Bourke, M. C. *et al.*, Lunar and Planetary Science Conference XXXV, Abs. #1453 2004. [7] Bourke, M. C. *et al.*, *Geomorphology* **81**, 440-452 (2006). [8] Norris, R. M. *et al.*, *Geological Society of America, Bulletin* **72**, 605-620 (1961). [9] Bourke, M. C., Lunar and Planetary Science Conference, XXXVI, Abs. # 2373 2005. [10] Long, J. T. *et al.*, *Geological Society of America Bulletin* **75**, 149-156 (1964).

Summary Statistics	Width (m)	Stoss Length (m)	Height (m)
Mean	741	246	65
Median	666	237	52
Mode	600	237	39
Standard Deviation	227	91	32
Minimum	440	120	26
Maximum	1343	500	130

Table 1: Summary morphometric data for 36 megabarchans in the north polar region of Mars.

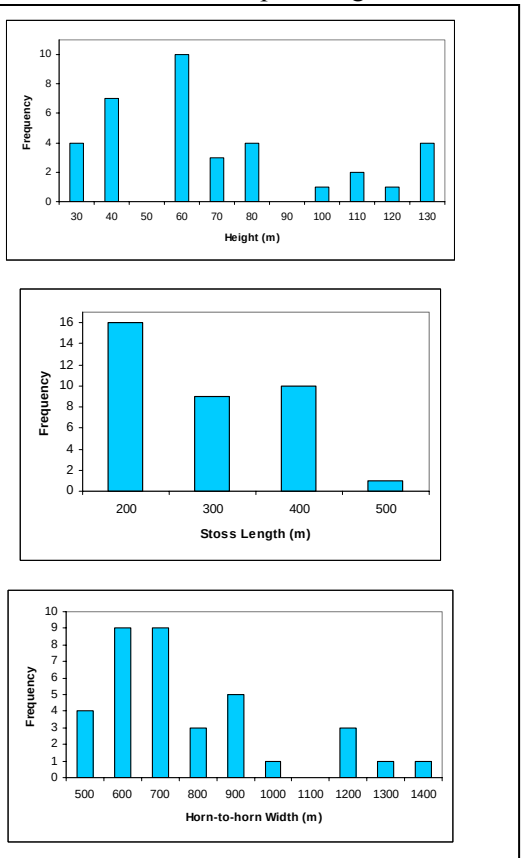

Figure 1: Frequency histograms of megabarchan height, length and width.

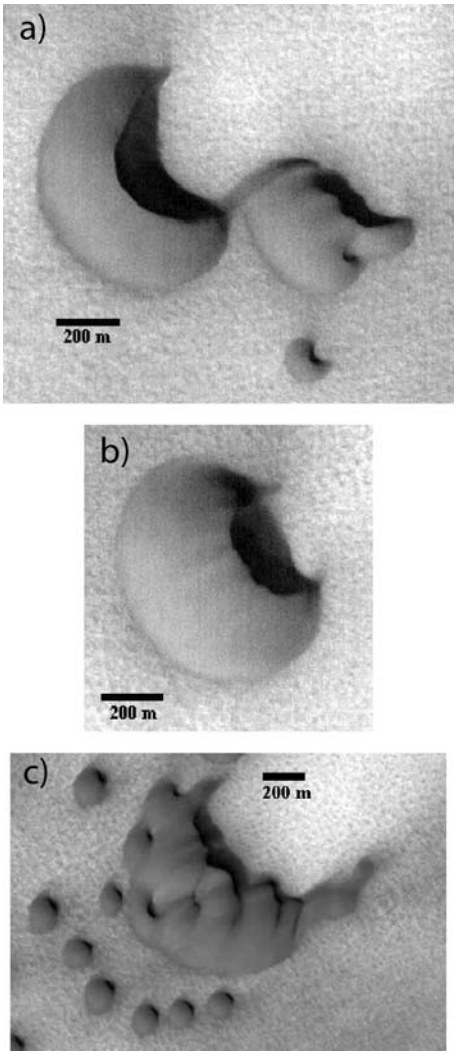

Figure 2: Megabarchan morphology on Mars.
a) Simple megabarchan form. Note the similar alignment with the small barchan. MOC E0400575
b) Megabarchan with a sinuous crestline. This crestline morphology represents the remnants of merged dunes on the windward slope. MOC E0400575
c) Complex megabarchan. MOC E0101781

MIGRATION RATES OF NIVEO-AEOLIAN DUNES IN ANTARCTICA: IMPLICATIONS FOR MARTIAN DUNES. M.C. Bourke[1], R. Ewing[2] D. Finnegan[3] and H. A. McGowan[4]. [1]Planetary Science Institute, Tucson, Arizona mbourke@psi.edu [2]Geological Sciences, University of Texas, Austin, TX,. [3]Cold Regions Research & Engineering Laboratory, Hanover NH 03755. [4]School of Geography, Planning and Architecture, University of Queensland, St. Lucia 4072, Australia.

Introduction: Dune migration has not yet been detected on Mars [1, 2]. There are however indications of active and significant sand transport. For example, two dome dunes in the north polar region on Mars disappeared over 3.04 Mars years [3]. HiRise data show arcuate ridges upwind of dunes in Chasma Boreal that mark previous dune positions suggestive of recent migration (Fig. 1) [4]. Dunes that currently display no change could be crusted, indurated, or subject to infrequent episodes of movement. One of the many agents of dune induration may be niveo-aeolian deposits [5]. The effect of niveo-aeolian deposits on dune migration rates remains unknown but is suggested by some to entirely restrict movement [6]. We present the results of a remote sensing study on the influence of niveo-aeolian desposits on dunefield morphodynamics. This data will assist in better understanding the potential transport-limiting effect not only on Earth, but also on Mars and other extraterrestrial surfaces.

Figure 1 Arcuate permafrost ridges upwind of barchan dunes in Chasma Boreale mark the former position of sand dunes. (HiRISE Image 85.0ºN, 339.0ºE, 32.1 cm/px).

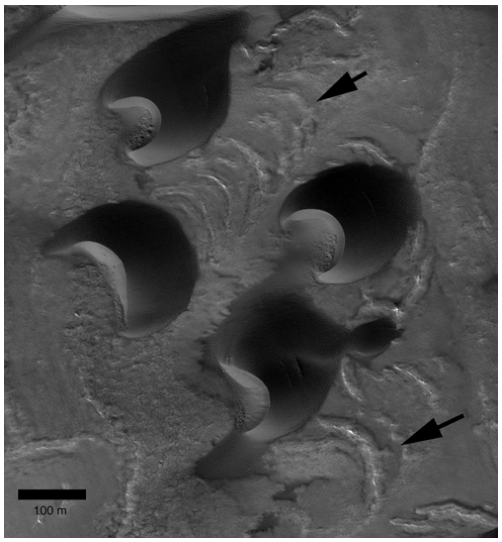

The Study Area: The Victoria Valley sand dunes lie in a hyper-arid polar desert with a present day mean annual temperature of -27.4°C [7]. Annual precipitation is <10 mm and summer snowfalls sublime rapidly. The recorded wind speeds exceed the threshold sand entrainment velocity of 5.5 m/sec for 27% of the time during winter and 74% of the time during summer [8]. The dune field consists of a series of transverse and barchan dunes that covers an area of ~1.1 km^2, in a belt which is about 3.1 km long and 0.5 km wide..

Niveo-aeolian Deposits: The aeolian deposits of the McMurdo Dry Valleys in Antarctica are the primary type site for understanding landforms and process rates for perennial niveo-aeolian environments [e.g., the work of 9, 10]. Shallow manual excavations of the dunes show inter-bedded snow and ice layers, likely annual winter or storm deposits [6] (Fig. 2). The snow laminae are discontinuous, and their thickness varies, as does the proportion of snow in the sand layers [11].

Methodology: In our analysis we have used vertical air photographs from 1959, 1961, 1972, 1981 and 1983) combined with high resolution LIDAR data, collected in 2001. The images were all projected to a common pixel dimension and registered to a Lambert Conformal Conic projection using a 1st order polynomial fit and nearest neighbor algorithm. Dune migration was estimated utilizing mapped crestlines (1961-2001) in ARCGIS (Fig. 3). We collected dune morphometric and spacing data (height, length and horn to horn width). We also estimated dunefield defect density (ρ). This is a field-scale measure of the number of the defect pairs per unit length of crestline [12], where defects represent terminations of dune crestlines.

Dune migration rates: Dunes in the Victoria Valley dune field moved on average 62 meters to the west during the 40 year survey period. This translates to an average dune migration rate of 1.5 m per year. Individual dunes displayed considerable variation in movement with values ranging from a total distance 20 m to maximum of 112 m over the 40 yr period. No correlation is observed between dune position in the dune field and migration rate, although terminations that extend toward the valley floor show the greatest degree of change.

Dune morphodynamics: Significant change occurred in the dune field. All crestlines have not only migrated downwind, but also changed position relative to each other. Dune merging, lateral linking and absorption occurred. The decrease in the coefficents of variation, total crest length and defect density and the increase in mean spacing indicate that the dune-field organization increased over time. These data match

well with other empirical studies of pattern evolution over time and models of dune-field pattern evolution as self-organizing systems [12-15].

Conclusion: The data show relatively low rates of dune migration for the Victoria Valley. When considered alongside other cold climate studies, these data suggest that dune migration rates are lower in polar deserts than in warm desert environments, which can be between 6 to 20 m/yr. The data from Victoria Valley show that while niveo-aeolian deposits lead to lower rates of dune migration, their presence does not extinguish dune movement on Earth or we would suggest, on Mars.

Acknowledgements: Funded by MFRP.

Figure 2 (Left)View across eroded windward slope of barchan dune in Victoria Valley. Snow and ice-cemented sand layers are visible.
(Right) Shallow manual excavation of a barchan dune in the Victoria Valley. Section reveals interbedded snow, ice and sand.

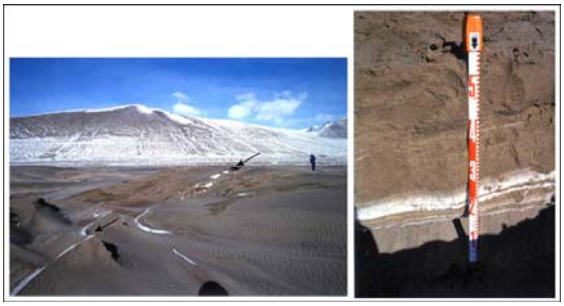

References

[1] Zimbelman, J. R., *Geophysical Research Letters* **27**, 1069-1072 (2000). [2] Schatz, V. *et al.*, *Journal of Geophysical Research (Planets)* **111**, 10.1029/2005JE002514 (2006). [3] Bourke, M. C. *et al.*, *Geomorphology* **94**, 247-255 (2008). [4] Bourke, M. C. *et al.*, *Permafrost and Periglacial Processes*, (submitted). [5] Bourke, M. C., *Eos Trans. Fall Meet. Suppl.* **85**, Abstract P21B-01 (2004). [6] Selby, M. J. *et al.*, *New Zealand Journal of Geology and Geophysics* **17**, 543-562 (1974). [7] Doran, P. T. *et al.*, *Journal of Geophysical Research (Atmospheres)* **107**, (2002). [8] Ayling, B. F. *et al.*, *Arctic, Antarctic, and Alpine Research* **38**, 313-324 (2006, 2006). [9] Cailleux, A., *Biuletyn Peryglacjalny* **17**, 57-90 (1967). [10] Calkin, P. E. *et al.*, *Geographical Review* **64**, 189-216 (1974). [11] Miotke, F.-D., *Polarforschung* **55**, 79-125 (1985). [12] Werner, B. T. *et al.*, *Geology* **27**, 727-730 (August 1, 1999, 1999). [13] Ewing, R. C. *et al.*, *Earth Surface Processes and Landforms* **31**, 1176-1191 (2006). [14] Wilkins, D. E. *et al.*, *Geomorphology* **83**, 48-57 (2007/1/15, 2007). [15] Werner, B. T., *Geology* **23**, 1107-1110 (1995).

Figure 3: Change in position of sand dunes in Victoria Valley. Digitized dune crest lines 1961 (dashed line) and 2001 (solid line).

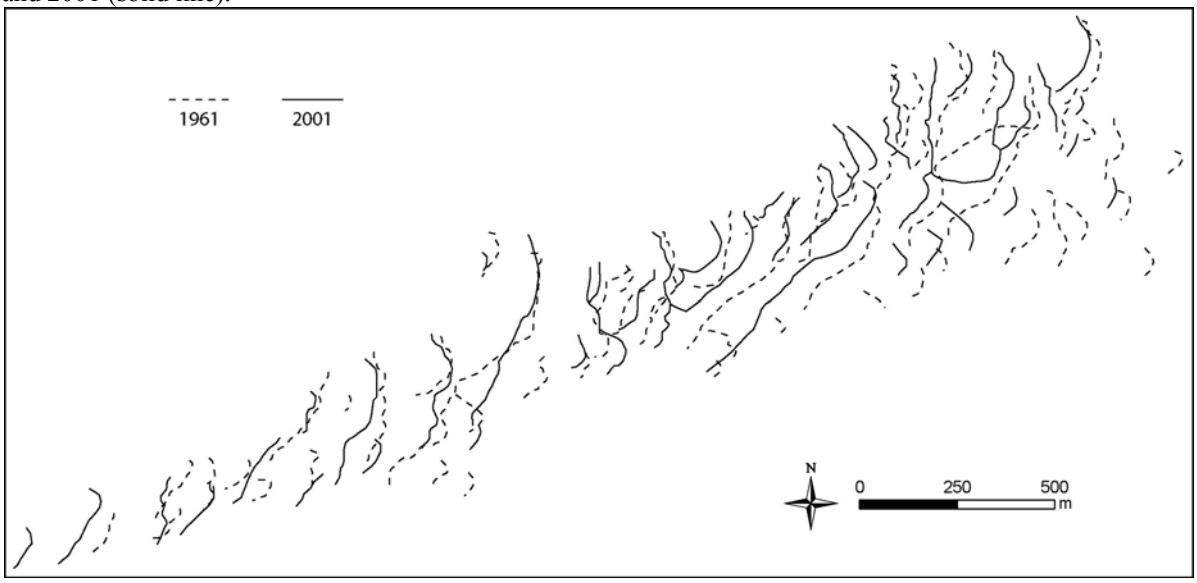

GPR Surveys of the Jurassic Navajo Sandstone: a Potential Analogue to the Burns Formation, Meridiani Planum, Mars

Charlie Bristow[1], Harry Jol[2]

[1] School of Earth Sciences, Birkbeck College, University of London, Malet Street, London WC1E 7HX email c.bristow@ucl.ac.uk

[2] Department of Geography and Anthropology, University of Wisconsin Eau-Claire, 105 Garfield Avenue, Eau Claire, WI 54702-4004, USA.

The Burns Formation of the Meridiani Planum, Mars, is interpreted as an aeolian sandstone (1), and images from the Mars Exploration Rover 'Opportunity' show exposures of cross-stratified aeolian sandstones of the Burns Formation exposed within the walls of the Victoria Crater. In this paper we show the results of GPR surveys across a terrestrial analogue for the Burns Formation, the Jurassic, Navajo Sandstone. The Navajo Sandstone has already been suggested as a possible terrestrial analog for heamatite bearing sandstones on Mars (2). At outcrop in Zion Canyon, Utah, the Navajo Sandstone forms spectacular outcrops of cross-stratified aeolian sandstones separated by beds of wet interdune sands. We used ground penetrating radar (GPR) with a range of antennas with central frequencies of 12.5, 25, 50,100, 200, 225, 450 and 900 MHz to successfully image the sedimentary structures and shallow stratigraphy within the sandstone. The results of the GPR surveys are very good, with good depths of penetration and high resolution. The longer wavelengths of the low frequency antennas (12.5 - 25 MHz) achieved depths of penetration to around 40m, while the higher frequency antennas resolve beds of cross-stratified sandstones, and the cross-strata (Figures 1 and 2).

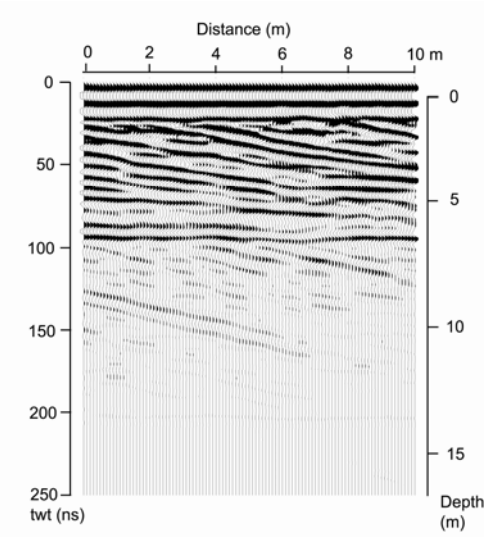

Figure 1. 200 MHz GPR profile showing first 10m of section images cross strata to 10 m

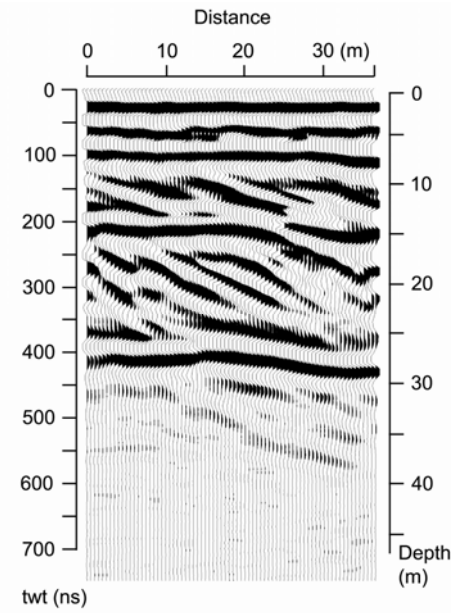

Figure 2. 25 MHz GPR profile shows strata resolved to a depth of around 40m but the shallow subsurface is obscured by the ground wave and air wave and the first two sets of cross-strata imaged in the 200 MHz profile are not resolved.

The results of the GPR surveys of the Navajo Sandstone illustrate the potential for GPR on future Mars rover missions to image the subsurface stratigraphy on Mars. On Mars where there is little or no liquid water in the shallow subsurface the depths of penetration might be greater permitting improved imaging of the shallow subsurface stratigraphy with GPR. Our results suggest that GPR mounted on a Mars rover should be able to image sedimentary structures within the Burns Formation and could be used to constrain the subsurface stratigraphy.

(1) Grotzinger, J.P., Arvison, R.E., Bell, J.F. III, Calvin, W., Clark, B.C., Fike, D.A., Golombek, M., Greely, R., Haldemann, A., Herkenhoff, K.E., Jolliff, B.L., Knoll, A.H., Malin, M., McLennan, S.M., Parker, T., Soderblom, L., Sohl-Dickstein, J.N., Squyres, S.W., Tosca, N.J., and Watters, W.A., 2005, Stratigraphy and sedimentology of a dry to wet eolian depositional system, Burns formation, Meridiani Planum, Mars. Earth and Planetary Science Letters 240, p.11-72.

(2) Chan, M.A., Beitler, B., Parry, W.T., Ormo, J., and Komatsu, G., 2004, A possible terrestrial analogue for haematite concretions on Mars. Nature, 429, p.731-734.

GPR surveys of Sand Dunes in Antarctica as Analogs for Dunes on Mars

Charlie Bristow[1], Harry Jol[2], Paul Augustinus[3], Irene Wallis[3]

[1] School of Earth Sciences, Birkbeck College, University of London, Malet Street, London WC1E 7HX, c.bristow@ucl.ac.uk

[2] Department of Geography and Anthropology, University of Wisconsin Eau-Claire, 105 Garfield Avenue, Eau Claire, WI 54702-4004, USA.

[3] School of Geography and Environmental Science, The University of Auckland, Private Bag 92019, Auckland, New Zealand

The cold, dry, windy conditions on Mars have created a variety of sand dunes especially in the areas surrounding the polar ice caps. Antarctica is the coldest, driest, and windiest continent on Earth. As a consequence, the areas on Antarctica that are free of ice and snow are analogous to the surface conditions on Mars. In this paper we report the results of a ground penetrating radar (GPR) survey of sand dunes in Antarctica. In Victoria Valley, one of the McMurdo dry valleys of Antarctica, there are areas of sand dunes that include reversing, transverse - barchanoid dunes, and slipfaceless 'whaleback' dunes (Fig. 1). We have used ground penetrating radar (GPR) systems with central frequencies between 100 and 900 MHz to image the sedimentary structures within the dunes.

The results of the GPR surveys are exceptionally good with good depths of penetration and very high resolution. The lack of attenuation is attributed to a lack of liquid water within the frozen dunes. Successive layers within the dunes imaged by the radar provide a record of sand accumulation on the dune surface and record the development of the dunes.

Interpretation of the GPR profiles indicate that the reversing dunes of the Packard dune field show net migration towards the west in response to easterly winds blowing along the Lower Victoria Valley in the summer. There is evidence for wind reversal with strata dipping towards the east at the crest of the dune (Fig. 2). These eastward dipping strata are interpreted as the deposits of katabatic winds that descend from the Antarctica Plateau which are stronger and more frequent during the winter months. The seasonal reversing winds reprofile the producing low-angle bounding surfaces that are imaged by all the GPR antennae. However, the higher frequency antennae (especially the 450 MHz) successfully image strata between the bounding surfaces. In addition, we have also identified frequency dependent anomalies from layers of snow and ice within the dunes. Discontinuous snow layers that appear to produce parabolic reflections on GPR profiles collected with lower frequency antennas have less obvious effects on the profiles collected with the high frequency antennas, although they may produce some multiples. Because the multiples are parallel to the snow layers and strata within the dune they could easily be mistaken for reflections from primary sedimentary strata.

The Victoria Valley dunes show evidence of topographic control on dune orientation and wind direction. The results of this study illustrate the potential for GPR surveys on future missions to Mars.

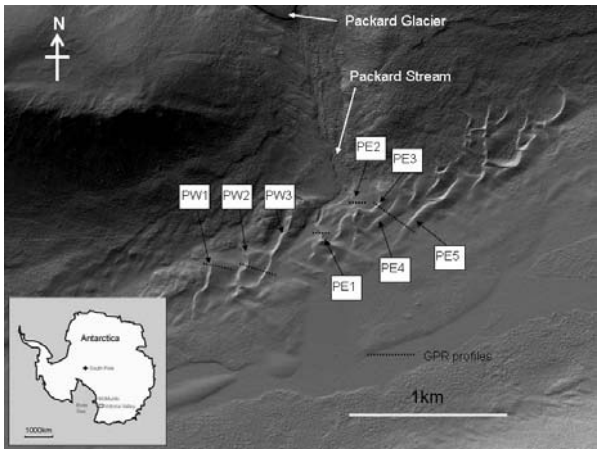

Figure 1. Locality map and Lidar image of sand dunes in the Victoria Valley, Antarctica

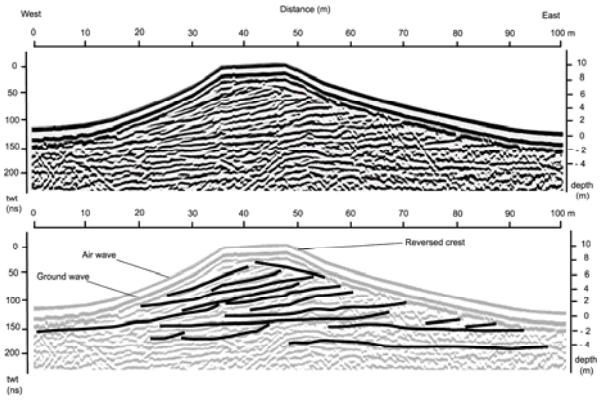

Figure 2. GPR profile PE1 (see location above) showing inclined reflections from bounding surfaces within a reversing dune. Data collected using Pulse EKKO 100 with 100 MHz antennas and 1000 volt transmitter.

Dunes on Mars, 'Venus', Earth, and subaqueous ripples: a scaling law for their elementary size

P. Claudin & B. Andreotti
Laboratoire de Physique et Mécanique des Milieux Hétérogènes (UMR CNRS-ESPCI-P6-P7 7636)
10 rue Vauquelin, 75231 Paris Cedex 05, France.
claudin@pmmh.espci.fr, andreotti@pmmh.espci.fr

Dunes and bedforms are observed in considerably diverse environments: aeolian dunes of sand as well as snow, dunes under water, but also dunes on Mars or Titan. Summarising our work published in [1], we would like to show in this paper that, although the fluid, the grains and the mode of sediment transport can be different in these various situations, the understanding of the size at which a flat bed destabilises – denoted below as the 'elementary' size – can be thought of in a common manner, i.e. independently of the above geological objects. Reasoning in terms of instability mechanism, we have then been able to evidence a scaling law for this elementary size, valid from centimetric subaqueous ripples to 600 m long Martian dunes.

A flat sand bed submitted to a turbulent flow spontaneously generates undulations due to the combined action of sediment transport and hydrodynamics. Because of the large separation between the hydrodynamical and dune growing time scales, these two aspects can be treated independently of each other. The amount of sediment that can be transported by a steady flow per unit time is finite above a certain threshold $u_{\rm th}$ and is a function of the shear velocity u_*. We call $q_{\rm sat}$ the corresponding 'saturated' sediment flux. Be the flux out of its saturated value, it relaxes toward equilibrium within some time or distance, depending on the nature of the perturbation. We call $\ell_{\rm sat}$ this saturation length. Consider now a wavy bottom of wavelength λ. The basal shear stress is also modulated at this wavelength, but not in phase with the bottom: the shear maximum is reached before the bottom crests. Because turbulence does not provide any intrinsic length scale, this up-flow shift is some (small) fraction of λ. As for a given shear, transport equilibrium is only reached after some lag $\ell_{\rm sat}$, the position at which the sediment flux is maximum can then be located either on the stoss side of the bottom bumps when λ is large, or on their lee side when λ is small. This position is crucial for the dune formation issue as it separates the erosion from the accretion zone. When erosion occurs at the crest, the bumps shrink, meaning that the bed is stable with respect to perturbations at this wavelength. Conversely, bumps can grow if their crest is in the deposition region. The mathematical linear stability analysis of these processes leads to a growth rate which is positive for all large wavelengths down to a cut-off value λ_c, with a maximum at λ_m. As expected, both λ_m and λ_c are proportional to $\ell_{\rm sat}$, which is the only length scale of the problem. Because it corresponds to the most unstable mode, we call λ_m the elementary size of this instability.

So far, we have not specified how $\ell_{\rm sat}$ is related to the grain, fluid and flow properties. In fact, there is not a single mechanism limiting the time and length of saturation transient but several, e.g., (i) the ejection of the grains from the bed, (ii) the grain inertia that controls the length needed for one grain to reach its asymptotic trajectory, (iii) the fluid inertia that controls the length needed for the wind to readapt to a change of the flux. One should consider for $\ell_{\rm sat}$, the *slowest* process i.e. the largest relaxation length amongst the modes of relaxation, which can be different depending on the value of $u_*/u_{\rm th}$ as well as that of the grain to fluid density ratio ρ_s/ρ_f. Initially motivated by the aeolian case at wind speeds reasonably above the threshold, we have focused on the grain inertia mechanism (ii), for which the typical length scale is the drag length $\ell_{\rm drag} = \frac{\rho_s}{\rho_f} d$, where d is the grain diameter. In order to test this analysis, the idea is then to plot the elementary size *vs* $\frac{\rho_s}{\rho_f} d$ for situations as various as possible.

The measure of the elementary size is easy in the lab, for a bed of grains submitted to a water flow. In this case, the emergence of the pattern can be well controlled, and its λ_m deduced from a correlation or a Fourier transform technique. The data plotted in figure 1 correspond to different grain diameters [2,3,4]. For dunes in the field, the measure is less strict. In particular, isolated small barchans are not necessarily at the elementary size: λ_m is a non-local measure of the typical initial wavelength of the dune pattern. Fortunately, large barchans often present corrugated flanks with superimposed undulations, especially after few days of storm or unusual winds. In fact, a large dune is not far from a flat sand bed, and these rows of undulations are precisely emergent pattern at the elementary size [5]. Although less accurately, these superimposed undulations can also be seen on photos of Martian dunes [6]. From the analysis of 'microscopic' photos taken by the rovers at the

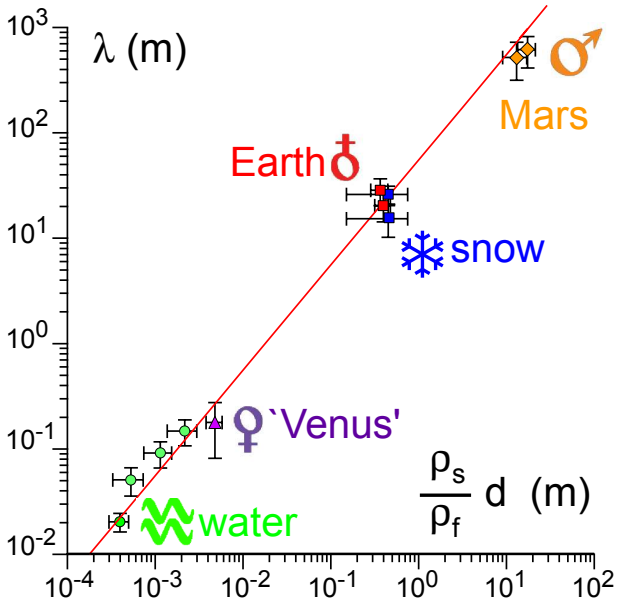

Figure 1: Scaling law for the elementary size of dunes. Symbols: aeolian sand dunes in Atlantic Sahara (♁); aeolian snow dunes in Antartica (⚹); Martian dunes (♂); bedforms in the Venus wind tunnel (♀); subaqueous ripples (♒).

surface of the planet, as well as theoretical calculations on the threshold for transport in the Martian conditions, one can deduce that the aeolian grains on Mars are rather small, with a diameter slightly smaller than 100μm. The plot of figure 1 is completed by two less documented situations: snow dunes in Antarctica [7,8], as well as bedforms obtained in a high pressure CO_2 wind tunnel reproducing conditions close to the Venus atmosphere [9]. Interestingly, the two aeolian Earth data point (sand and snow dunes) coincide on the plot although the very different values of d and ρ_s, but which compensate. Overall, the scaling law $\lambda \propto \frac{\rho_s}{\rho_f} d$ is well verified over almost five decades.

Given the few information available on Titan [10] and following this scaling law, one expects the elementary size there to be of the order of one or few meters. This size is much too small to be detectable on the Cassini radar images showing the dunes [11], which are presumably of 'giant' type, like terrestrial star dunes. Aeolian sand ripples are another pattern that should not be included in this law, as their formation mechanism is of different nature – a screening rather than hydrodynamical instability. Finally, we shall emphasize again that we do not claim to capture all the dependences on this plot, but that $\frac{\rho_s}{\rho_f} d$ is the dominant scaling factor. As mentioned above, we expect subdominant dependences on the wind speed, on finite size effects, etc, related to other relaxation mechanisms.

This scaling law at hand, one can finally address the more speculative issue of the time scales of Martian dunes. The linear stability analysis predicts that the dune growth rate scales with $\ell_{\rm sat}^2/\bar{Q}$, where $\bar{Q}$ is the mean sand flux. Its value is difficult to estimate because we do not know the fraction of the time for which Martian winds are above the transport threshold. Assuming that this is the case few days per year, we end up with a factor of the order of 10^5 between terrestrial (a week) and Martian (tens of centuries) dunes. Similarly, one gets a factor 10^{-4} between the propagation velocities. As some satellite high resolution pictures definitively show some evidence of aeolian activity – e.g. avalanche outlines – it may then well be that the martian dunes are fully active but not significantly at the the human scale.

References

[1] P. Claudin and B. Andreotti, Earth and Planetary Science Letters **252**, 30 (2006).
[2] P. Hersen, S. Douady and B. Andreotti, Phys. Rev. Lett. **89**, 264301 (2002).
[3] S.E. Coleman and B.W. Melville, J. Hydraulic Eng. **122**, 301 (1996).
[4] S.E. Coleman and B. Eling, J. Hydraulic Res. **38**, 331 (2001).
[5] H. Elbelrhiti, P. Claudin and B. Andreotti, Nature **437**, 720 (2005).
[6] `http://barsoom.msss.com/moc_gallery/`
[7] R.A. Massom, *et al.*, J. Geophys. Res. **103**, NO. C11, 24837 (1998).
[8] R.A. Massom *et al.*, Rev. Geophys. **39**, 413 (2001).
[9] R. Greeley, J.R. Marshall and R.N. Leach, Icarus **60**, 152 (1984).
[10] R.D. Lorenz, J.I. Lunine, J.A. Grier and M.A. Fisher, J. Geophys. Res. **100**, 26377 (1995).
[11] R.D. Lorenz *et al.* Science **312**, 724 (2006).

THERMOPHYSICAL PROPERTIES OF PROCTOR DUNE FIELD, MARS. G.E. Cushing, T.N. Titus and R.K. Hayward. U.S. Geological Survey, 2255 N. Gemini Dr. Flagstaff, AZ 86001, gcushing@usgs.gov

Introduction: Since first observed by Mariner 9 in the early 1970s, the dune field in Proctor crater has been the subject of many investigations because its large expanse of homogeneous, unconsolidated granular material provides a predictable and convenient surface for testing and comparing thermal models and theories of heat transfer within granular materials (e.g. [1,2,3]). In this study of dune-field thermophysical properties, we validate our technique by comparing results from these previous investigations, with those from our own, and conclude by discussing the implications of our results.

To date, probably the most vigorous examinations of this dune field were performed by Fenton et al. [4] and Fenton and Mellon [5], who determined the average thermal inertia of the dune field to be ~300 J m^{-2} $s^{-1/2}$ K^{-1} (units henceforth referred to as tiu [6]), which were consistent with global datasets created by Putzig et al. [7] and Christensen [8]. Using the particle-size / thermal-conductivity relation described by Presley and Christensen [3], average grain sizes in this dune field were calculated to be on the order of ~0.5–2.0 mm [5].

Data: We use data collected by a variety of instruments onboard several spacecraft orbiting Mars. We obtained atmospheric opacity and albedo information from the Mars Global Surveyor (MGS) Thermal Emission Spectrometer (TES) [8]. The MGS Mars Orbiter Camera (MOC) [9] provided high-resolution visible-wavelength coverage as well as albedo information. We used both visible-wavelength and diurnally obtained thermal infrared information from the Mars Odyssey Thermal Emission Imaging System (THEMIS) [10]. The Mars Reconnaissance Orbiter (MRO) High Resolution Imaging Science Experiment (HiRISE) provided images at a resolution of 25 cm/pixel [11].

Atmospheric pressures were adjusted to scale height, and were calculated assuming a mean annual pressure of 6.1 mb at zero elevation, adjusted for the annual CO_2 sublimation cycle.

Modeling: To model dune-field terrain at high-resolution, we applied the photoclinometry technique developed by Kirk [12] to THEMIS VIS image V09563005. Photoclinometry cannot distinguish between shaded terrain and albedo variations, so the synthetic terrain models generated from images of variable-albedo surfaces will show non-real topographic variations. In many cases however, such as in the centers of the dune field discussed here, the albedo variations can be relatively minor (compared with topographic shading) and the real topography in these synthetic terrain models is easily distinguished from artifacts introduced by albedo boundaries. Therefore, we can still accurately represent the 'apparent' topography of local terrain features such as the locations and general features of dune crests and troughs, even though other information such as regional topography and the relative heights of adjacent features may be incorrect.

We generate maps of slope & atmospherically corrected Lambertian albedo values by first creating a map of I/F values from a THEMIS VIS image (multiplied by the cosine of observed incidence angle and scaled to MGS TES bolometric albedo). This I/F information and the digital-terrain map are then applied to a photometry algorithm, which determines albedo values according to the slope-corrected solar illumination and atmospheric dust opacity (from TES observations).

To calculate thermal inertia values, we use the Kieffer 'KRC' thermal-diffusion model [13] to create a lookup table of temperature values that represent appropriate ranges of slope, azimuth, solar longitude, time, albedo and thermal-inertia values. An interpolation routine compares this lookup table with maps of albedo, terrain, and observed nighttime temperatures and determines the best-fit thermal inertia at each pixel.

Results: TES-observed albedo values were 0.08-0.085 in the dark-dune areas in Proctor crater, while the surrounding surfaces were somewhat brighter. Our best-fit thermal inertia for these dunes is 304 +/- 14 tiu, which is very similar to values given by Fenton et al. [5] as well as to the global datasets provided by Putzig et al. [7] and Christensen [8]. Using the method described by Presley and Christensen [3], we calculate grain sizes to be on the order of 0.5 +/- .1 mm. These diameters are consistent with the lower end of values calculated by Fenton and Mellon [5]. Differences between our values can be easily explained if a different value for bulk density was used. We used 1700 kg m^{-3}.

Discussion: Fenton and Mellon [5] described a scene where the interdune areas and dune troughs are cooler than the crests at night, therefore consisting of lower-thermal-inertia materials. Difficult registration between THEMIS VIS and predawn IR observations gave an appearance that the crests were particularly warm at night and were therefore composed of materials with higher thermal inertia. However, overlaying THEMIS nighttime IR over photoclinometric topography shows that the warmest locations at night are associated with the north-faces of the dune crests rather than the crests themselves. Figures 1-A and 1-B show a colorized thermal-radiance map that has been com-

bined with a visible-radiance map (in B&W) and draped over photoclinometric topography. Figure 1-A shows the dune field from a south-facing 3-D perspective where warm spots on the northern crest faces are clearly visible. From a perspective that faces north, however (Figure 1-B), the warmest spots can no longer be seen. This thermal behavior suggests that the north-facing slopes are probably warmer because that is the orientation to receive the most solar insolation each day, and retains more residual heat each day (Figure 2). It is also possible that the north-facing slopes have exposed, partially indurated surfaces, with higher thermal inertia, while their unconsolidated, low-thermal-inertia weathering products fall into the troughs.

Aside from the north-facing hot spots, our results agree with Fenton and Mellon [5] that low-lying areas in this dune field appear to have lower thermal inertia than the upper-dune surfaces. We were thus surprised to find a significant population of boulders in MOC and HiRISE images with diameters up to ~25 m covering the surfaces surrounding the dune field, as well as the exposed intra-dune surfaces at the outer edges of the dune field. These boulders must confirm Fenton and Mellon's conclusion that a mantle of dust is covering these low-lying surfaces [5], because without such a mantle, they would stand out as patches of warm, high-thermal-inertia material at night.

Additional support for dust mantling occurs in the form of the seasonal presence of numerous dust-devil tracks we find in both MOC and HiRISE images. These tracks indicate the presence of dust, and their formation has been shown by Rossi and Marinangeli to be critically dependent upon vertical particle-size sorting of the surface materials (such as dust over sand) [14]. These tracks appear to cover all slopes of the dune field, including the crest areas, suggesting there is at least some amount of dust on all dune surfaces.

Many large boulders are partially buried at the edges of sand dunes, so changing amounts of sand observed on and around these boulders could indicate an active dune field. MOC and HiRISE have sufficient resolution to monitor this type of activity [9,11], and could probably document dune activity over shorter timescales than would be necessary to the track the motion of larger dune features.

Future work: We will present results for Russell crater at the workshop. Further in the future, we will incorporate data from CRISM, which may identify distinct mineral components and possibly help distinguish and explain different types of dune fields.

References: [1] Edgett K.S. and Christensen P.R. (1991) *JGR*, 96, 22765-22776. [2] Edgett K.S. and Christensen P.R. (1994) *JGR*, 99, 1997-2018. [3] Presley M.A. and Christensen P.R. (1997) *JGR*, 102, 6551-6566. [4] Fenton L.K. et al. (2005) *JGR*, 110, E06005. [5] Fenton L.K. and Mellon M.T. (2006) *JGR*, 111, E06014. [6] Putzig N.T. (2006) Ph.D. Thesis, Univ. Colorado. [7] Putzig N.T. et al. (2007) Icarus, 191, 1, 68-94. [8] Christensen P.R. et al. (2001) *JGR*, 106(E10), 23,823-23,871. [9] Malin M.C. et al. (1992) *JGR*, 97(E5), 7699-7718. [10] Christensen P.R. et al. (2004) *Sp. Sci. Rev.*, 110(1), 85-130. [11] McEwen A.S. et al. (2007) *JGR*, 112(E5), E05S02. [12] Kirk R.L. (1987) Ph.D. Thesis, Caltech, 165-258. [13] Kieffer H.H. (1977) *JGR*, 82, 4249-4291.[14] Rossi A.P. and Marinangeli L.(2004) *GRL*, 31, #6.

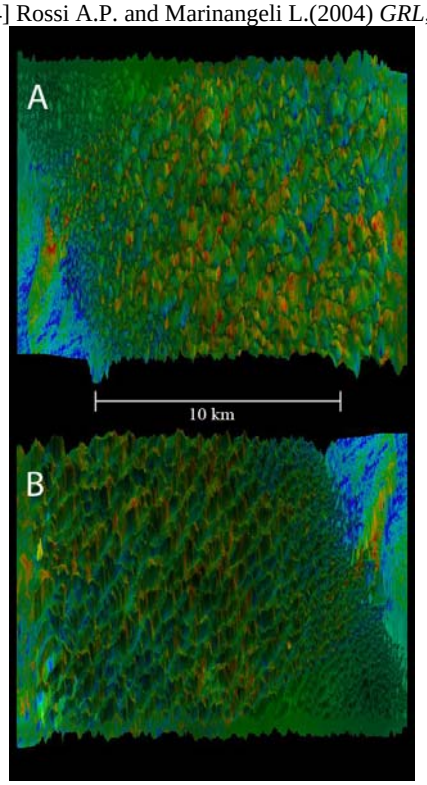

Figure 1: 3-D perspectives of the Proctor crater dune field. This is a synthetic terrain model overlain with THEMIS VIS (V09563005) in B&W, and colorized nighttime temperatures from THEMIS IR I00967002. Figure 1-A has a perspective looking south--upon the northern faces of the dunes, while 1-B (same image, rotated) looks northward at the southern faces. Hot spots are confined to the north-facing slopes.

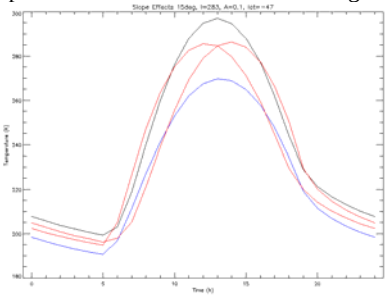

Figure 2: Modeled 24-hour temperature profiles of surfaces with 15° slopes facing: north (black), south (blue), east (red) and west (red). Thermal inertia=283 tiu, and albedo=0.1. At 3.33 hrs. (the time of THEMIS IR I00967002), the modeled north-facing slopes are ~5 K warmer than east or west-facing slopes, and more than 10 K warmer than south-facing slopes.

DEFROSTING PROCESSES ON DARK DUNES: NEW INSIGHTS FROM HIRISE IMAGES AT NOACHIS AND AONIA TERRAE, MARS. G. Di Achille[1], S. Silvestro[1], and G. G. Ori[1,2], [1]International Research School of Planetary Sciences, Università "G. D'Annunzio", Pescara, Italy; [2]Ibn Battuta Centre, Universite Cady Ayyad, Marrakech, Morocco. (gadiachi@irsps.unich.it)

Introduction: Morphological surveys of Martian ergs have recently revealed the occurence of gullies and scars on dark dune slopes [1-7]. They have been classified according to their morphology [1,2] and interpreted to be the results either of regular dry avalanching or fluid erosion and transport [1-7]. In particular, *Bourke* interpreted alluvial-like lobate deposits, developed at the base of dune slip faces, as possible evidence for niveo-aeolian and denivation processes [6, 7]. However, the origin of these features is often still enigmatic and likely related to the peculiar environmental conditions of Mars in relation to the behavior of volatiles and thermophysical properties of sand. Here, we present new HiRISE observations (Fig. 1 and 2) of dunes belonging to dark ergs formed within two unnamed craters [8]. Our survey identified unusual meter-scale circular depressions at the termini of grooves and gullies (Fig. 1 and 2). The latter features are interpreted to be the results of a combination of possibly overlapping processes, occurring during the seasonal defrosting at this latitude region. These likely involve frost vaporization, reprecipitation, snowball-like downslope rolling of frost/sand aggregates, glacial-like creep sustained by ephemeral liquid flow, and terminal sublimation at the base of dunes.

Observations: Studied ergs are located within two unnamed craters in Noachis (48-km-diameter; Fig. 1) and Aonia (10-km-diameter; Fig. 2) Terrae, respectively. The first covers an area of about 210.7 km^2 and can be classified as a giant complex dome (200-400 m

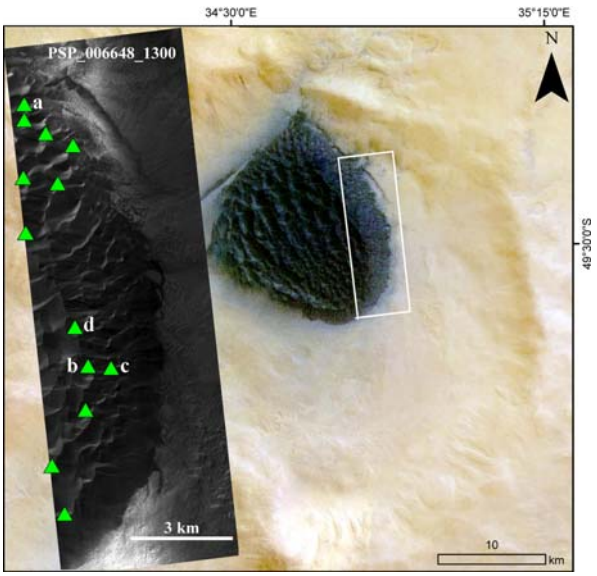

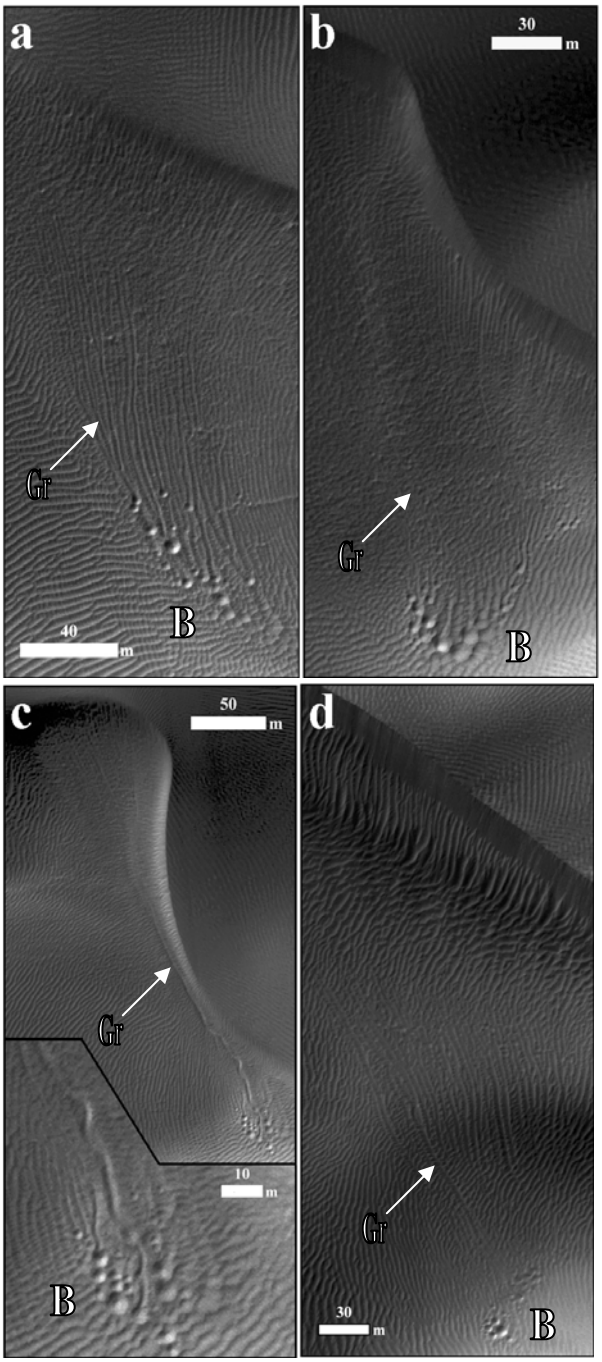

Figure 1. (left) Overview of the studied erg in Noachis Terra: HRSC color mosaic showing the dark erg with superimposed footprint of PSP_006648_1300 HiRISE image shown as inset. Green triangles indicate possible defrosting features. (above: a, b, c, d) Close-up from HiRISE image (see overview for location; **Gr** indicate grooves; **B** the bowl-shaped meter-scale depressions).

high), comparable to terrestrial examples occuring in the northern Saudi Arabia [9]. The second erg covers an area of about 10.8 km^2 and is mainly composed of barchan dunes with slipfaces reflecting dominant winds from northeast (Fig. 2).

Grooves, gullies and small circular depressions. HiRISE images of both the above described ergs show extensive occurrence of shallow grooves (**Gr**) and gullies (**Gu**) that occur mostly along the SE-facing dune slopes and terminate with bowl-shaped shallow depressions (**B**) (Fig. 1 and 2). However, **Gr** and **Gu** appear rather different from previously recognized gullies on Martian dunes (e.g. Russel crater [1]), first of all, for the previously unidentified presence of **B** features at their termini, but also for the lack of levees and terminal debris aprons, and for their lower depth. **Gr** and **Gu** are a few meters wide, start from dune crests and extend downslope of dune slipfaces with length ranging from tens up to a few hundreds meters (Fig. 1 and 2). **Gr** are generally arranged in series of low-sinuosity and parallel lineations (Fig. 1a, b, d). Occasionally the lineations originate from alcove-like crenulations along the dune crests, then converge at mid-slope into a main groove, which wanes downslope into a series of **B** features (Fig. 1c). **Gu** have usually same dimensions with respect to **Gr** but are deeper and wiggler than grooves (Fig. 2b, c). Like **Gr**, they also start from dunes crests, however, their upslope portions often show low-order dendritic patterns and convergence of several lineations into a single gully. Bowl-shaped features (**B**) usually occur as small clusters at the base of dune slipfaces, or at local topographic lows surrounded by dune crests, in association with the sharp terminations of grooves and gullies (Fig. 1 and 2). **B** diameters range from tens of centimeters up to a few meters and never exceed 10 m. In some cases the diameters of the small circular depressions appear to be proportional to the length of the associated grooves (Fig. 2b).

Discussion and conclusion: On this base, we interpret the formation of **Gr**, **Gu** and **B** at their termini to be the results of seasonal defrosting occurring along the dune slipfaces. In particular, we hypothesize that the spring/summer defrosting of the dune slopes could explain the formation of the observed morphologies without involving a significant role of fluid erosion and transport. In fact, shallow grooves and gullies, shown by HiRISE images, display low sinuosity, lack of levees and distributary deposits at their mouths, and the presence of bowl-shaped depressions, which we interpret as resulting from the sublimation of meter-scale aggregates of CO_2-H_2O frost and sand. These could have arrived at the base of the dunes mainly through snowball-like rolling and glacial-like creep. The latter might have been sustained by alternate evaporation and reprecipitation of volatiles during the downslope movement, possibly also enhanced by the presence of an ephemeral basal liquid fraction, especially for the **Gu** features (Fig. 2). In conclusion, **Gr**, **Gu**, and **B** could have formed due to an almost "dry" mechanism and represent remnants of transport of frost along dune slopes and its terminal basal sublimation. Therefore, preliminary HiRISE investigation of Martian dunes likely suggests that defrosting processes might involve less amount of liquid water than previously thought [e.g. 1, 2, 6, 7]. Further observations and repeated surveys of regions affected by seasonal defrosting could help to test this perspective and asses the role of the liquid component during Martian defrosting processes.

References: [1] Reiss D. and Jaumann R. (2003) *GRL*, 30, 1321. [2] Reiss et al. (2007) *LPSC XXXVIII*, 1993. [3] Mangold N. et al. (2003) *JGR*., 108, 5027. [4] Malin M. C. and Edgett K. S. (2001) *JGR*, 106. [5] Edgett K. S. and Malin M. C. (2000) *JGR*, 105, [6] M. C. Bourke, (2004) *Eos Trans*., 85, pp. Abstract P21B-01. [7] Bourke M. C. (2005) *LPS XXXVI*, 2373. [8] S. Silvestro S. and G. G. Ori, *this volume*. [9] McKee E. D. (1978) *USGS Prof. Paper*, 1052. [10] Malin M. C. and Edgett K. S. (2000) *LPSC XXXI*, 1056. [11] Kossacki K. J. and Kopystinsky J. (2004) *Icarus*, 168.

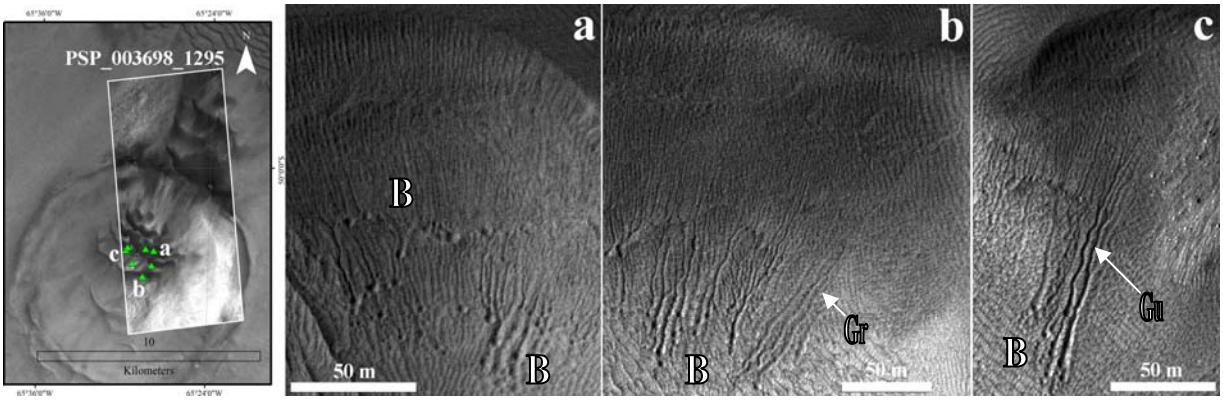

Figure 2. (left) Overview of the studied erg in Aonia Terra: HRSC image of the erg with superimposed PSP_003698_1295 HiRISE image. Green triangles indicate possible defrosting features. (a, b, c) Close-up from HiRISE image (see overview for location; **Gr** indicate grooves; **Gu** indicate gullies; **B** the bowl-shaped meter-scale depressions).

MODELING 2-D DUNE INTERACTIONS. Serina Diniega[1] and Karl Glasner[2], [1]Program in Applied Mathematics, The University of Arizona (Tucson, AZ 85721, serina@math.arizona.edu), [2]The University of Arizona

Introduction: This research aims to understand, through the analysis of simple equations and numerical simulations, the general trends and processes involved with transverse dune formation and evolution. Towards this end, the linearized version of the two-dimensional dune evolution equations derived by [1-3] have been analyzed and numerically simulated. Relationships between different environmental and dune parameters have been derived and/or calculated.

Additionally, this research seeks to understand the different types of dune interaction and the parameter regimes in which these interactions occur. This will aid in developing a macroscale model of dune field evolution, as models based on the movement of sand onto and over individual dunes are unfeasible.

The Model: To evolve a given sand (over rock) topography into a dune, the model first considers the interactions between the wind and sand by calculating the shear stress exerted by the wind onto the surface, via the Jackson-Hunt equation [4]. Corrections are applied to account for the separation of airflow and formation of shadow zones [5] to the lee of sharp topography (like dune crests).

This shear stress is then used to calculate the local maximal sand flux. The actual sand flux attains this amount after a spatial delay: the saturation distance. Additionally, the type of substrate the sand flux is moving over (non-erodible bedrock vs. sand) is taken into consideration.

The sand flux is then related back to changes in the dune profile, via the Exner equation. Additionally, a diffusion term is included in the dune sand evolution equation to mimic avalanching effects.

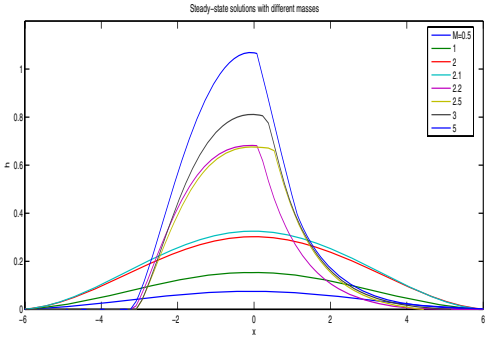

Figure 1: Plot of steady-state dune profiles for different initial system masses (height axis exaggerated). Notice the abrupt transition in shape: below the threshold mass dome dunes with smooth profiles form; above this mass crests form and the dune's aspect ratio increases.

Isolated Dunes: Steady-state dune profiles were found for a range of initial dune masses. Two types of dunes were observed to form: dome dunes when the initial mass was small and crested dunes above a mass threshold (figure 1). The crested dunes, corresponding to cross-sections of transverse or barchan dunes, were also observed to exhibit an inverse relationship between dune velocity and height, as expected (figure 2).

Additional analysis was done using a reduced dimensional model: the dune was approximated as a simple piecewise linear function. Thus, the profile of the dune could be expressed as a function of three variables: total volume of the dune, its windward slope, and the position of the dune's crest. Assuming that volume is conserved, the time derivative of the two remaining dynamic variables (windward slope and position) can be found by projecting the time derivative of the dune profile (calculated via the Exner equation in the full model) onto the space spanned by the partial derivatives of the function with respect to the windward slope and position.

The phase portrait of the windward slope (figure 3) shows that there is a stable equilibrium windward slope value (dependent on volume) that the dune profile naturally moves towards. Additionally, when the dune has this slope, the velocity of the simplified dune is inversely proportional to its height (figure 4).

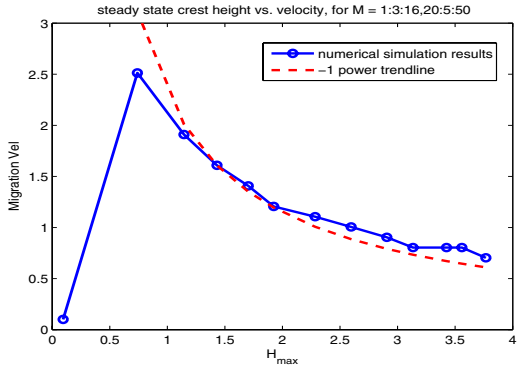

Figure 2: Plot of crest height vs. migration velocity for steady-state dune profiles with different masses. The trendline illustrates the expected inverse relationship.

Interacting Dunes: Due to the inverse relation between dune size and velocity, if a small dune is upwind of a large dune then an interaction will occur: the smaller dune's shadow zone will catch up to the larger dune and begin to steal sand. However, as the sand is stolen from the leading (initially larger) dune, the downwind dune shrinks in size/moves faster and the

upwind dune grows/moves slower. Depending on the interplay between the changes in size (and speed) of the two dunes, several different types of interactions can occur: (1) Coalescence: the upwind dune catches up to the downwind dune faster than this dune can lose sand/migrate faster, and the two dunes merge into one dune; (2) Run Away: the downwind dune, by shrinking and thus migrating faster, manages to escape from the (now larger) upwind dune, resulting in two dunes with different speeds and sizes; (3) Disappear (or Attempted Run Away): the downwind dune manages to escape, but is too small to remain stable. The result is one dune with most of the sand, as the downwind dune separates, flattens, and then disappears.

It was hypothesized that the different interactions could be predicted based on the model dunes' relative and absolute sizes: for small dunes, the actual dune sizes matter as the saturation length is comparable with the dune sizes and will influence the interactions; once the two dunes are large enough, the dune mass ratio should be the deciding factor . This was found to be the case (figure 5); these results are similar to the three dimensional model results found by [6].

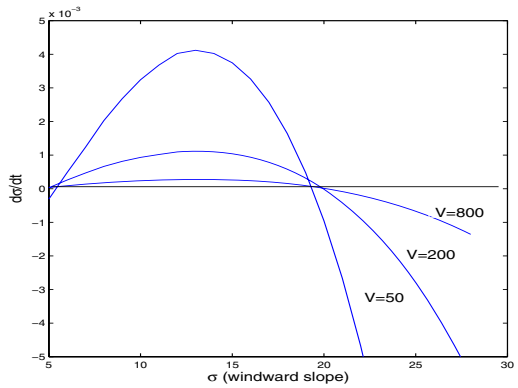

Figure 3: Phase portrait of the windward slope (in degrees), computed with the reduced dimension dune model. Note that there are two equilibrium slopes for each volume: the lower value (close to 0) is unstable and the upper value (around 20) is stable.

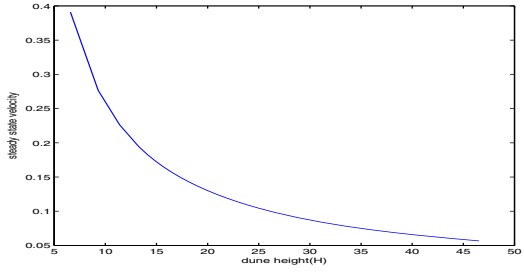

Figure 4: Plot of dune height vs. calculated dune velocity once the equilibrium slope is achieved. Note that it exhibits the expected inverse relationship.

Summary: This model appears to capture the main dynamics of dune formation and evolution: sand transport, avalanching, and separation of air flow/shadow zone, yielding physically realistic dune profiles and relations in the study of isolated dune structures. By applying the model to two dune structures, different possible interactions have been categorized and were shown to depend on the two dunes' initial masses (and only on the mass ratio for sufficiently large dunes).

Work is ongoing to understand analytically why certain interactions occur for a particular mass ratio between the dunes. Additionally, studies concerning interactions between more than two dunes will be completed to better understand and allow simulation of dune dynamics in large dune fields.

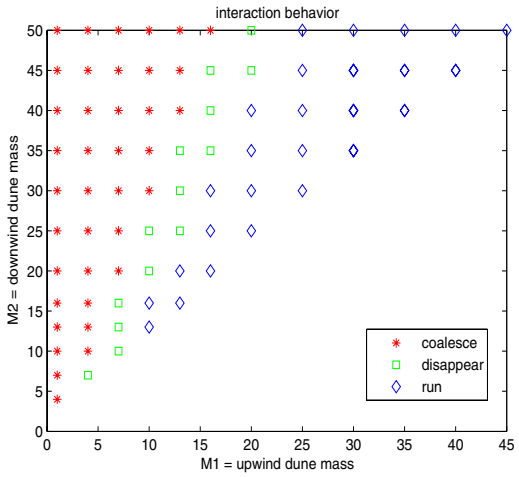

Figure 5: Plot showing the interactions observed in the simulations of two dunes, as a function of their initial masses. The axes are of the upwind dune's initial mass vs. the downwind dune's initial mass (larger). Notice that the regimes of interaction behavior (red stars = coalescence, green squares = disappear, blue diamonds = run away) depend only on the mass ratio (slope of regime boundaries) for larger dunes.

Acknowledgements: This research is supported by a NASA Harriet G. Jenkins Pre-doctoral Fellowship.

References: [1] Sauermann G., Kroy K. and Herrmann H. J. (2001), *Physics Review E, 64*, 031305. [2] Kroy K., Sauermann G. and Herrmann H. J. (2002), *Physical Review E, 66*, 031302. [3] Andreotti, B., Claudin, P. and Douady, S. (2002), *The European Physical Journal B, 28*, 341–325. [4] Jackson P. S. and Hunt J. C. R. (1975), *Quarterly Journal of the Royal Meteorological Society, 101*, 929–955. [5] Schatz V. and Herrmann H. J. (2006), *Geomorphology, 81*, 207–216. [6] Durán O., Schwämmle V., and Herrmann H. J. (2005) *Physics Review E, 72*, 021308.

Three-dimensional characterization and morphological dynamics of gypsum sand dunes at White Sands National Monument using airborne LiDAR. Ewing, R.C.[1*], Kocurek, G. [1], Peyret, A.P.B. [1], Mohrig, D. [1],
[1] Department of Geological Sciences, The University of Texas at Austin, 1 University Station C1100, Austin, TX 78712-0254. *rce@mail.utexas.edu

Introduction: Aeolian dune fields form some of the most striking patterns on Earth and other planetary surfaces. These patterns are thought to evolve through self-organization [1,2,3]. Self-organization refers to the spontaneous emergence of a pattern from a non-pattern state as a result of interactions between the elements of the system. In aeolian dune fields, the pattern is the result of the interactions between the dunes themselves and is largely decoupled from the smaller scale processes such as grain/fluid interactions. This hypothesis offers an approach to understanding dune-field pattern evolution which translates across dramatically different settings including subaqueous environments and different planetary surfaces.

On Earth, aeolian dune-field patterns form and persist on landscapes for over thousands of years and record important climatic and basinal events. Extracting this information requires an understanding of how large-scale dune-fields evolve through time and respond to environmental boundary conditions. Within the self-organization approach, crest spacing, crest length and defect density (number of defect pairs per unit crest length) are time dependent variables that characterize the dune-field pattern [4]. Spacing and crest length increases and defect density decreases through time owing to dune-dune interactions [5]. Boundary conditions, such as wind regime, influence dune-dune interactions, which in turn, affect the pattern formation and account for the diversity seen in aeolian dune-field patterns [6,7].

Recognizing the time-dependence of the pattern evolution and the influence of boundary conditions suggests that aeolian dune-field patterns can be used to interpret the climatic and geomorphic histories of dune fields. Essentially, spacing, crest length, and defect density reflect the constructional age of the pattern and the arrangement reflects the climatic and basinal conditions under which the pattern formed. Simple pattern analysis studies using aerial and satellite imagery and GIS have demonstrated that pattern variables can be statistically quantified and the dune-field patterns decomposed to provide robust interpretations of a dune field's evolution [8,9,10]. Absent from these studies, however, is the statistical quantification of the three-dimensional dune-field pattern components.

This study characterizes the three-dimensional dune parameters and morphological dynamics of the White Sands Dune Field at White Sands National Monument in New Mexico. In doing so, this research addresses how dune-dune interactions are coupled to boundary conditions to influence the field-scale pattern formation.

Methods: Airborne LiDAR was collected over a 40sqkm area in the core of White Sands. The data have a vertical accuracy of ~ 6 to 10 cm and were gridded to a 1 meter spatial resolution DEM. In order to extract the three-dimensional dune parameters the dune surface was first detrended from the underlying topography using an algorithm developed in Matlab. To characterize the underlying surface, the algorithm searches for the local minima in the downwind directions then creates a surface based on these points (Fig. 1). The surface was subsequently smoothed in the across-field direction The original DEM was then subtracted from the extracted surface to generate a de-trended dune surface.

The three-dimensional dune and dune-field pattern parameters were measured from the de-trended dune surface using Matlab and ArcGIS. These parameters include: (1) dune volumes and surface area, (2) crestline lengths, spacing, elevations, and sinuosity, (3) the slope and curvature of the stoss and lee slopes, and (4) size and shape of interdune areas. All parameters were calculated for individual dunes and the distributions characterized over the entire dune field. Dunes were separated from interdune areas based on the change in slope at 2.5 degrees. Volumes and surface area were calculated from ArcGIS. Crest lines were extracted using an automated algorithm developed in Matlab in which the local maxima were picked in the down wind and across field directions, and manually from visual inspection. Slopes and curvature were calculated using ArcGIS.

Results: Results indicate a strong control on dune form and field-scale pattern by changes in the field boundary conditions. The topography of the underlying surface reveals the presence of two previously unrecognized shorelines of Paleo-lake Otero (Fig. 1). Water-table heights related to this antecedent topography control local changes in sediment supply, which, in turn influences the nature of the dune slopes, crestline lengths, crest spacing, and interdune area (Fig. 2). The water table is perched at its highest between the two paleo shorelines and lies very near the surface at the core of the dune field. The presence of the high water table reduces sediment flux as sediment is accumulated in the interdune areas. Dunes in this area have more rounded crests, more continuous crestlines, more widely spaced crests, and wider interdune areas. At the change in slope of each shoreline the dunes are have sharper crests, more defects, more narrowly spaced crests, and minimal interdune areas.

Conclusions: Overall, the boundary condition of antecedent topography imposes the strongest control on the

dune-field pattern evolution at White Sands National Monument. Extracting the three-dimensional parameters of the dunes and dune-pattern reveals the significance of this control and emphasizes the importance of recognizing boundary conditions in interpreting dune-field evolution. Comparison of these static data with subsequent surveys will show the dynamic response of dunes to the boundary conditions. Changes in the location and magnitude of dune deformation on a seasonal and annual time scale, as well as, dune migration rates and dune-dune interactions will be determined with new surveys.

References: [1] Hallet, B. (1990) Earth-Science Reviews, 29, 57-75. [2] Werner, B.T. (1995) Geology, 23, 1107-1110. [3] Baas, A.C.W. (2007) Geomorphology, 91, 311-331. [4] Werner, B.T. (1999) Science, 284, 102-104. [5] Werner, B.T. and Kocurek, G. (1999) Geology, 27, 771-774. [6] Ewing, R.C. and Kocurek, G. (in prep) [7] Kocurek, G. (in review) JGR- Earth Surface. [8] Ewing, R.C., Kocurek, G., and Lake, L.W., (2006) Earth Surface Processes and Landforms, 31, 1176-1191. [9] Beveridge, C., Kocurek, G., Ewing R.C., Lancaster, N., Morthekai, P., Singhvi, A.K., and Mahan, S.A., (2006) Sedimentology, 53, 183-195. [10] Derickson, D., Kocurek, G., Ewing, R.C., Bristow, C., (in press) Geomorphology.

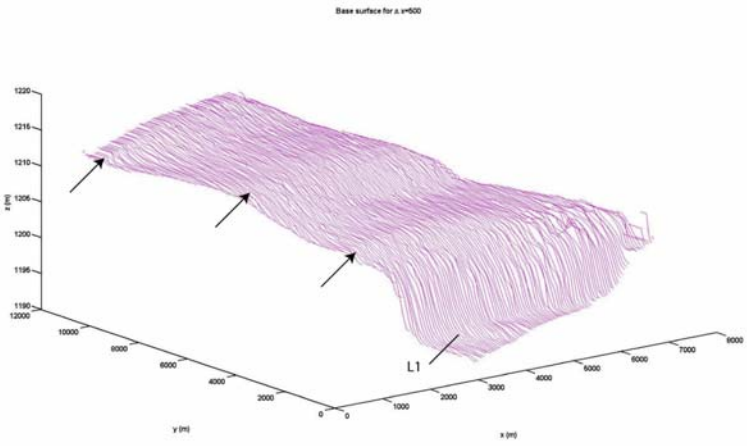

Figure 1. MATLAB curve fitting through interdune troughs to show the substrate upon which the dunes are developed. The lowermost hint of a terrace is the L1 shoreline of Langford (2003, *Quaternary International* 104: 31-39). Higher elevation breaks in slope (arrows) probably represent earlier shorelines and terrace development.

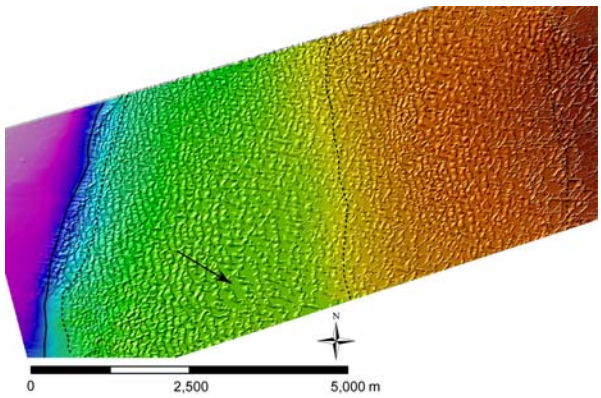

Figure 2. Area shown covers the airborne LiDAR survey of White Sands Dune Field. The image is a hillshade of the 1 m DEM overlain on the extracted underlying topographic surface. Cold colors are lower in elevation. Dunes are migrating to the northeast. Dashed lines indicate slope changes interpreted as paleo shorelines and correspond to arrows in Fig. 1. The solid line corresponds to the L1 shoreline indicated in Fig. 1. The arrow points to the deflated interdune areas between shorelines.

ESTIMATE AND EXPRESSION OF WATER ICE IN POLAR SAND DUNES. W.C. Feldman[1] and M.C. Bourke[1] [1]Planetary Science Institute, Tucson, Arizona, 85719, USA, mbourke@psi.edu, feldman@psi.edu

Introduction: The most extensive sand dune deposits on Mars encircle the north-polar residual water-ice deposit. The Olympia Undae, located between 130° and 245° E and 78° and 83° N is the largest sand sea on Mars covering an area of 185,00 Km^2 [1]. Although the dunes have been studied extensively using visible and infrared imaging data of the Viking orbiters [e.g., 2, 3-6], many fundamental issues regarding the origin, evolution, and internal structure of the dunes remain unknown. Omega and CRISM data confirm that there is a strong calcium sulfate signature (most likely gypsum) in the dune surface sediments in the eastern part of the dunefield that decreases westwards [7-9]. More recently, hydrated minerals have been detected throughout the north polar region including many of the deeper chasma and re-entrants in Planum Boreum [10]. Here we estimate the hydrogen content of the Olympia Undae and explore the dune-scale geomorphic features of north polar dunes to explain concentrations of hydrogen detected.

Hydrogen signature: We use two data sources in our analyses. First, neutron currents were measured using the Mars Odyssey Neutron Spectrometer. Second, seasonally varying temperatures were measured using the Thermal Emission Spectrometer. Details of this approach are outlined in Feldman *et al* [11]. Both the neutron and thermal infrared data are best represented by a two-layered model having a water-ice equivalent hydrogen content of 30±5% in a lower semi-infinite layer, buried beneath a relatively desiccated upper layer that is 9±6 g/cm^2 thick (about 6 cm depth at a density of 1.5 g/cm^3).

Dune geomorphology: We use High Resolution Imaging Science Experiment (HiRISE) images to detect dune-scale geomorphic signatures (Fig. 1b).We present four features that suggest induration of the dune sediments and potential sublimation of dune volatiles.

Indurated layers and arcuate ridges: Narrow, often curvilinear ridges protrude from the windward slope of dunes on Mars. These may be indurated layers that are exposed when windward-side erosion occurs. On Earth, induration is know to result from geochemical process [12] and from layers of frozen sand, ice and snow in dunes [13].

The remnants of partially eroded dunes that moved across the area are preserved as arcuate ridges. These may mark the base of the windward slope, slipface or may outline the entire position of the dune (Fig.1a). Similar features are found upwind of dunes on Earth. They can be formed as vegetation traps sediment [14], geochemical induration of sediment during periods of high groundwater or interdune flooding [12], or they result from ice induration of dune sediment [15].

Sinkholes: Circular depressions that resemble sinkholes are located periodically along dune crests (Fig. 1c). These circular depressions are found on polar desert dunes on Earth and are formed by the sinking/collapse of surface sediment due to a loss in volume of underlying volatiles [16]. Their position along the dune crest and not elsewhere may be linked to larger diurnal insolation receipts at that location on the dune. These features identify locations of potential denivation, but do not necessarily map out the potential full extent of subsurface volatiles.

Tensional fissures: Sinuous, narrow, rectilinear and branching depressions are observed on the lee face of the larger dunes (Fig. 1d). These features suggest cohesion of the surface sediments and the operation of tensional stresses. They are similar to tensional cracks reported on dune surfaces in polar deserts. On Earth, the cohesion is a function of moisture content (from snowmelt). The source of tensional stress is a loss of subsurface volatile volume [16]. On Mars, cohesion of the surface sediment may be provided by crusting [17, 18].

Are these signatures a product of geochemical induration? The neutron and thermal infrared data coupled with the dune geomorphology suggest that the dunes contain a relatively desiccated top layer, which overlays a hydrogen-enriched lower layer. A stratigraphic model that is consistent with all three data sets is that the dunes contain a surface dry layer which overlays a niveo-aeolian lower layer.

However, the origin of the hydrated signature is under discussion. Two of the geomorphic features presented here may be consistent with a geochemical cementation process (protruding indurated layers and arcuate ridges). However, the crestline pits suggest a loss of volume, triggered by melting, evaporation or sublimation of volatiles that are located close to the surface. If the indurated laminae, arcuate ridges and tensional fissures are due to the presence of hydrated minerals,require repeated episodes of (melt)water production and this presents a challenge under current polar climatic scenarios.

The multispectral data indicate the presence of hydrated minerals on the surface (*i.e.* ≤ 20 μm depth). Neutron data detect a hydrogen signature at greater depth (6cm) and the geomorphic features allow a potentially deeper view into the internal composition of the dunes. Based on our combined approach our preferred hypothesis is that the dunes contain niveo-aeolian deposits. These are deposits of wind-driven snow, sand, and dust [19]. They consist of inter-bedded sand and ice that are often indurated and resistant to erosion [20]. They are preserved by rapid burial of precipitated snow and frost layers by rapidly aggrading sand. On Mars water ice may be emplaced in the dune by the diffusion of water vapor or by direct precipitation of snow and ice crystals.

References: [1] Hayward, R. K. *et al.*, LPSC XXXIX, abs. # 1208, 2008. [2] Cutts, J. A. *et al.*, *Science* **194**, 1329-1337 (1976). [3] Tsoar, H. *et al.*, *Journal of Geophysical Research* **84**, 8167-8180 (1979). [4] Ward, A. W. *et al.*, *Icarus* **55**, 420-431 (1983). [5] Thomas, P. C., NASA Planetary geology and Geophysics technical memorandum, 1987. [6] Lancaster, N. *et al.*, *Journal of Geophysical Research (Planets)* **95**, 10921-10927 (1990). [7] Langevin, Y. *et al.*, *AGU Fall Meeting Abstracts* **21**, 06 (2007). [8] Langevin, Y. *et al.*, *Science* **307**, 1584-1586 (2005). [9] Horgan, B. H. N. *et al.*, *LPI Contributions* **1353**, 3241 (2007). [10] Horgan, B. H. N. *et al.*, LPSC XXXIX, abs. # 2122, 2008. [11] Feldman, W. C. *et al.*, *Icarus*, (in press). [12] McKee, E. D., *Sedimentology* **7**, 1-60 (1966). [13] Morris, E. C. *et al.*, *52* US Geological Survey Interagency report:Astrogeology, 1972. [14] Jimenez, J. A. *et al.*, *Sedimentology* **46**, 689-701 (August 01, 1999, 1999). [15] Lindsay, J. F., *Geological Society of America Bulletin* **84**, 1799-1806 (1973). [16] Koster, E. A. *et al.*, *Earth Surface Processes and Landforms* **13**, 153-170 (1988). [17] Sullivan, R. *et al.*, *AGU Fall Meeting Abstracts* **21**, 04 (December 1, 2004, 2004). [18] Richter, L. *et al.*, European Geosciences Union, Abs. 05489 2006. [19] Cailleux, A., *Niveo-eolian deposits*. R. W. Fairbridge, J. Bourgeois, Eds., Encyclopedia of Sedimentology (Academic Press, New York, 1978), vol. 6, pp. 501-503. [20] Bourke, M. C. *et al.*, LPSC XXXIX, abs. # 2166, 2008.

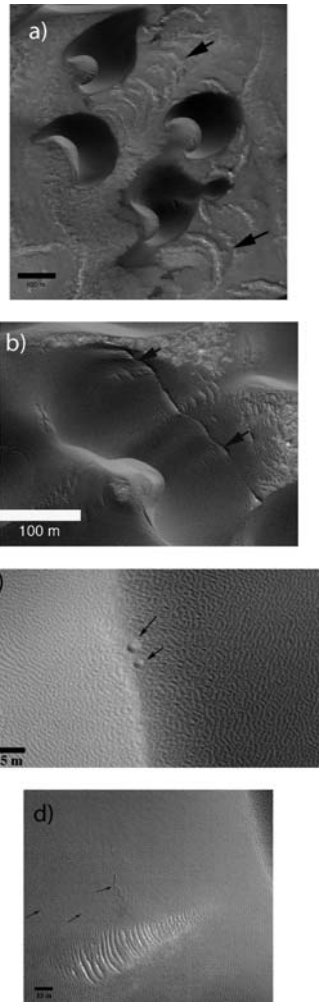

Figure 1 a) Arcuate ridges upwind of barchan dunes in Chasma Boreale mark the former dune position. (PSP_1374_2650. b) Indurated layer protruding from the windward slope (PSP_1374_2650). c) Section of dune crest from black arrows indicate locations where the dune crest has been altered by hypothesized sublimation pit formation. (PSP_001736_2605).d) Tensional crack development on a dune lee slope (PSP_001736_2605).

SOUTHERN HEMISPHERE DUNES OF MARS: MORPHOLOGY TRENDS AND CLIMATE CHANGE.
L. K. Fenton[1] and R. K. Hayward[2], [1]Carl Sagan Center, NASA Ames Research Center, MS 245-3, Moffett Field, CA 94035-1000, lfenton@carlsagancenter.org, [2]U.S.G.S. 2255 N. Gemini Dr., Flagstaff, AZ 86001.

Introduction: A major focus of Mars science over the past few decades is the impact of recent climatic shifts on geological, polar, and atmospheric processes. Sand dunes and other aeolian features are unique in their contribution to understanding climate change because they are geological features formed by atmospheric forces. In particular, cold climate sand dunes are surface features that become more active under windy, nonicy conditions, but less active under non-windy and/or icy conditions. Thus they are extremely sensitive to changes in temperature, humidity, and atmospheric dynamics that drive climate change.

Here we present the continuing work of mapping, classification, and morphological analysis of 1196 (to date) martian dune fields located poleward of 50º S. Part of the study represents a southward extension of the Mars Global Digital Dune Database (MGD^3) [1], and it complements a similar study in the high northern latitudes [2].

Mapping: Dune fields between 50º - 60º S were obtained from the MGD^3. Dune fields poleward of 60º S were identified using the nearly complete spatial coverage of daytime Thermal Emission Imaging System (THEMIS) IR images (as part of the original MGD^3 study). Further work using THEMIS VIS, Mars Orbiter Camera (MOC) Narrow Angle (NA), and Mars Reconnaissance Orbiter (MRO) Context Camera (CTX) images has aided in refining dune field boundaries and identifying smaller dune fields than the THEMIS IR images can resolve.

Dune Field Classification: Southern high- and midlatitude dune fields have been classified into six types that are interpreted to relate to their present level of aeolian activity and state of degradation. Characteristics of each are listed below, progressing from the least to the most degraded.

Sharp: Typical of dune fields in the equatorial MGD^3, minimal degradation at THEMIS VIS scale, dune crests appear sharp.

Sharp/Aproned Intermediate: Part of dune field consistent with "sharp" category, part consistent with "aproned". Apron around dune field perimeter is not complete.

Aproned: Presence of a distinctive sharp-edged apron surrounding dune field, between dunes. Dune crests may be either sharp or slightly rounded.

Aproned/Degraded Intermediate: Apron surrounding dune field is apparent, possible signs of dune degradation, possible exposure of layered material beneath dune field.

Degraded: Clear degradation of dunes, possible exposure of layered material beneath dune field.

Sand Patch: Sandy area without dunes. Possible layering (some cases may be polar layered deposits). Unclear if dunes were ever present.

Dune Field Distribution: Figure 1 shows the distribution of dune fields by type (see Figure 2 for a legend). Dune fields are common, especially between 60º - 80º S. Histograms of dune fields by type are shown in Figure 2 with a bin of 1º latitude. The histograms indicates that there is considerable overlap in dune field type, but that there is a general progression in type (interpreted here to indicate an increase in degradation) towards the pole. For example, sharp dune fields dominate equatorward of 65º S and aproned dune fields dominate between 60º - 70º S.

Influence of local topography: Local topography appears to account for some (but not all) of the latitudinal overlap in dune type. In forty of sixty pairs of adjacent dune fields, the less degraded dune field is located at a higher elevation.

CROCUS Date: Equatorward of ~65º S, dune fields retain seasonal frost longer than the surrounding terrain [3] by 10º-40º L_s. It is possible that some thermal property of dune sand (or perhaps ice in the subsurface) allows dune slopes to act as a cold trap for frost.

Discussion and Future Work: The progression in dune degradation towards the south pole is likely indicative of climate change postdating dune field formation. Dune fields will accumulate in an environment in which the wind can blow above the saltation threshold stress and sand is both plentiful and available for transport (*e.g.*, not indurated) [4]. The increasingly inactive and eroded appearance of dunes towards the pole indicates that at these latitudes, erosion (and perhaps induration by ground ice) currently dominates over saltation.

Future work will include investigating higher resolution images for morphological patterns and wind orientations; comparison of morphology and location to sand mineralogy, and ground ice modeling of dune sand as a function of recent orbital variations.

References: [1] Hayward R. K. et al (2007) *JGR, 112,* E11007. [2] Tanaka K. L. and Hayward R. K. (2008) *Planet. Dunes Wkshp.* (this mtg.). [3] Titus T. N. (2005) *LPSC XXXVI,* Abst. #1993. [4] Kocurek G. and Lancaster N. (1999) *Sediment., 46,* 505-515.

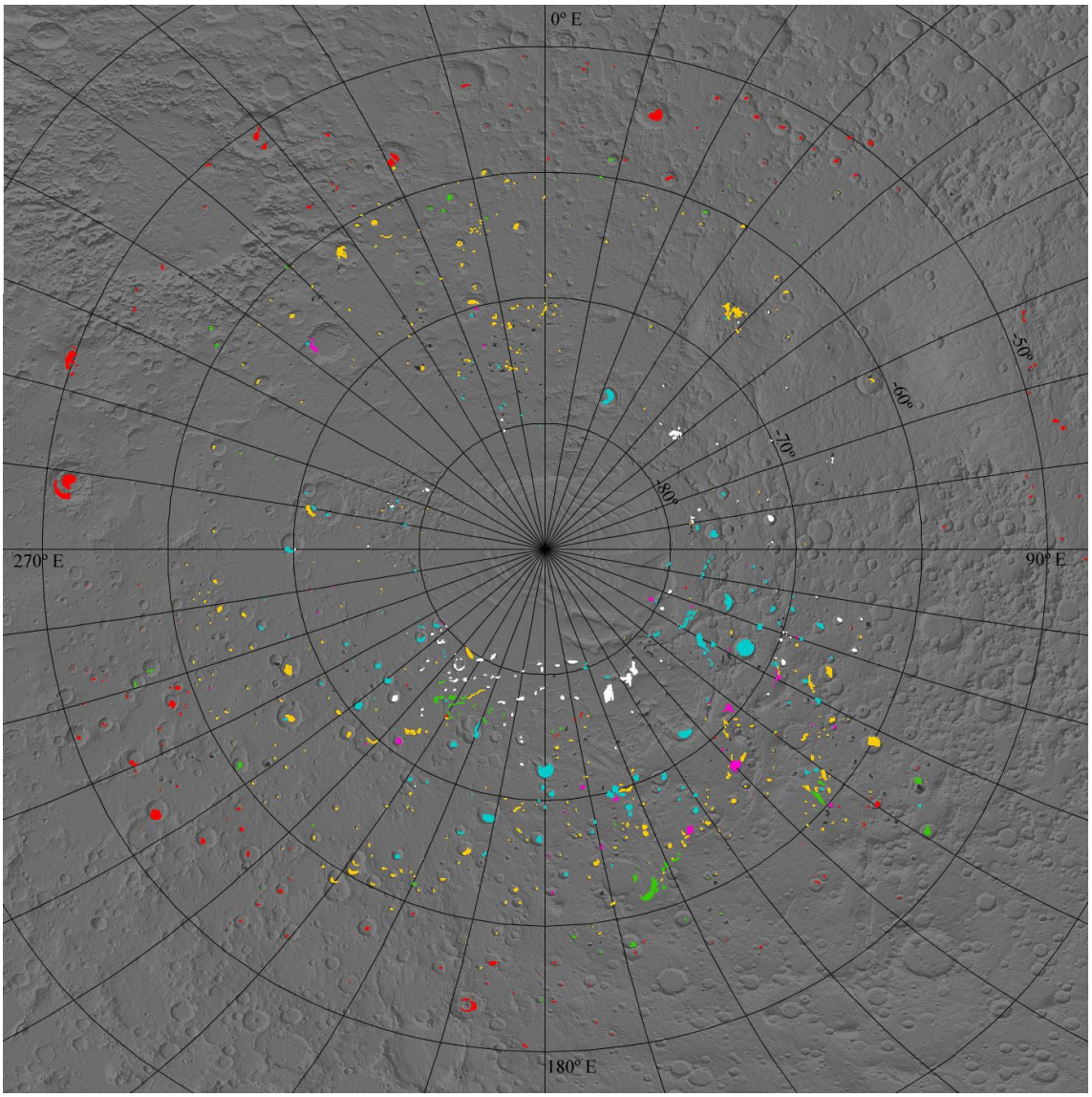

Figure 1. Distribution of dune fields by type poleward of 50° S (see legend in Fig. 2).

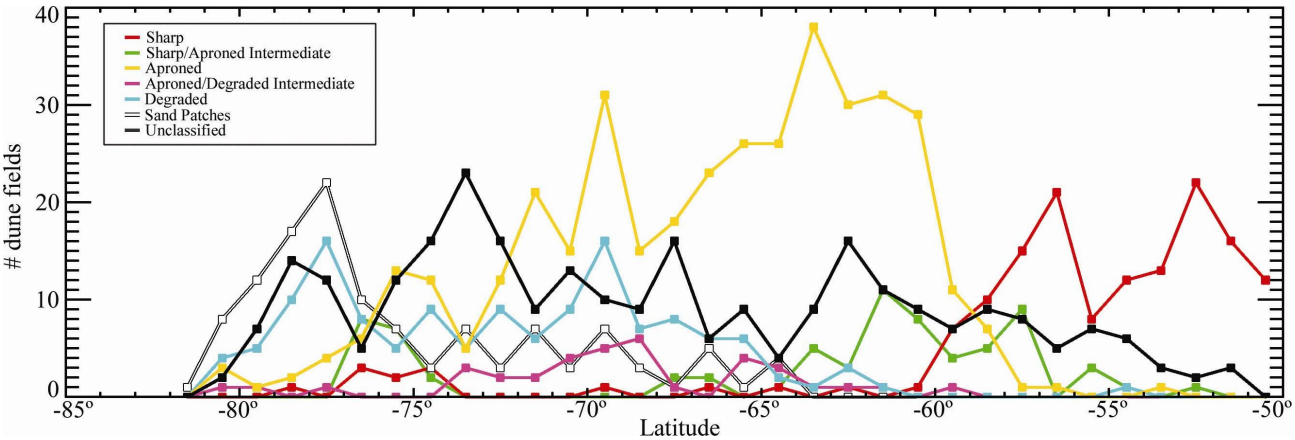

Figure 2. Histograms of dune fields per 1° latitude, shown by type. Note prevalence of sharp dune fields equatorward of 60° S and aproned dune fields between 60°-75° S.

DUNE FIELDS ON MARS: MARKERS OF CLIMATIC CHANGES? E. Gardin[1], C. Quantin[1] and P. Allemand[1], [1] Laboratoire des Sciences de la Terre, Université de Lyon, Ecole Normale Supérieure de Lyon, Université Claude Bernard Lyon 1, CNRS, France, Bat Géode, 43 bd du 11 Novembre, 69622 Villeurbanne cedex, France (emilie.gardin@univ-lyon1.fr).

Introduction: On Earth, the shapes of dunes are controlled by wind regime and sediment supply. The geometry of each dune of a dune field is generally similar and reflects the present wind conditions. On Mars, dune fields are not homogeneous as on Earth [1, 2, 3]. Several types of dunes can coexist in the same Martian area [4].

For some authors, dunes are current. In some example of [5], dunes fit well with present wind azimuths obtained by atmospheric Global Circulation Models (GCM). However, physical formation of Martian dunes develop by [3] show a turn-over time of a dune formation estimated at 100,000 years. If dunes are formed at this timescale, dune fields should have recorded last climatic variations. In such scenario, dune field should expose aeolian morphology overlaps.

The aim of this work is to describe five examples of dune fields which record several aeolian events.

Method: A global digital Martian dune database is available to the scientist community which contains informations on more than 550 dune fields stored in a Geographic Information System (GIS) [5]. From this database, we constructed individual GIS for each dune fields. For that, we have geo-processed all available high resolution images covering dune fields: MOC-NA images, THEMIS VIS images, and HIRISE images. That allows us to obtain image mosaics at optimal resolution for each dune fields until 25cm per pixel. The individual dune fields GIS are named by the ID Barlow's method [6]. The first number corresponds to longitude coordinates and the second to latitude coordinates of the field. In this abstract we present a selection of five dune fields.

Dune_field ID	0104-584	0126-545	0386-448	0326-500	0168-589
Lat (°S)	58.44	54.51	44.84	50.07	58.98
Lon (°E)	10.47	12.66	38.69	32.61	16.88
Dune types	B,Bd,T,L	B,Bd,T,L	B,Bd,T	B,Bd	B,Bd,T,L
Fields area (km^2)	30	1704	116	117	264
∅ of host crater (km)	68	134	no crater	103	70
chronology	yes	yes	no	no	yes

Table 1: Characteristics for each studied dune field. Their name employed the Barlow_ID method [6], Latitude and longitude are added. Dunes types found on dune fields are listed (B: Barchan dune, Bd: Barchanoïd form, T: transversal dunes, L: Longitudinal dune). Diameter of host crater provided and surface of fields are mentioned up to global GIS [5] measurements. Aeolian chronology or not is indicated.

Morphological Observations: The five dune fields are all located in the Southern hemisphere between 45° and 60° of latitude (Table 1). The surface of each field is from 30 and 1704 km^2 calculated by [5]. Four of them are localized in craters. Only one of them is located outside a crater.

0104-584: Three types of dunes can be observed in this field (Figure 1A). Barchans and transversal dunes, located in the eastern part of the field, reflect the existence of a unidirectional wind regime coming from the ESE. Longitudinal dunes, well-recognized by their symmetric geometries and frontal progress forms [1, 7], reflect the existence of a bidirectional wind regime from both SW and SSE directions. Some pre-existing barchans are clearly reshaped in longitudinal dunes.

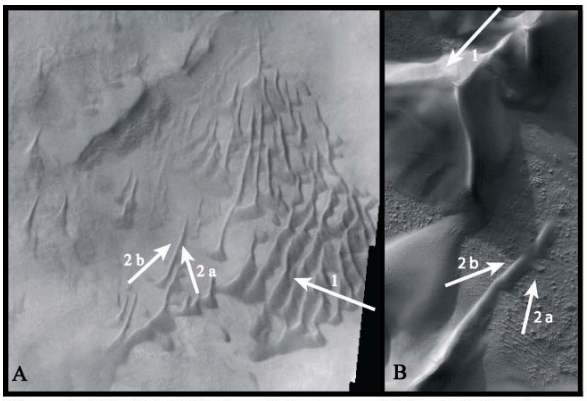

Figure 1: [A]: 0104-584 dune field shows a ESE wind direction in the eastern part of the field (arrow 1); and two contemporary aeolian directions:SW and SSE (respectively arrows: 2-a and 2-b) on a visible THEMIS image (V09849007). [B]: Russell Crater dune field (0126-545) shows a pre-existant barchan formed by a NE wind (arrow 1) and two comtemporary wind directions: SSE and WSW (respectively: arrows 2-a and 2-b) on a MOC image (E2100396).

0126-545: the dune field of Russell crater presents two types of dunes (Figure 1B): barchans formed by a NE wind direction and reshaped by both SSE and WSW wind to create longitudinal dunes. This observation of two aeolian regimes can be generalized to the whole dune field of the Russell crater. Material of pre-existent barchans seems to be recycled with the bidirectional aeolian regime. History of aeolian activities can be done on this field.

0386-448: presents barchanoïd forms and barchan dunes (Figure 2A). Their slipfaces show clearly two opposite azimuths implying two opposite wind directions: (i) a west origin on the western part and (ii) an east origin on the eastern part. Both directions are observed all over the field however there are no

evidence of coexistence of both aeolian orientations at dune scale. It is so challenging to determine a chronology.

0326-500: presents transversal and barchan dunes (Figure 2B1). Like the precedent dune field, barchans slipfaces show two opposite orientations. Some barchan structures like in Figure 2B2 have two coexisting slipfaces. Such geometries have no equivalent on Earth. Singular dunes recorded two wind directions. Our geomorphologic survey on this field didn't allow us to determine an event succession.

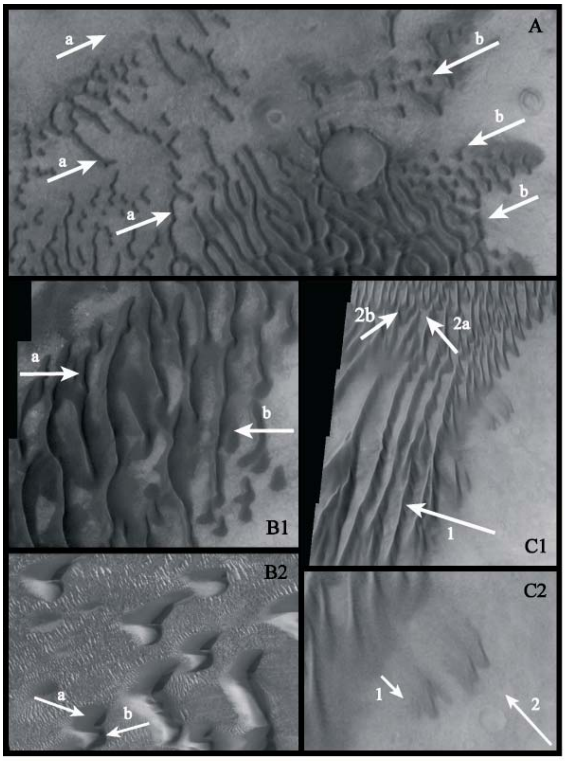

Figure 2:[A]: 0386-448 dune field presents two aeolian directions on the visible THEMIS image (V17598008). A first one from the WSW (arrow a) and a second one from the ENE (arrow b). No chronology is visible. [B1]: 0326-500 dune field has some evidence of two opposite aeolian directions: one from the west (arrows a) and one from the east (arrrows b) on the visible THEMIS image (V16475005). A zoom of the field is shown on the MOC image (E0300618) [B2]. It presents unusual barchan forms that seem to be created by two directions (a and b) of winds.[C1]: 0168-589 dune field shows that 3 wind directions occured on the field, on visible THEMIS image (V10011001) [C2]: Records of pluri-aeolian directions are shown on a zoom of visible THEMIS image (V10011001). A pre-existent barchan formed by a NW wind (arrow 1) and a second SE wind (arrow 2) re-uses the material to create dark streaks.

0168-589: presents a barchan dune created by a NW direction wind and dark streaks [8] formed by a SE wind, on Figure 2C2. Material of the pre-existent barchan is re-used to form dark streaks. Two consecutive winds have been acting on the dune. This field is the best example for dunes to be recorders of several aeolian events.

Discussion: The morphological observations presented in this paper reveal that dunes record different wind orientations. Theses variations are observed at different scales: (i) at dune-scale: pre-existent material is re-employed by two successive winds. (ii) At dune field-scale, two aeolian directions coexist but there are no chronological evidence at dune-scale. Only coexistence of aeolian directions at dune-scale allows us to propose a chronology.

The 0386-448 and 0326-500 dune fields present barchans created by two opposite wind azimuths. Taking into account the timescale dune formation, one wind direction might have succeeded to the other one. However, there are no evidence for dune overlaps. Thus a chronology can not be proposed.

0104-584, 0126-545 show evidence of a recycling of barchans by longitudinal dunes and allow us to foresee a chronology of wind directions. A first regime creates barchans with a NE wind and a second regime alternating both SSE and WSW winds forms longitudinal dunes. Thus longitudinal dunes are younger than barchans.

0168-589 show a barchan created by a NW wind direction which is reworked by dark streaks supporting a SE wind. Dark streaks refresh the barchan and thus are younger.

The third last dune fields show clearly evidence that dune fields recorded different consecutive wind regimes. However, it is challenging to correlate which climatic changes induced theses wind regime variations.

Conclusions: We conclude that some dune fields are formed by several aeolian regimes.

In some cases, when there is no overlapping between different kinds of dunes, it is impossible to establish a chronology. In other cases, aeolian chronology is possible and shows destabilization of the previous type of dunes, what indicates a variation of the wind azimuth over the last 100,000 years at least. Dunes are so pertinent markers of climatic change.

References: [1]: Lee, P. and Thomas, P. C., *JGR*, 100, E3, 5381-5395pp, (1995). [2]: Hersen, P., phd thesis:0 Morphogenèse et dynamique des barchanes, (2004). [3]: Claudin, P. and Andreotti, B., *EPSL*, 252, 30-44pp, (2006). [4]: Fenton, L. K., *JGR*, 110, E11004, doi:10.1029/2005JE002436, (2005). [5]: Hayward, R.K. et al, *JGR*, 112, doi: 10.1029/2007JE002943, (2007). [6]: Barlow, N. G. et al. *JGR*, 105, E11, 26,733-26,738, (2000). [7]: Tsoar, H., *Sedimentology*, 30,567-30,578, (1983). [8]: Thomas, P. C., Verveka, S., Lee, S. and Bloom, A., *Icarus*, 45, 124-153, (1981).

MODELING AEOLIAN SEDIMENT TRANSPORT THRESHOLDS ON MARS: A SHEAR STRESS PARTITIONING APPROACH. J.A. Gillies[1], W.G. Nickling[2], J. King[1], and N. Lancaster[3], [1]Division of Atmospheric Sciences, Desert Research Institute, 2215 Raggio Parkway, Reno NV USA 89512, jackg@dri.edu, [2]Department of Geography, University of Guelph, Guelph ON Canada N1G 2W1, [3]Division of Earth and Ecosystems Sciences, Desert Research Institute, 2215 Raggio Parkway, Reno NV USA 89512.

Aeolian sediment entrainment and transport processes play a crucial role in the evolution of the Martian landscape. The most dramatic demonstration of aeolian activity on Mars is the planet-wide dust storm [1] [2], but dust storms on the scale of $>10^2$ km^2 to $>10^6$ km^2 are frequent. Data presented by Martin [2] and more recently by Cantor [3] indicate dust storms are a common occurrence on Mars. Other features observed on Mars, as evidenced by the presence of bedforms such as sand dunes, sand sheets, ripples, and megaripples provide further evidence of aeolian activity. In addition to smaller scale aeolian bedforms, which are observed in plains areas [4] there is evidence of sand entrainment and transport in areas among roughness elements in the size range from pebbles to cobbles, to boulder size [5]. This surface type has been imaged by the Mars Exploration Rover Mission (http://marsrovers.jpl.nasa.gov/home/) and covers extensive regions of the planet's surface. These rough surfaces are areas where it can be expected that the presence of the roughness create conditions whereby entrainment of sediments by wind requires increased wind speeds compared to the aerodynamically smoother plains areas.

This paper explores the effect that larger roughness elements may have on entrainment of sediment by Martian winds using a shear stress partitioning approach based on a model developed by Raupach et al. [6]. The Raupach et al. [6] model predicts the shear stress partitioning ratio, i.e., the percent reduction in shear stress on the intervening surface between the roughness elements as compared to the surface in the absence of those elements [7], based on knowledge of the geometric properties of the roughness elements, the characteristic drag coefficients of the elements and the surface, and the assumed effect these elements have on the spatial distribution of the mean and maximum shear stresses.

Recent work by King et al. [8] and field testing by Gillies et al. [9] [10] have demonstrated that this model [6] can effectively predict roughness effects on entrainment threshold and be used to assess, in part, roughness effects on aeolian sediment flux rates for terrestrial atmospheric conditions. As the model can be used for different fluid properties it makes it applicable to evaluating how the atmospheric conditions and winds of Mars interact with the roughness to predict the effect that roughness will have on sediment entrainment there. On Mars, unlike on Earth, the shear stress partitioning caused by roughness is non-linear as drag coefficients for the surface as well as for the roughness itself show Reynolds number dependencies for the reported range of Martian wind speeds. Based on the results of Gillies et al. [10], which provide data on the effect large solid roughness elements of varying roughness density have on shear stress partitioning and particle threshold and aerodynamic parameters, the shear stress partitioning model of Raupach et al. [6] was used to evaluate how Martian atmospheric conditions will affect the threshold shear stress ratio on Martian surfaces with the same range of roughness evaluated by Gillies et al. [9] [10]. Using, as an example, a 125 µm diameter particle with an estimated threshold shear stress on Mars of ~0.06 N m^{-2} (shear velocity, $u_* = \sim 2$ m s^{-2} on a smooth surface), Figure 1 shows the effect roughness density has on the threshold shear stress ratio for this diameter particle. For comparison, Figure 1 also shows the same relationship for terrestrial conditions. Based on available estimates of roughness density for Mars drawn from the literature, estimates of threshold wind speeds for rough surfaces can be estimated for a range of particle sizes using this approach.

References::

[1] Gierasch, P.J. (1974) *Rev. of Geophys. & Space Sci*., 12, 730-734. [2] Martin, L.J. and Zurek, R.W. (1993), *J. Geophys. Res*. 98, E2, 3221-3246. [3] Cantor, B.A., et al. (2001), *J. Geophys. Res*., 106, E10, 23653-23688. [4] Sullivan, R. et al. (2005), *Nature*, 436, doi:10.1038, 58-61. [5] Jakosky, B.M. and Christensen, P.R. (1986), *Icarus*, 66, 125-133. [6] Raupach, M.R., et al. (1993), *J. Geophys. Res*. 98, D2, 3023-3029. [7] Wolfe, S.A. and Nickling, W.G. (1996), *Earth Surf. Proc. & Land*., 21, 607-619. [8] King, J., et al. (2005), *J. Geophys. Res*. *E-S*, 110, F4, F04015 doi:10.1029/2004JF000281. [9] Gillies, J.A., et al. (2006), *J. Geophys. Res*. *E-S*, 111, F02006, doi:10.1029/2005JF000434. [10] Gillies, J.A., et al. (2007), *B.-L. Met*., 122, 2, 367-396.

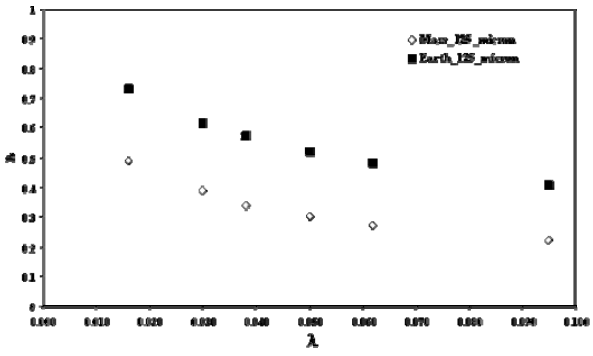

Figure 1. R_t for 125 µm particle on Mars and Earth as a function of λ, when roughness is that described by Gillies et al. [10].

VARIETIES OF BARCHAN FORM IN THE NAMIB DESERT AND ON MARS. Andrew S. Goudie[1] and Mary C Bourke[2]. [1]Saint Cross College, Oxford. andrew.goudie@stxox.ac.uk [2]Planetary Science Institute, Tucson, Arizona, 85719 mbourke@psi.edu

Introduction: Barchans are individual, mobile, crescentic shape dunes, the two horns of which face in the direction of movement. Generally they occur in areas of limited sand supply, with a low precipitation and vegetation cover, on planar surfaces and where winds are unimodal to narrowly bimodal. On Mars, the most common dune is transverse and within the barchan group there is a wide variety of forms [1] (Fig. 1).

Morphological classifications: There is little work that describes or explains the morphological variety of barchans. One useful hierarchical classification considers barchans as simple, compound or complex [2]. Another attributes barchan form to a stage in dune evolution [e.g., barchanic shield dune, 3]. Long and Sharp [4] use a ratio between the length of the windward slope (*a*) and the horn to horn width (*c*) to categorize barchans: Fat (≥1), Pudgy (0.75) Normal (0.5) and Slim (0.25). This classification may be useful for Martian dunes and give insight into the controls on dune form.

Barchan shape is a function of grain size, wind flow velocity, sand saturation, and wind variability [5]. For example, a smaller grain size or higher wind speed both produce a steeper and blunter stoss-side. A low saturation of the inter-dune sandflow produces an open crescent-moon shaped dune [5]. Dunes in areas characterized by coarse sediment (higher effective wind threshold) and/or low speeds may have lower, longer profiles compared with those in areas with fine sediments and/or strong winds [6]. Dune shape is not necessarily scale invariant. The windward profile has been found to be nearly a straight line for tall dunes, but becomes increasingly convex for smaller ones [7, 8]. Equally, the relative position of the slip face within the whole dune varies with dune size, but also the ratio of horn length to total length increases with the height [9-11].

A satellite image survey of the Namib Desert found that there was a wide range of barchan morphologies present that are more varied and complex than is often assumed. The purpose of this paper is to report on those findings and to present similar forms found on Mars.

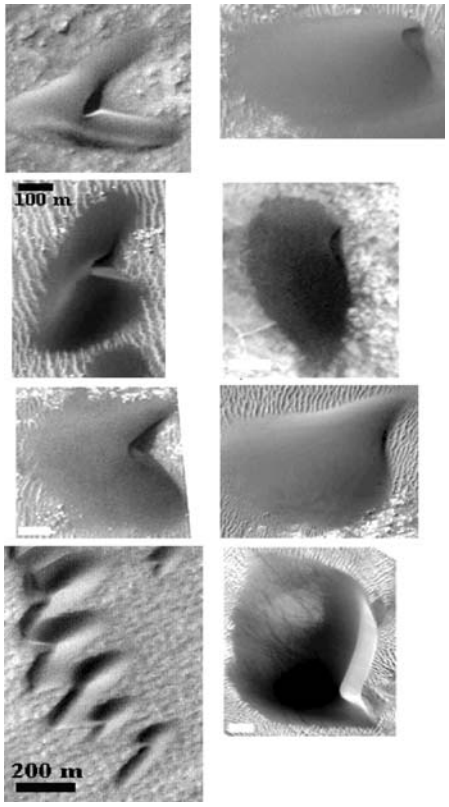

Figure 1: Variety of barchan forms on Mars. Dunes have variable width/length ratios, horns length and stoss slope curvature. These forms suggest differences in local conditions.

*Type 1: Classical symmetrical barchans-Normal & Slim:*The simplest form of barchan is the classic individual crescentic feature. Some of these are elegantly slim (Fig.2a) found on the rocky plains to the south and east of Luderitz and Elizabeth Bay. They also appear to be rather angular in plan. They display a wide range of sizes, with some having widths as great as 500-600 m, and some only a few tens of metres. These are a feature of areas with unidirectional winds, low sand influx and high values for shear velocity [12]. The examples in southern Namibia occur on rock surfaces that have a very limited sand cover, and because of their proximity to the coast have high wind velocities from a relatively constant direction with a total annual sand flow potential that exceeds 1200 tonnes/m/yr. As a

consequence rates of barchan migration are particularly high [13].

Slim barchans, are also found on Mars (Fig. 3a). Dunes that most closely resembled a classic crescentic shape were preferentially selected in a study of barchans [1]. As expected, all barchans surveyed are in the 'Slim' category. However, the north polar barchans were slimmer (a/c = 0.37) than the inter-crater dunes (a/c = 0.52). The example shown (Fig. 3a) is extraordinarily 'slim' (a/c = 0.17) and similar values have not been reported from surveys on Earth.

Type 2: Classic symmetrical barchans – Pudgy & Fat: Dunes in this class have horns that are relatively small in relation to the total mass of the dune (Fig. 2b). Fat dunes occur in areas where there is a substantial sand influx and lower shear velocity [12]. Many of the world's barchans described in the literature appear to be fat and pudgy rather than slim. On Mars dune fields of Pudgy and Fat barchans are found in the north polar region, particularly on the margins of large dune fields and in locations where the topography may concentrate windflow (Fig. 3c). This may indicate a higher (local) sediment supply and lower shear velocity. This is also suggested by changes observed in dome dunes [14].

Type 3: Classic symmetrical barchans – large, fat and unstable: Mega-barchans (>500 m wide) often have secondary features on their flanks, which may be indicative of instability. They often shed small barchans downwind (Fig. 2c). Megabarchans are also found on Mars. They are larger than those in Namibia and have simple, rather than complex or compound forms [15].

Type 4: Classic symmetrical barchans composed of smaller barchans. One remarkable barchan was identified in southern Namibia. It is a classic barchan form some 400 m across and 700 m long that is predominantly made up of a cluster of smaller barchans. It may be an extreme form of the Type 3 barchan and an example of proto-mega-barchans [16]. A similar form has not yet been detected on Mars although there are examples of degraded and modified barchans that may, in time, approach this morphology.

Other barchan dune assemblages were noted in Namibia but are not explored in this abstract. They include, *Type 5:* asymmetrical barchans that form linear dunes; *Type 6:* coalescing barchans that form transverse ridges; *Type 7:* barchan convoys that form linear ridges.

Application to Mars: Although useful, there remains a large variability of barchan forms on Mars that is not adequately differentiated by this approach. Other morphometric ratios may be more appropriate and are being explored.

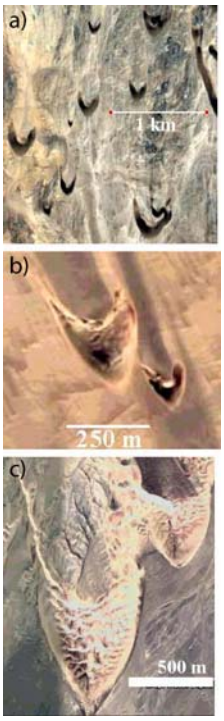

Figure 2 Barchan dunes in Namibia
a) Normal (0.5)
b) Pudgy (0.74)
c) Fat (0.99)

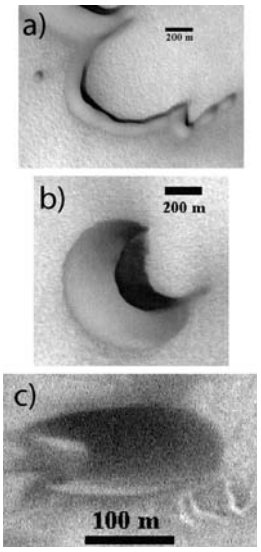

Figure 3 Examples of dune shapes on Mars according to the classification of Long and Sharp (1964).

a) Slim (0.17)
b) Pudgy (0.67)
c) Fat (2.43)

References: [1] Bourke, M. C. *et al.*, Lunar and Planetary Science Conference XXXV, Abs. #1453 2004. [2] Breed, C. S. *et al.*, in *A study of global sand seas,* E. D. McKee, Ed. (United States Geological Survey, Professional Paper, 1052, 1979), pp. 253-304. [3] Mainguet, M., in *Deserts and arid lands,* F. El-Baz, Ed. (Martinus Nijhoff, Boston, 1984), pp. 31-58. [4] Long, J. T. *et al.*, *Geological Society of America Bulletin* **75**, 149-156 (1964). [5] Howard, A. D. *et al.*, *Sedimentology* **25**, 307-338 (1978). [6] Mckenna Neuman, C. *et al.*, *Sedimentology* **47**, 211-226 (2000). [7] Hastenrath, S. L., *Zeitschrift fur Geomorphologie* **11**, 300-311 (1967). [8] Schwaemmle, V. *et al.*, *European Physical Journal, E* **16**, 57-65 (2005). [9] Herrmann, H. J., *Comptes Rendus Physique* **3**, 197-206 (2002). [10] Herrmann, H. J. *et al.*, *Physica A* **358**, 30-38 (2005). [11] Sauermann, G. *et al.*, *Geomorphology* **36**, 47-62 (2000). [12] Parteli, E. J. R. *et al.*, *Physical Review E - Statistical, Nonlinear, and Soft Matter Physics* **75**, (2007). [13] Lancaster, N., *The Namib Sand Sea: Dune Forms, Processes, and Sediments*. (A.A. Balkema, Rotterdam, 1989), pp. 200. [14] Bourke, M. C. *et al.*, *Geomorphology* **94**, 247-255 (2008). [15] Bourke, M. C. *et al.*, This volume. [16] Cooke, R.U. *et al.Desert geomorphology* (UCL Press, London, 1993)

MARS GLOBAL DIGITAL DUNE DATABASE (MGD[3]): User's Guide R. K. Hayward[1], K. F. Mullins[1], L. K. Fenton[2], T. N. Titus[1], K. L. Tanaka[1], M. C. Bourke[3], A. Colaprete[4], T. M. Hare[1], and P. R. Christensen[5], [1]U.S.G.S. 2255 N. Gemini Dr., Flagstaff, AZ 86001, rhayward@usgs.gov. [2]Carl Sagan Center/Ames Research Center, [3]Planetary Science Institute, Tucson, AZ, [4]NASA/Ames Research Center, [5]Arizona State University, Tempe, AZ.

Introduction: The Mars Global Digital Dune Database (MGD[3]) is a GIS-based database of moderate- to large-size dark dune fields on Mars. The database currently covers the area from 65°N to 65°S and will soon be expanded to include the entire planet. MGD[3] can be accessed at a variety of internet locations in a variety of formats, including a non-GIS table. The database makes it possible to look at dunes in a global context, comparing their geographic locations and attributes to other global coverages, such as the NASA/Ames General Circulation Model (GCM) [1] that is included with this database. The Viking-based Atlas of Mars 1:15,000,000 Geologic Series maps (USGS I-1802A-C) [2] and the Mars Orbiter Laser Altimeter (MOLA) elevation data set [3], two existing coverages that are not part of the database, are also included with MGD[3] for the user's convenience.

Comparisons between dune field distribution and global coverages provide significant perspective on global and regional-scale aeolian processes that have shaped and continue to influence the surface of Mars. MGD[3] can also be used to locate areas of potential interest for local studies by querying the attributes provided for each dune field. These attributes include, but are not limited to: longitude, latitude, dune type, dune field area, estimated mean height of dune field, estimated dune field volume, average elevation, and slip-face orientation (if measured). Also listed are the ID numbers of Thermal Emission Imaging System (THEMIS) infrared (IR), THEMIS Visible (VIS) [4], and Mars Orbiter Camera narrow angle (MOC NA) [5] images used to create the MGD[3] database. In addition, the following information is provided for dune fields that are located within craters: crater centroid to dune centroid azimuth, crater diameter, and crater area.

Discussion: *Where to find MGD[3] and how to access the database once you have found it.* MGD[3] was released as United States Geological Survey (USGS) Open-File Report (OFR) 2007-1158. It can be downloaded from the following website (http://pubs.usgs.gov/of/2007/1158/) as a complete package, ready to use, with many layers and backgrounds. For users that do not require the entire package, its shapefiles, tables, images, and documentation are also available as separate, smaller downloads. Parts of MGD[3] can also be accessed at other internet locations. The following is a guide to finding and accessing the level of MGD[3] that suits individual user needs.

Accessing MGD[3] if you do not want to use GIS. While MGD[3] is GIS-based, we recorded data within its attribute tables that would make MGD[3] valuable to non-GIS users as well. The Dune Field layer table (547 rows, 37 columns) summarizes most of the information in the database, with the notable exception of the GCM output. The table is available in both a tab delimited text version and an Excel spreadsheet format. The table can be downloaded from the USGS OFR 2007-1158 website (http://pubs.usgs.gov/of/2007/1158/). Under "Database Organization group," the table is in the "Tables.zip" file. For those with access to the online *Journal of Geophysical Research Planets*, the table can be downloaded as "Table S2" in the auxiliary material associated with Hayward et al. [6].

Accessing MGD[3] if you do not have GIS software, but would like to use MGD[3] in a GIS environment. **Option 1.** The easiest way to view MGD[3] in a GIS environment is through the USGS Planetary GIS Web server – PIGWAD (http://webgis.wr.usgs.gov). The most important part of MGD[3], the Dune Field layer, and its attribute table, can be viewed at this location with no need for downloads or special software. The user can access the Dune Field layer from the PIGWAD home page by selecting "Mars" under "PIGWAD Maps," then selecting "Crater/Dunes Database Viewer" under "Intermediate," or use the following direct link to the MarsCrater/Dune Image Viewer page, http://webgis.wr.usgs.gov/website/mars%5Fcrater%5Fhtml/viewer.htm. On the Mars Crater/Dune Image Viewer page, choose the "Dune_Field (Dune Consortium)" layer and click the Refresh Map button. Using the identify tool, click on an individual dune field to display its attributes, which will appear at the bottom of the screen.

Option 2. If you want to view all the layers, backgrounds, and images included in MGD[3], you can do so by downloading the entire database at the OFR website http://pubs.usgs.gov/of/2007/1158/ (of2007-1158.zip). Be aware that the entire database, zipped, is a 1.8 Gigabyte download. For users that would like the entire database but encounter difficulty with the large download, MGD[3] is available on DVD upon request (contact rhayward@usgs.gov). Users will also need to download the free ArcReader software at http://www.esri.com/software/arcgis/arcreader/download.html. Unzip the database and find the ArcReader folder. The folder contains a series of ArcReader projects that cover the equatorial region. If you double

click on an ArcReader project file, ArcReader will open it and you will be able to view all layers in MGD[3], and their attributes.

Option 3. If you want to go beyond viewing the layers and attributes included in MGD[3], and manipulate them and compare them to other data sets, you can download the shapefiles (Shapefiles.zip only is needed, NOT the entire download) from the OFR website and upload them to a free GIS software package. Arizona State University's JMARS, http://jmars.asu.edu, is an excellent choice for this. Be sure to upload the geocentric version of the shapefiles to JMARS, as the sinusoidal version will not project correctly in JMARS. Also note that when loading the shapefiles, choose "ESRI™ Shape File" in the "Files of Type" dropdown box, then choose "Dune_Field.shp" as the "File Name." For more help with loading shapefiles in JMARS go to http://jmars.asu.edu/wiki/index.php/Shape_Layer. When using the Dune_Field layer attribute table, bypass the "Shape_Area" column and use the "Area_sinu_" column for accurate dune field areas.

Accessing MGD[3] if you have GIS software. **Option 1.** MGD[3] was created using ESRI ArcMap9® software. For users with ArcMap9® software, the ArcMap projects included in the database are the most powerful option, allowing access to all layers included in the database, with the opportunity to manipulate existing layers and add more data. Download the entire database (of2007-1158.zip) from the OFR website, http://pubs.usgs.gov/of/2007/1158/. As noted in the section above, be aware that the entire database is quite large and may be difficult to download. When opened, the projects in the ArcMap folder will provide all the layers, backgrounds, and map projected THEMIS IR, THEMIS VIS, and MOC NA images used to create the database.

Option 2. If you do not want to use all the backgrounds and projected images included in MGD[3], or if you use a GIS software that will not open ArcMap9 project files, you can download just the shapefiles (Shapefiles.zip, 58 MB) and add them to your own project. The shapefiles are provided in both ESRI™ shapefile format and Geography Markup Language (GML) format for maximum compatibility.

Future versions of MGD[3]. The north pole region of MGD[3] will soon be released as a USGS OFR, followed by an OFR of the south pole region. We plan to combine the three regions and release a streamlined version of the MGD[3] as a USGS Data Series.

Summary: MGD[3], a GIS-based database of moderate- to large-size dark dune fields on Mars, can be a useful tool in Mars aeolian research. Although MGD[3] is GIS-based, non-GIS users can access the database through spreadsheet tables, while those without GIS software can view MGD[3] with easy to use, free online GIS software. The planet-wide scope of the database, combined with the detailed attributes of the dune fields, allows MGD[3] to be used to address global, regional, and local research questions. MGD[3] has been released as USGS OFR 2007-1158 and can be found at http://pubs.usgs.gov/of/2007/1158/. A more complete description of MGD[3] can be found in the "Dunes_ReadMe" file and the "ReadMe_GIS" file in the Documentation folder at the OFR website. The Mars Dunes Consortium website, http://www.mars-dunes.org/, is a central location that provides links to the websites in this abstract.

Links to MGD[3] and related sites.
USGS OFR 2007-1158
http://pubs.usgs.gov/of/2007/1158/
JMARS
http://jmars.asu.edu
PIGWAD
http://webgis.wr.usgs.gov
Mars Dunes Consortium
http://www.mars-dunes.org/
ArcReader
http://www.esri.com/software/arcgis/arcreader/download.html

Suggested Citation for MGD[3]. If you use MGD[3] in your research, please use the following citation: Hayward, R.K., Mullins, K.F., Fenton, L.K., Hare, T.M., Titus, T.N., Bourke, M.C., Colaprete, A., and Christensen, P.R., 2007 Mars Global Digital Dune Database: MC2 - MC29: U.S. Geological Survey Open File Report 2007-1158. [http://pubs.usgs.gov/of/2007/1158/] or, Hayward, R.K., K.F. Mullins, L.K. Fenton, T.M. Hare, T.N. Titus, M.C. Bourke, A. Colaprete, and P.R. Christensen (2007), Mars Global Digital Dune Database and initial science results, J. Geophys. Res., 112, E11007, doi:10.1029/2007JE002943.

References: [1] Haberle, R.M., et al. (1999), General circulation model simulations of the Mars Pathfinder atmospheric structure investigation/meteorology data, *JGR., 104* (E4), 8957-8974. [2] Skinner Jr., J. A. et al. (2006) *LPSC XXXVII*, Abstract #2331. [3] Smith, D., et al. (1999), NASA PDS, MGS-M-MOLA-3-PEDR-L1A-V1.0. [4] Christensen, P.R., et al., THEMIS Public Data Releases, PDS node, ASU, http://themis-data.asu.edu. [5] Malin, M.C., et al., Malin Space Science Systems Mars Orbiter Camera Image Gallery http://www.msss.com. [6] Hayward, R.K., et al. (2007), JGR., 112, E11007, doi:10.1029/2007JE002943.

Hydrated Minerals in the North Polar Chasmata and Circum-polar Erg B. H. N. Horgan[1], J. F. Bell III[1], P. C. Thomas[1], E. Z. Noe Dobrea[2]. [1]Cornell University Dept. of Astronomy (briony@astro.cornell.edu); [2]JPL/Caltech.

Background: The north polar region of Mars is situated at the lowest elevation of a basin that encompasses much of the northern hemisphere, making it an ideal place for the potential deposition of outflow channel fluids and sediments [1]. Results from the Mars Express OMEGA near-IR imaging spectrometer investigation have indicated the presence of extended deposits of hydrated calcium sulfates in the Olympia Planitia (OP) region, which have been identified as gypsum ($CaSO_4$•$2H_2O$) [2]. Gypsum formation generally requires a source of sulfur and H_2O interacting with Ca-bearing minerals [3].

We are examining hydration in the entire north polar region to establish a regional context for the OP sulfates and to test the proposed OMEGA global mineralogic history [6]. If the sulfates are limited to OP, then they are most likely intimately related to the dunes and may be much younger than sulfate deposits elsewhere; alternately, hydrated minerals elsewhere in the region may suggest otherwise.

Methods: The OMEGA image cubes that we have used in this study have average resolutions between 1 and 4 km/pixel, lie between 75°N and 85°N, and are limited to L_S 90° to 115° (the summer season). To compensate for atmospheric absorption, we have employed an empirically-derived correction based on the ratio of OMEGA spectra of high and low elevation regions on Olympus Mons [8].

To map hydrated minerals, we first calculated the 1.94 μm band depth using the OMEGA parameters [8]; however, this algorithm is also sensitive to water ice, which has a large band around 2 μm. To determine if a spectrum contains hydrated minerals as opposed to water ice, we require the band minimum wavelength to be at 1.941 or 1.955 μm (see [9] for more details).

Because the hydration band is located inside the 2 μm ice band in ice-rich terrains, using the OMEGA parameters gives an artificially inflated band depth, offset by as much as 10% band depth. To evaluate the approximate 1.94 μm band depth inside ice bands, we instead have approximated the continuum value at 1.94 μm with the equivalent value on the opposite side of the ice band, at 2.12 μm. Because the ice band is symmetric around 2.03 μm, this has provided us with much improved band depth estimates.

The maps and spectral averages presented here have a minimum 1.94 μm band depth of 4%, compared to

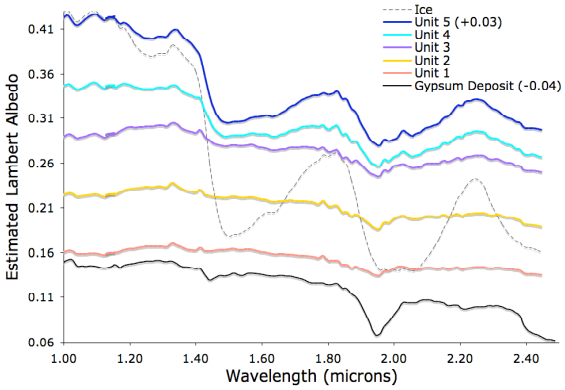

Figure 2: *Regionally averaged spectra of hydrated and ice-rich terrains in the north polar region. OP gypsum-rich deposit shown for comparison.*

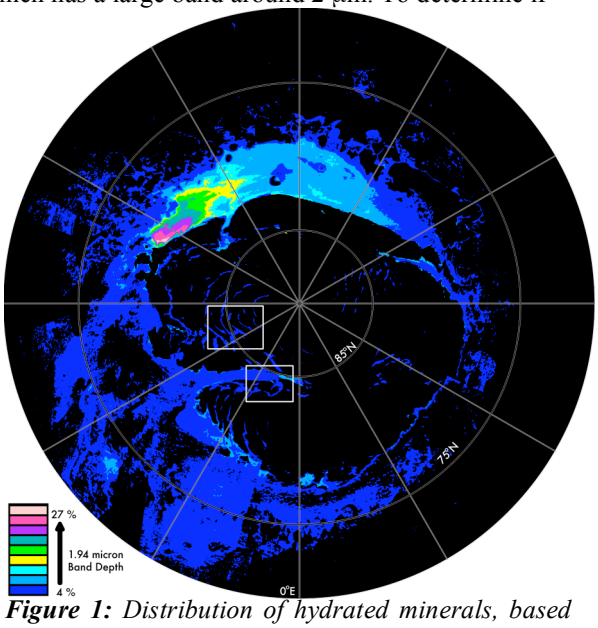

Figure 1: *Distribution of hydrated minerals, based on 1.94 μm band depth. Band depths range from 4 to more than 27% below the continuum.*

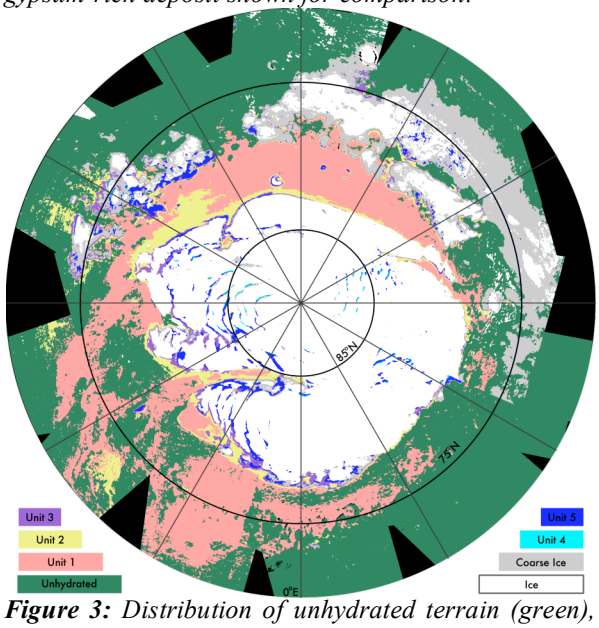

Figure 3: *Distribution of unhydrated terrain (green), fine and/or solid water ice (white), coarse grained water ice (grey), and hydrated units identified above.*

the OMEGA noise level of ~2% [8]. All maps have been orthographically projected at 1 km/pixel resolution.

Results: Figure 1 shows our 1.94 μm band depth map, created using the combination of band depth algorithms described above. Hydration is detected in Olympia Planitia, as expected [2,4], but also in much of the remaining circumpolar erg, on the floor of reentrants, and in scarps exposed by troughs troughout Planum Boreum. In the plains around Planum Boreum, the hydration signature correlates geographically with the Olympia Undae geologic unit [10]. The band depth values appear to be bimodaly distributed, with the majority of Olympia Planitia exhibiting band depths between 7 and 25%, and the rest of the deposits exhibiting band depths between 4 and 7%.

The spectral character of the hydrated units is remarkably consistent. Figure 2a shows regional averages for 4 hydrated spectral types, representing a continuum parametertized by increasing ice content and/or decreasing ice grain sizes. The distribution of the spectral types is shown in Figure 3. In Planum Boreum, hydration is found along with coarse ice in the chasmata, while the resdual ice cap appears to be devoid of hydration.

To search for correlations of hydration with geologic features or units, we have directly compared our hydration maps with THEMIS images and MOLA topography, as shown in Figure 4. Our initial investigations have suggested that in Planum Boreum, hydration is associated with troughs that expose dark PLD on slopes and scarps large enough to be resolved by OMEGA. Although OMEGA does not have the resolution to link hydration with specific layers, such correlations may be revealed in future investigations with CRISM.

Implications: Our finding that sulfates are present in nearly all dune fields in the north polar region as well as in the polar layered deposits suggests that the sulfates were formed prior to the emplacement of most of Planum Boreum; however, the vast range of hydration band depths in the region implies that hydrated minerals are not homogeneously distributed throughout a single set of sediments. The order of magnitude higher hydration band depths observed by CRISM in eastern OP [11] may be due to aeolian mining of a locally enriched gypsum deposit [12]. This deposit may be separate in composition and origin to the hydrated minerals in the other dune fields and in Planum Boreum, or may have been the source for these hydrated minerals in an earlier epoch.

References: [1] Zuber *et al*. (1998) *Science*, *282*, 2053. [2] Langevin *et al.* (2005) *Science*, *307*, 1584. [3] Deer *et al*. (1992) *The Rock-Forming Minerals*, Pearson, 612. [4] Fishbaugh *et al.* (2007) *JGR*, doi: 10.1029/2006JE002862. [5] Feldman *et al*. (2007) *Icarus*, doi: 10.1016/j.icarus. 2007.08.044. [6] Bibring *et al*. (2006) *Science*, *312*, 400. [7] Cloutis *et al.* (2006) *Icarus*, *184*, 121. [8] Poulet *et al*. (2007) *JGR*, doi: 10.1029/2006JE002840. [9] Horgan *et al*. (2008) *39th LPSC*, #2122. [10] Tanaka *et al*. (2007) *7th Mars*, #3276. [11] Roach *et al*. (2007) *38th LPSC*, #1970. [12] Tanaka (2006) *4th Mars Polar Sci. Conf.*, #8024.

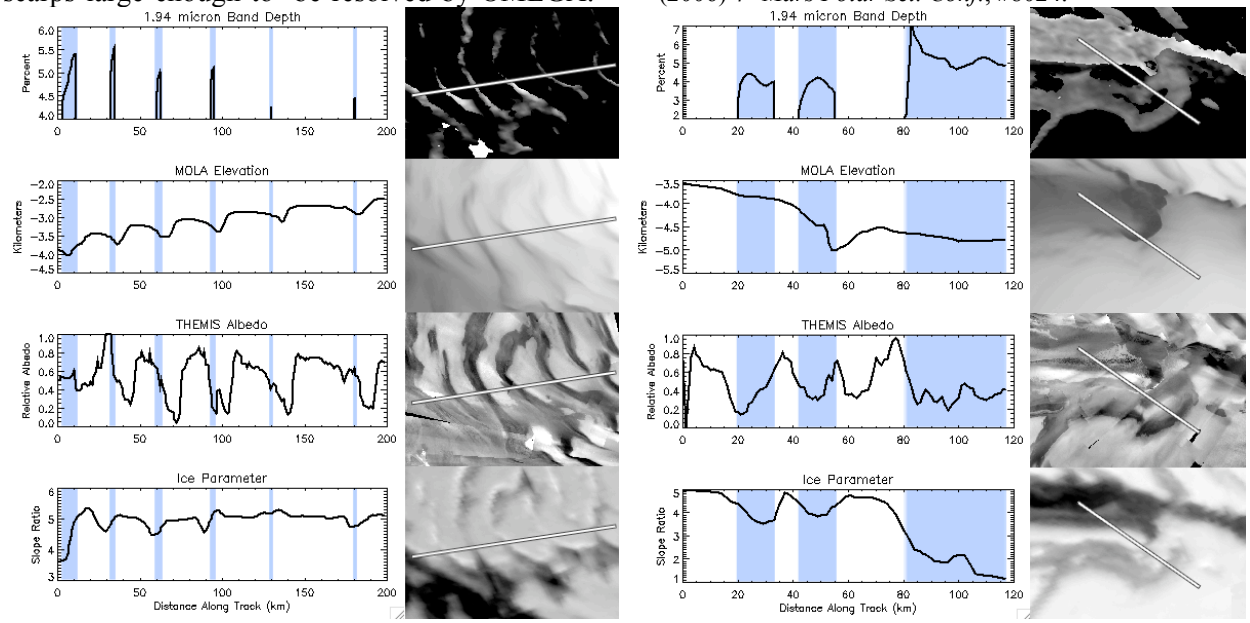

Figure 4: *From top: Hydration band depth compared to elevation, albedo, and relative ice content, as defined by a ice spectral parameter (see [9]). Blue bars indicate hydration. Left: Profiles taken on Planum Boreum show preferential hydration on poleward slopes. Right: Profiles taken at Chasma Boreale head scarp show preferential hydration on equatorward slopes. Context shown in Fig. 1 – upper box is left image, lower box is right image.*

AEOLIAN SAND TRANSPORT SYSTEMS – A TERRESTRIAL PERSPECTIVE. N. Lancaster[1] (Desert Research Institute, 2215 Raggio Parkway, Reno, NV 89512, USA; nick@dri.edu.

Sand dunes of different types are a key component of all aeolian sand transport systems. Their dynamics and morphology, as well as their response to the effects of external forces, such as changes in climate, cannot be considered in isolation from the dynamics of the sand transport system of which they are a part.

Aeolian sediment transport systems, in which sand is moved by wind from source areas via transport pathways to depositional sinks (e.g. dune fields, sand seas), have been identified at regional- and local-scales in many deserts using a combination of wind and remote sensing data [1]. Principles of sediment budgets show that accumulation of sand is the product of spatial changes in transport rates and/or temporal changes in sediment concentration [2]. Following principles of conservation of sediment mass, sand seas and dune fields accumulate downwind of source zones wherever sand transport rates decrease as a result of regional and/or local changes in wind speed and directional variability, so that the influx of sand exceeds outflux. Reductions in sand transport rates may be a result of topographic or regional climatic factors, so that many sand seas and dune fields occur in areas of low total or net sand transport and/or in topographic lows.

The dynamics of eolian sediment transport systems on any time scale are determined by the relations between the supply, availability, and mobility of sediment of a size suitable for transport by wind [3]. Sediment supply is the emplacement of sediment that serves as a source of material for the eolian sediment transport system. Sediment availability is the susceptibility of a sediment surface to entrainment of material by wind; and sediment mobility can be described by potential sand transport rates (or wind speed as a proxy). The relationships between the controls of sediment dynamics can be used to define the state of the system and how it varies through time. These key variables may be affected by changes in climate, including variations in the magnitude and frequency of winds capable of transporting sediment, so enabling the response of sand transport systems to climate and other external changes to be assessed and modeled. In many cases, periods of sediment input are relatively short compared to the much longer episodes of reworking and stability and even depletion of the sand body (Fig. 1) [4].

Terrestrial sand seas contain large volumes of sand (10's to 100's of cubic km) and have accumulated episodically during the Quaternary Era. Their construction has therefore been determined by climatic, tectonic, and sea level changes that have affected sand supply, availability, and mobility, as well as the preservation and inheritance of deposits and landforms from prior episodes of aeolian construction. Given that the reconstitution time (time to completely rework a sediment body) increases exponentially with sediment volume, the legacy of past climatic conditions therefore plays a major role in determining the present morphology and distribution of many areas of dunes [5]. One effect of climate change is the development of multiple generations of dunes, which in many sand seas are manifested by clear spatial patterning of dune types (often with sharp transitions between dune types), dune size and spacing, crest orientation, and sediment characteristics (Fig. 2). Different dune morphological units were most likely formed at different times in a specific wind regime [6].

Despite significant conceptual and methodological advances, many aspects of the dynamics of aeolian sand transport systems remain difficult to resolve. One example is the identification of the source(s) of sediment for many large-scale systems. In many cases, the input of sediment may no longer be active, so that it is not possible to physically trace the transport pathway from source to sink. Mineralogical information (determined from field or remote sensing studies) can offer insights [7, 8]. Remote sensing and climate data may however give a false impression of the regional nature of aeolian sediment transport. In Australia, for example, dune patterns suggest a continent-wide system of dunes, yet mineralogical data suggest that many dunes are sourced locally and inter-basin transport does not occur [9, 10]. High spectral resolution remote sensing data can provide valuable data to identify distant and local sediment sources [11].

Assessment and modeling of the sand budgets of sand seas and dunefields remains uncertain in many areas. The potential for using climate models and reanalysis data to understand regional winds and sand transport patterns is considerable and can follow methods established to understand dust generation areas in the Sahara [12] and martian dune fields [13].

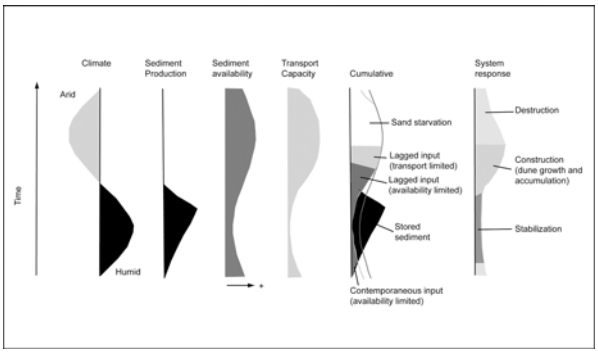

Fig. 1: Conceptual diagram of changes in sediment state over time [4**].**

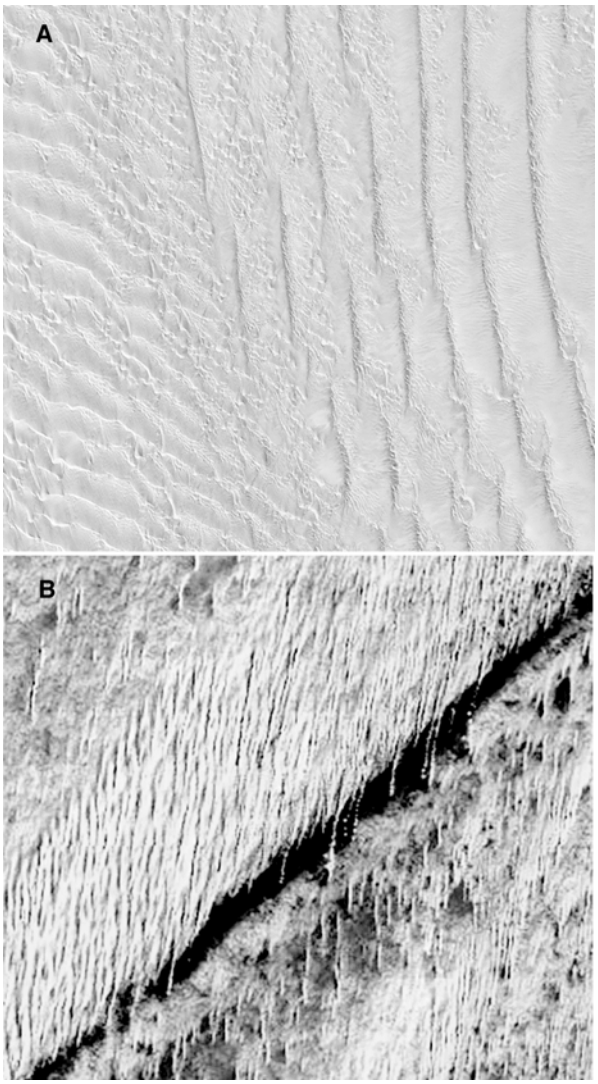

Fig 2: Examples of dune generations: (A) juxtaposition and superposition of compound crescentic and complex linear dunes, Namib Sand Sea; and (B) superimposition of modern N-S oriented linear dunes on NE-SW oriented late Pleistocene linear dunes, Azefal Sand Sea, Mauritania.

References

1. Fryberger, S.G. and T.S. Ahlbrandt (1979) Z. für Geomorphologie, 23, 440-460.
2. Kocurek, G. and K.G. Havholm, (1993) in Siliciclastic Sequence Stratigraphy, AAPG, 393-409.
3. Kocurek, G. and N. Lancaster, Sedimentology, 46, 505 - 515.
4. Kocurek, G. (1998), in Quaternary Deserts and Climatic Change, 327-338.
5. Lancaster, N. (1999) in A.S. Goudie, I. Livingstone, and S. Stokes, Eds, 49 – 70.
6. Ewing, R., C., G. Kocurek, and Lake.L.W., (2006) ESPL, 31, 1176-1191.
7. Ramsey, M.S., et al., (1999). GSA Bulletin, 111, 646-662.
8. Muhs, D.R., (2004), Geomorphology, 59, 247-269.
9. Wasson, R.J., et al. (1988) Australian Geographer, 19, 89-104.
10. Pell, S.D., I.S. Williams, and A.R. Chivas (1997), Sedimentary Geology, 109, 233-260.
11. Scheidt, S., M. Ramsey, and N. Lancaster (in press) Remote Sensing of Environment.
12. Washington, R., et al. (2006). GRL,33(L09401).
13. Fenton, L.K. (2005) JGR, 110 (E110004).

IN-SITU GEOCHRONOLOGY FOR MARTIAN DUNES: A REVIEW OF OPTICAL DATING CONCEPTS AND EXPERIMENTS WITH ANALOG MATERIALS. K. Lepper. Optical Dating and Dosimetry Laboratory, Department of Geosciences, North Dakota State University, 218 Stevens Hall, Fargo, ND, 58105; ken.lepper@ndsu.edu.

Introduction: Eolian dunes are a direct geomorphic expression of the dynamic interaction between the atmosphere and the lithosphere of planets. The timing, frequency and spatial extent of dune mobility reflect changing climatic conditions. However, one of the greatest challenges to deciphering the record of climate variability on Mars will be the need for absolute dating techniques, particularly those techniques applicable to the timeframes and materials involved in Mars surface processes [1]. Lepper and McKeever [2-4] have proposed developing optical dating (a.k.a. OSL), an established terrestrial Quaternary dating method based on principles of solid-state physics, for remote *in-situ* application to Martian sediments. Eolian transport provides the optimal conditions for successful optical dating and the technique has been used successfully to make absolute age determinations for numerous terrestrial eolian deposits (reviewed in [5, 6]).

The MER rovers and the orbital instruments OMEGA and CRISM have identified sulfate minerals as important constituents of Mars surface deposits. Orbital observations also suggest that sulfates may be concentrated by eolian processes and may occur as primary components of dunes (Fig. 1). The goals of this presentation are to introduce optical dating to the community of planetary scientists that are conducting research on dunes and to review nearly a decade of OSL experimental work with terrestrial analogs of Mars surface sediments focusing on our recent work with sulfate minerals.

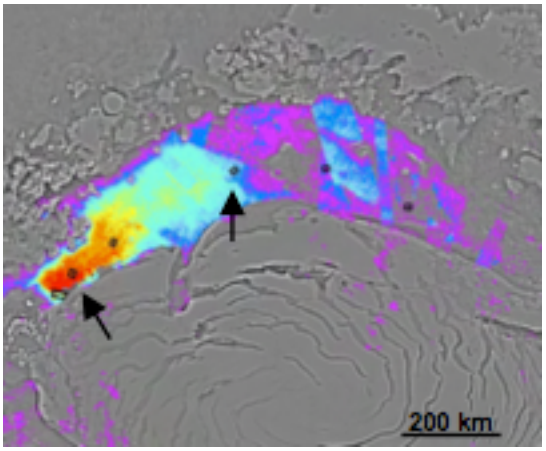

Fig. 1. Image of Mars' Northern Polar ice cap and adjacent erg. OMEGA 1.9 μm spectral mapping data overlain on the sand deposits. Red indicates highest concentrations of sulfates grading to purple (from [7]).

Methodological Background: Over geologic time, ionizing radiation from the decay of naturally occurring radioisotopes and from cosmic rays liberates charge carriers (electrons and holes) within mineral grains. The charge carriers can subsequently become localized at crystal defects leading to accumulation of a "trapped" electron population. Recombination of the charge carriers and relaxation results in photon emission, i.e. luminescence. The intensity of luminescence produced is proportional to the amount of trapped charge, and thereby to the radiation dose absorbed by the mineral grains since deposition at the sampled site. A determination of the ionizing radiation dose rate at the sample location allows the age of the deposit to be determined (from *Age = Absorbed Dose / Dose Rate*). Experimentally, optical excitation is used to initiate the measurement process which gives rise to the method's name - optically stimulated luminescence (OSL) dating or, simply, optical dating.

Methods and Samples: We have examined the fundamental optical dating properties of (i) radiation dose response, (ii) measurement induced sensitivity change (MISC) and (iii) signal fading for a variety analog materials including:

- the soil simulant JSC Mars-1 [3,8]
- evaporated mixtures of JSC Mars-1 and geologic salts [9]
- natural and synthetic gypsum as well as synthetic anhydrite [10-13]
- synthetic thenardite [14]
- synthetic kieserite and hexahydrite [10,13,15]

using blue light or infrared stimulation and monitoring the resultant luminescence in the UV or blue region (blue monitoring with infrared stimulation only). Other research groups have conducted similar studies on pyroxenes [16,17] mixtures of plagioclase feldspars [16], and mafic rocks [17,18].

Synopsis of Sulfate Experimental Results:

Calcium Sulfates [10-13]. The OSL measurements made on natural and synthetic gypsum as well as synthetic anhydrite indicated OSL dose response in all stimulation and monitoring combinations used. Signal stability (MISC and fading) varied considerably among the samples and stimulation methods. Anhydrite exhibited a high degree of signal instability with fading ranging from 23 to 40% per decade. An important exception, however, were the results from natural gypsum, including a sample from White Sands National Monument, which yielded stable signal characteristics

and large saturation doses (~3000 to ~4500 Gy) when utilizing the infrared stimulation and UV signal measurement configuration.

Singhvi and others [19,20] have directly dated sand dunes at White Sands, New Mexico with OSL methods, but found small amounts of quartz incorporated in the dunes to give more precise results than measurements made on the gypsum grains. Although developmental work may be needed, it appears that gypsum may have the potential to serve as an OSL geochronometer on Mars.

Sodium Sulfates [14]. Our measurements of unannealed dopant-free thenardite (Na_2SO_4) indicated UV phosphorescence following beta irradiation and both infrared and blue stimulated UV luminescence. However, all of these luminescence signals were highly unstable over short time scales (fading at a rate of up to 70% per decade) suggesting that natural unheated thenardite is an unlikely candidate for an in-situ OSL dating.

Magnesium Sulfates [10,13,15]. We have also carried out preliminary optical dating characterizations on kieserite ($MgSO_4 \bullet 1H_2O$) and hexahydrite ($MgSO_4 \bullet 6H_2O$). These magnesium sulfates did not exhibit phosphorescence or infrared stimulated luminescence, but they did show blue stimulated OSL response with saturation doses of ~3000 Gy and ~600 Gy for kieserite and hexahydrite, respectively. The signal stability characteristics of the magnesium sulfates exhibited similarities to both quartz (MISC) and feldspars (fading), which warrant more detailed examinations.

Summary: Based on our current data and interpretations of the optical dating properties of sulfates, their presence as trace or minor components in Martian eolian deposits will need to be considered when developing *in-situ* dating protocols, however, they should not preclude the application of optical dating to silicates in Martian dunes. Moreover, our characterizations suggest that gypsum may have the potential to be dated directly using OSL techniques. Certainly, more detailed examinations of the optical dating properties of calcium and magnesium sulfates are warranted. With proper development and deployment strategies optical dating holds the potential to help establish a geochronology for Martian eolian activity and, by extension, a geochronology for important aspects of climate change in the latest Amazonian epoch on Mars.

Acknowledgements: This abstract/presentation incorporates the work of numerous students; graduate students Vanessa O'Connor and Marissa Detschel, as well as undergraduate students Dan Thorstad, Todd Morken, and Andrew Podoll. The White Sands natural gypsum sample and permission to use were provided by David Bustos of W.S.N.M. This work is supported by the NASA Mars Fundamental Research Program, grant NNX06AB24G and by undergraduate research awards from the North Dakota NASA Space Grant Consortium.

References: [1] Clifford S.M. et al. (2000) *Icarus,* 144, 210-242. [2] Lepper K. and McKeever S.W.S. (1998) LPI Contribution No. 953. [3] Lepper K. and McKeever S.W.S. (2000) *Icarus*. 144, 295-301. [4] McKeever, S.W.S. et al. (2003) *Radiat. Meas.* 37, 527-534. [5] Aitken M.J. (1998) An Introduction to Optical Dating. Oxford Univ. Press. [6] Murray A.S. and Olley J.M. (2002) *Geochronometria*. 21, 1-16. [7] Roach, L.H. et al. (2007) LPSC 38, Abst.# 1970. [8] Lepper K. (2003) LPSC 34, Abst.# 1962. [9] Lepper K. et al. (2000) 2nd Mars Polar Science Conf. Abst.# 4027. [10] Lepper K. et al. (2006) *Martian Sulfates Workshop,* Abst.# 7054. [11] O'Connor V. and Lepper K. (2007) *GSA Abst. w/ Prog.* 39(6), 570. [12] Thorstad D. and Lepper K. (2007) *GSA Abst. w/ Prog.* 39(6), 321. [13] O'Connor V. and Lepper K. (2008) LPSC 39, Abst. #2089. [14] Morken T. and Lepper K. (2006) *GSA Abst. w/ Prog.* 38(7), 359. [15] Podoll A. and Lepper K. (2005) *GSA Abst. w/ Prog.* 37(7), 208. [16] Kalchgruber R. et al. (2006) *Radiat. Meas*. 41, 762-767. [17] Jain M. et al. (2006) *Radiat. Meas.* 41, 755-761. [18] Abbott N. et al (2001) LPSC 32, Abst.# 1974 [19] Singhvi, A. (2006) 4th NWLDDW, *Abst. Vol*. VI: 22. [20] Kocurek G. (2007) *Sed. Geol.* 197, 313-331.

THE SAND SEAS OF TITAN : DISCOVERY AND IMPLICATIONS FOR METHANE CLIMATOLOGY AND WIND PATTERNS R.D. Lorenz[1], J. Radebaugh[2] and the Cassini RADAR Team, [1] JHU Applied Physics Laboratory, Laurel, MD 20723 (Ralph.lorenz@jhuapl.edu) [2]Brigham Young University, Provo, UT 84602.

Introduction: Cassini's radar instrument discovered that Saturn's giant moon Titan has remarkably abundant sand dunes, apparently made of organic-rich material, bringing a new set of materials and physical parameters to the pantheon of dune-worlds. Here we review their discovery and the implications for Titan's exotic climate.

Discovery: Initially [e.g., 1] seen in February 2005 on T3 (north of Xanadu) as enigmatic dark streaks (nicknamed with the nongenetic term 'cat scratches') Titan's unexpected dunes were identified as such [2] on a more equatorial pass [T8, October 2005] that covered the dark region Belet. Titan's dunes were unexpected [3] because of the expectation of a damp, if not completely submerged, surface and the expectation that the feeble sunlight at Titan would be too weak to exceed the saltation threshold of 0.5-1 m/s.

The low latitude dark regions seen optically since maps of Titan were first made with Hubble and other data in the mid-1990s appear to correlate with areas with more abundant sand supply and perhaps higher dunes. The viewing geometry and/or the height of the dunes seen on T8 was such as to display their positive relief via slope-dependent radar reflectivity, and their slopes have recently been resolved in the near-infrared[5]. While dune sands are radar-dark compared to alluvial terrain and highlands[4], they are not as dark as the methane-ethane lakes seen at high latitudes[6]. A striking aspect [7] of Titan's dunes is that they are linear or longitudinal in form – often forming 'tadpole'-like flow patterns around topographic obstacles (e.g. Fig.1).

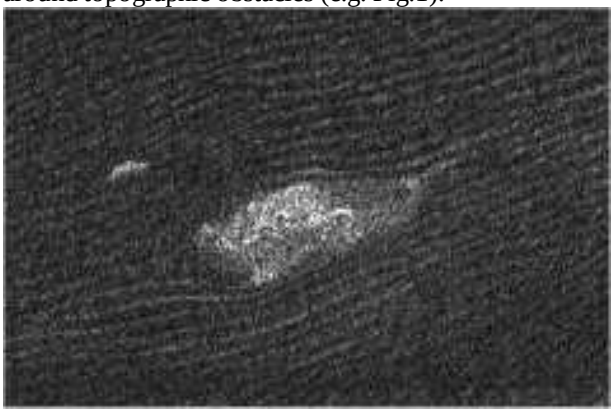

Figure 1. 75x50 km segment of Cassini Ku-band SAR acquired October 2005 during T8 flyby over Belet. The dunes part around and reconverge behind (east) of a bright mountain.

Implications for Humidity: Saltation requires dry conditions. The Huygens probe (at 10°S) observed a couple of dune streaks in the distance, within 30km of fluvial channels near its landing site which was itself an alluvial deposit which was physically damp. The proximity of dunes requiring dry conditions to form with moisture is in a sense paradoxical, but is not very unusual for Earth – it merely shows that Titan's climate is as variable and complex as that of our planet. Models suggest humidity should indeed be lower onslowly-rotating Titan near the equator (rather than in midlatitude belts as on Earth where the planetary rotation forces downwelling of dry air in the Hadley circulation) which is consistent with the observed dune distribution. It remains to be determined by further modeling and observation how often a given location may experience rainfall (under the present climate, or perhaps during epochs when the cryovolcanically-replenished methane humidity may have been different) and what the implications for present-day sand transport might be.

Implications for Sediment Supply: Even before Cassini [3] it was recognized that sand-producing processes might be weak on Titan. Glacial and freeze/thaw processes are not expected in the present climate, and the inventory of impact craters is not enough to produce much sand-sized material. It is estimated that the dune sands comprise some $>2x10^5$ km^3 of material [8]. Fluvial processes appear to be more pervasive than had been expected pre-Cassini (perhaps because rainstorms are, while rare, violent) although it is not yet clear whether the observed fluvial channel networks can account for this volume of material. Perhaps more likely, especially given the distinct near-infrared spectral characteristics of the dune-covered areas [5] is that the dunes are formed predominantly of organic material formed by photochemistry in the atmosphere. An open question, however, is how the micron-sized atmospheric organic haze particles are processed into sand-sized particles that can be saltated into dunes. It may be that some intermediate physical or chemical processing is required (perhaps associated with drying-up of lakes and their sediments).

Implications for Zonal Winds: Titan's winds are far from understood, and Titan presents the unique (in our solar system) situation of a dense atmosphere on a slowly-rotating body, with weak seasonally-variable solar forcing, a condensable fluid, and significant forcing by a gravitational tide. This tide produces a ~1mb pressure bulge and associated windfield (0.2-1 m/s) that

propagates around the body once per Titan day. Thus this curious setting (which may be common on extrasolar planets and their satellites) leads to winds that are both strong enough for saltation (since deep in Titan's atmosphere, the solar heating is diminished and the air is denser, so a given heat flux can drive only weak winds [3]) and that fluctuate in direction (which may be responsible for the longitudinal geometry seen for the vast majority of Titan's dunes). Simulations of Titan's winds with a Global Circulation Model (GCM) [9] have indeed indicated that bimodal wind patterns are likely, although perhaps more due to seasonal variations than the tide. A major challenge that is emerging is that models tend to produce (and indeed crude planetary-scale angular momentum balance requires) winds that are predominantly Easterlies (i.e. E-W) at low latitude, whereas the dune pattern [Fig. 2] clearly indicates W-E sand transport. However, there are major uncertainties in the input parameters for present models (not least the role of Titan's significant but poorly-known topography, which via mountain pressure torques as well as surface drag may substantially) and there are indications that substantial angular momentum may be exchanged between crust and atmosphere on seasonal timescales [10].

Conclusions: Titan's dunes bring a new world to the fore for the study of aeolian processes, in a physical and chemical setting very different from those of Earth and Mars, and its widespread sand seas (with a whiff of organic spice?) make it somewhat reminiscent of the Herbert's fictional Dune planet Arrakis [11] The observed style, distribution and orientation each provide important constraints on understanding Titan's winds and hydrological cycle.

References: [1] R D Lorenz and J Mitton, Titan Unveiled, Princeton University Press, 2008 [2] R. D. Lorenz et al., The Sand Seas of Titan : Cassini RADAR observations of Longitudinal Dunes, Science, 312, 724-727, 2006 [3] R. D. Lorenz, et al., Prediction of Aeolian Features on Planets : Application to Titan Paleoclimatology, Journal of Geophysical Research (Planets), 88, 26,377-26,386, 1995 [4] F. Paganelli, et al, Titan surface from Cassini RADAR SAR and high resolution radiometry data of the first five flybys, Icarus, 191, 211-222, 2007 [5] J. Barnes et al., Spectroscopy, Morphometry, and Photoclinometry of Titan's Dunefields from Cassini/VIMS, Icarus, in press [6] E.R. Stofan et al., The Lakes of Titan, Nature, 441, 61-64, 2007 [7] J. Radebaugh, Dunes on Titan Observed by Cassini Radar, Icarus, in press. [8] R. D. Lorenz et al., Titan's Inventory of Organic Surface Materials, Geophysical Research Letters, 35, L02206, 2008 [9] T. Tokano, Dune-forming winds on Titan and the influence of topography, Icarus, 194, 243-262, 2008. [10] R. D. Lorenz et al., Titan's Rotation Reveals and Internal Ocean and Changing Zonal Winds, Science (in press, 2008) [11] R. D. Lorenz, The Dunes of Dune, in K. Grazier (ed) The Science of Dune, Benbella Books, 2008

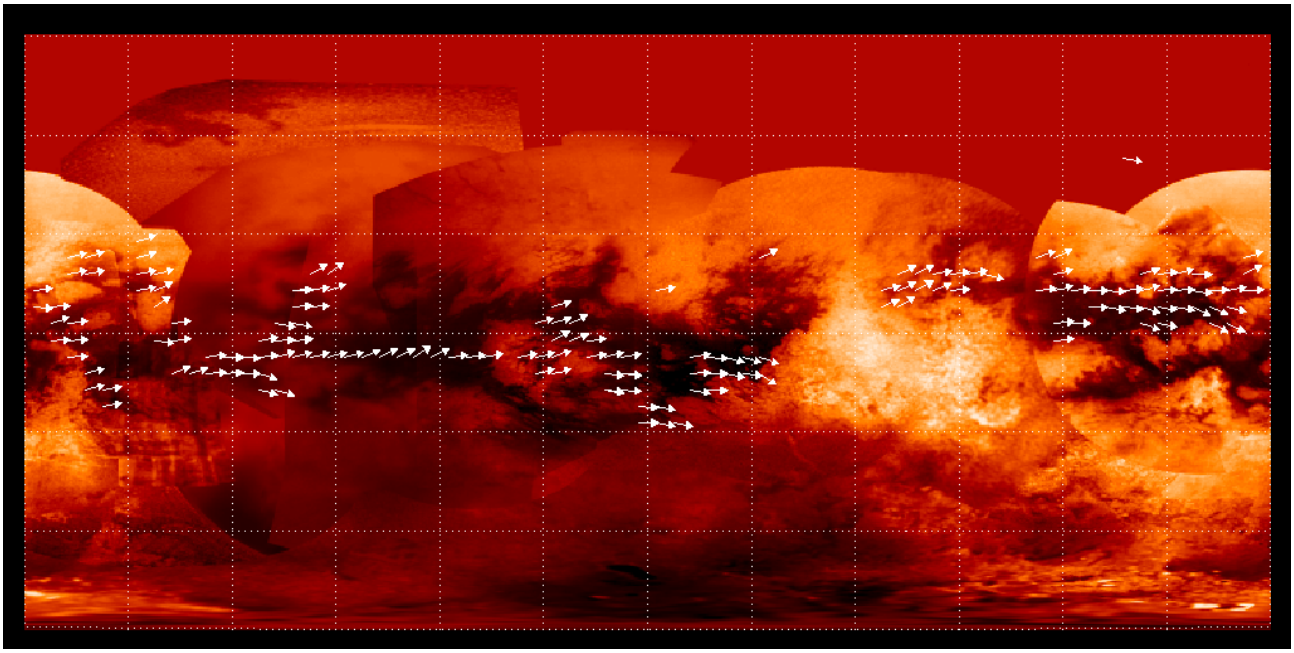

Figure 2. Cylindrical projection map showing observed dune orientations (arrows) overlaid on an optical (940nm) map generated by the Cassini ISS (www.ciclops.org). The predominantly eastwards flow is evident and is a challenge to models. Large areas of Titan (>70%) are presently unmapped – the dunes plotted here are from radar data acquired on TA,T3,T8,T13,T16,T17,T19,T21,T23 and T41.

UNLOCKING THE ENVIRONMENTAL CONDITIONS RECORDED BY AEOLIAN BEDFORMS WITH THE AID OF HIGH-RESOLUTION ATMOSPHERIC MODELING. T. I. Michaels[1], [1]Southwest Research Institute, 1050 Walnut St Suite 300, Boulder, CO 80302, tmichael@boulder.swri.edu.

Introduction: Aeolian bedforms are, by definition, formed and/or strongly modulated by complex interactions between a solid (often particulate) surface and atmospheric motions (*i.e.*, winds). As such, they are an intermediate expression of a fundamental erosional process, a standing exemplified by the fact that they are known to exist on all reasonably well-explored bodies that possess a significant atmosphere and a solid surface (*i.e.*, Earth, Mars, Titan, and Venus). Morphologically, aeolian surface features exhibit myriad individual forms, such as dunes, ripples, and streaks. They also have a penchant for occurring at multiple scales (and/or in a variety of forms) at a single location. Perhaps most importantly, these features are tangible records of invisible winds both contemporary and ancient, of rocks long since pulverized and those that were broken up yesterday, and of events in both the immediate neighborhood and regions greatly distant.

Unraveling this recorded information can be daunting. Three general approaches may be employed: i) *In situ* measurement of winds, structure, composition, and/or time evolution, ii) the analysis of remote sensing (perhaps multispectral) images and data, and iii) numerical modeling techniques, such as high resolution atmospheric simulations and specialized sediment transport models. It should be noted, however, that truly thorough *in situ* sampling is often impractical at best, even for aeolian features on Earth.

Comprehensively deciphering what aeolian features record about their atmospheric environment involves challenges that are outlined here. Past, present, and future approaches aimed at overcoming or reducing these challenges are also briefly discussed.

Challenges: One must have sufficient knowledge about the processes that have likely generated and modulated a given aeolian feature in order to correctly and entirely interpret the environmental conditions that it records. Such processes consist of complex interactions at multiple scales. It is important to fully recognize that much of this complexity is contributed by the nature of the atmosphere itself.

Atmospheric realities. Real atmospheres do not exhibit laminar, steady-state flows. Neutral atmospheric stability is the exception, rather than the rule. Turbulence is not random, nor is it stationary. Atmospheric circulations and processes are not one- or two-dimensional.

Real atmospheres consist of time-dependent flows of a turbulent nature, although the magnitude of the turbulence may be highly variable. They also exhibit chaotic tendencies (in the mathematical sense), where small changes in initial conditions may result in vastly different end states. Neutral atmospheric stability is a theoretical/statistical construct that exists only fleetingly in the instantaneous reality of the natural world. Turbulence exhibits significant scale-dependent three-dimensional structure. Atmospheric circulations and processes are three-dimensional. Real atmospheres are awash with a quasi-continuum of three-dimensional turbulent structures and myriad interfering waves (*e.g.*, acoustic (sound) waves, buoyancy ("gravity") waves; see Figure 1). Circulations and processes at larger spatial scales affect those at smaller scales, and vice versa.

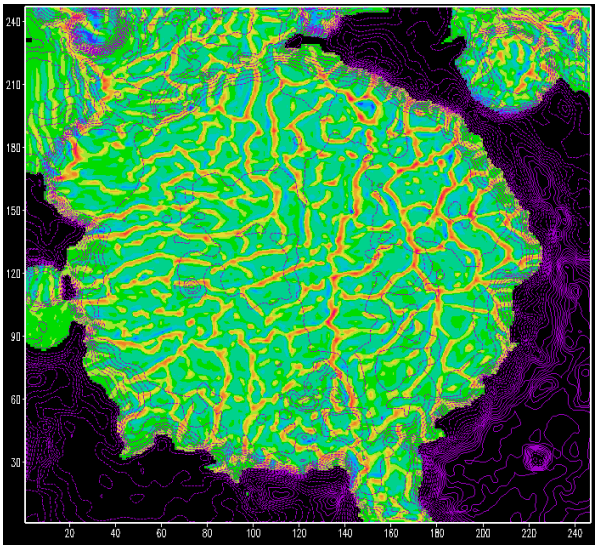

Figure 1 . Example of modeled (with a mesoscale model) midday dry convective structures in Gusev Crater, Mars, illustrating some of the complexity that a real atmosphere exhibits. Note that the full range of small-scale structure is not able to be shown here, since the grid-cell width is ~750 m. These structures are highly time-variable – translating with the mean wind, merging with one another, etc. [area shown is ~180 km wide; violet contours are model topography, shaded field is vertical velocity ("warm" colors = upwards, "cool" colors = downwards) on a constant geopotential surface ~800 m above the crater floor].

One particularly relevant consequence of a real atmosphere is that even though it may be obvious that an

aeolian feature is associated with a certain wind direction, it is often not clear whether that wind direction occurs only 1% of the time, only in a certain season, or in a stochastic fashion – the associated wind direction may even be very localized due to small-scale local effects.

Paradigm shifts and empiricisms. A given atmosphere-related approximation, assumption, theory, or empirical parameterization may seem to outwardly "work" in one situation/location, but fail in the next. This is particularly likely for "extrapolations" of Earth empirical relationships to other solar system bodies, such as Mars or Titan, where significantly different "exotic" paradigms may hold sway (above and beyond simply changing obvious physical parameters). "First principles" physics-based parameterizations tend to perform better in such situations, when available and/or possible. Of course, explicit calculation is always preferred, but even in this age of formidable computer capabilities, such detailed computation of many surface-atmosphere interactions is still often impractical.

Dealing With These Challenges: Numerical atmospheric models offer a way to explicitly simulate the real atmosphere, subject to certain assumptions, approximations, and the limitations of other input datasets and knowledge. This approach is particularly useful for winds, since they are notoriously difficult to observe/measure (especially in three dimensions), either *in situ* or by remote means, even on Earth.

General circulation models (GCMs) are global in extent, and simulate years at a time. However, such versatility currently requires significant simplifications (due to practical limits on computational time) that translate into disadvantages with respect to comparisons to aeolian surface features. For example, due to a relatively large grid-cell width, typically on the order of 200 km, GCM wind velocities may poorly correlate with real-world wind magnitudes and directions driven by subgrid-scale processes and/or topographic variations. Thus in general, investigating/comparing aeolian surface features with the currently available coarse-resolution GCM wind fields is to be discouraged, *unless* no better information (*e.g.*, observations or mesoscale model output) is available.

Mesoscale atmospheric models offer the next level of numerical modeling realism. These models currently employ regional (*i.e.*, less than global) computational domains, with a grid-cell width that can range from ~100 km to less than ~1 km. Mesoscale models use output from a GCM to provide an initial state and boundary conditions, and are typically run for several sols at a time. Furthermore, these models often contain more realistic approximations of physical processes than GCMs do. Mesoscale models have recently been used to compare with wind directions inferred from aeolian features on Mars (*e.g.*, [1], [2])

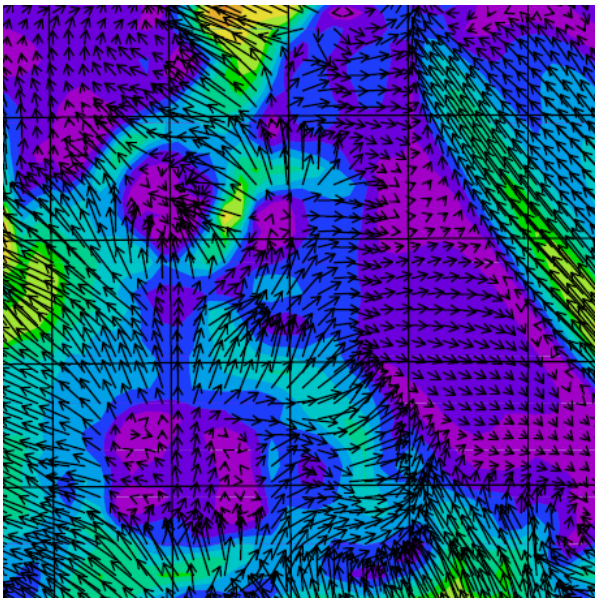

Figure 2. A near-surface nighttime wind field from a mesoscale model (wind speed shaded) near Gusev Crater, Mars – illustrates the wealth of detail gained versus using a GCM, where the 130 x 130 km area shown here would be ~0.25 of a single GCM grid-cell.

Conclusions: The natural complexity and variability of an atmosphere may present challenges with respect to correctly interpreting the record of environmental conditions that an aeolian surface feature represents. A higher-resolution type of numerical atmospheric model known as a mesoscale model can greatly aid in such investigations by providing a reasonably realistic three-dimensional atmospheric context to help guide the interpretation of aeolian surface features. A synergistic relationship is even possible, with aeolian features providing a form of "ground truth" guidance with which to "validate" and improve the mesoscale model.

References: [1] Fenton, L. K. et al. (2005) *JGR*, *110*, E06005.*GR, 90,* 1151–1154. [2] Greeley, R. et al. (2006) *JGR*, *111*, E02S09.

THERMOPHYSICAL ANALYSIS OF THE NORTH POLAR ERG ON MARS. N. E. Putzig[1], M. T. Mellon[2], K. E. Herkenhoff[3], and R. J. Phillips[1]. [1]Southwest Research Institute, Department of Space Studies, 1050 Walnut St, Suite 300, Boulder, CO 80302 (contact: nathaniel@putzig.com), [2]University of Colorado, Laboratory for Atmospheric and Space Physics, Boulder, CO, [3]United States Geological Survey, Astrogeology Team, Flagstaff, AZ.

Introduction: We are conducting an investigation into the reported anomalously low thermal inertia of the north polar erg on Mars, incorporating daytime observations and forward modeling of heterogeneity. Near-surface heterogeneity and normal basaltic sand may explain the thermal behavior of the erg, obviating the need for exotic sand-sized agglomerations of dust.

Background: The polar regions contain an array of geologic features that are crucial to understanding Mars' past and present global climate. The most prominent feature is the layered deposits that are believed to be largely composed of water ice and to result from cyclical climate variations over a broad range of time scales [1, 2]. After seasonal CO_2 frosts sublime, the layered deposits remain capped by bright residual water ice and surrounded by a dark annulus (Fig. 1a) of dune-forming materials known as the polar erg.

The dune morphology and the color and low albedo of the north polar erg materials are quite similar to those of dunes seen at lower latitudes [3] that have been interpreted to be composed of sand-sized basaltic materials [4, 5, 6]. The lower-latitude dunes exhibit intermediate values of thermal inertia (~ 250 tiu, where tiu = J m^{-2} K^{-1} $s^{-1/2}$), consistent with sand-sized grains. In contrast, the north polar erg has much lower values (~ 75 tiu), which has been interpreted to require that the materials be much finer grained [7, 8].

A widely accepted solution to this discrepancy is the bonding of fines into larger, low-density aggregate particles that are capable of forming dunes [9, 10]. The agglomeration of dust particles presumably occurs as they are weathered out of the layered deposits [1, 2, 10], and these sand-sized composite grains are subsequently transported within the erg by saltation. Recent studies associate the dune materials to a newly identified unit at the base the polar layered deposits [11, 12].

Thermal inertia and heterogeneity: A potential alternative explanation for the low apparent thermal inertia of the erg materials is surface heterogeneity, the anomalous thermal effects of which have been investigated in recent model studies [13, 14]. In particular, some configurations of near-surface layering may produce values of apparent thermal inertia at certain times of day and season that are substantially lower than the intrinsic thermal inertia of both the surface layer and its substrate [14]. If true for the polar erg, then it may be surfaced by ordinary basaltic sand, and the low values of apparent thermal inertia could then be attributed to an effect of surface heterogeneity rather than to sand-sized agglomerations of dust.

Large diurnal and seasonal variations in apparent thermal inertia (up to a few hundred tiu) derived from Mars Global Surveyor Thermal Emission Spectrometer (TES) data suggest that heterogeneity is a major factor in the global thermal behavior of the martian surface, and the polar regions show thermal characteristics that are broadly consistent with layered surfaces (Figs. 1b, 1c) [15]. A key element in this analysis is the use of both nighttime and daytime results, particularly for the polar regions where the seasons free of CO_2 ice largely overlap those when the Sun is predominantly above the horizon.

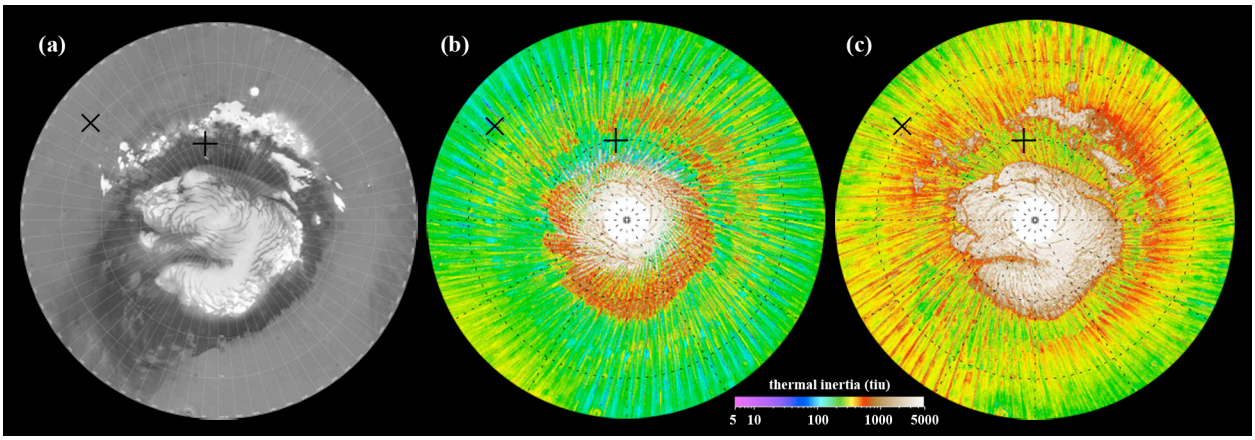

Figure 1. North polar region, 65–90° N, 0°W at bottom. (a) Mars Orbiter Camera wide-angle image mosaic; north polar erg is the irregular, dark annulus surrounding bright layered deposits. NASA/JPL/MSSS. (b, c) TES annual-median apparent thermal inertia near (b) 2 AM and (c) 2 PM [15]. Orbit-track-aligned streaks are due to seasonal variations. × is proposed Phoenix Lander site (Fig. 2). + is HiRISE image center (Fig. 3) within Olympia Undae (area of lower thermal inertia at 120-210° W, 78-83° N).

A comparison of seasonal TES results with those from models of sand (223 tiu) overlying 'rock' (2506 tiu) at the proposed Phoenix Lander site [16] is shown in Fig. 2. The rock value is also representative of the ground ice expected at this site. For the models with sand thicknesses approaching or exceeding a diurnal skin depth ($\geq \delta_S/26$), the 2-AM annual-mean apparent thermal inertia will be substantially less than that of the sand. Thus, analyses that focus solely on nighttime observations—or even those such as the Viking studies that take the annual mean of values fit to diurnal temperatures—may underestimate the inherent thermal inertia of the surface materials in this scenario.

Heterogeneity in the Erg: At the higher latitudes where the polar erg is located, the seasonal range of useful TES data becomes quite limited and the season-to-season changes in apparent thermal inertia are even larger than at the Phoenix site. To resolve these short-term, rapid changes, we will remap the north polar region with a finer seasonal increment—originally chosen at 10° L_S to optimize global results [15]. Our goal is to distinguish whether models having dust-sized surface materials (or agglomerations thereof that allow dune formation) or those having typical sand-sized surface materials provide the best match to the observed thermal behavior. We expect consistency with an ice-cemented substrate beneath a dry surface layer, and our analysis techniques may allow us to constrain the upper-layer thickness to within a few centimeters.

For some geometries, horizontal heterogeneity may have thermal behavior similar to that of layering [15].

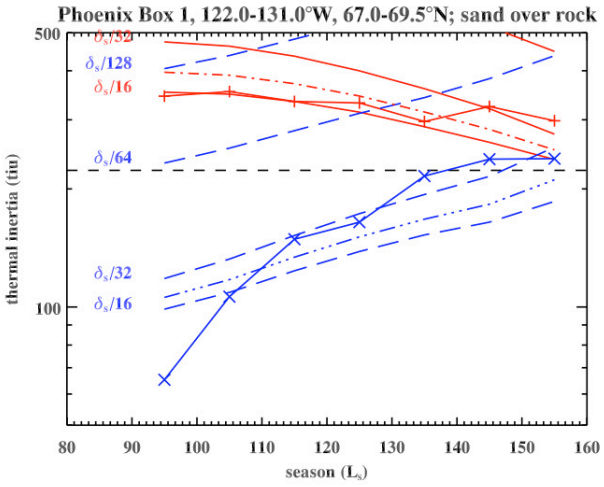

Figure 2. Seasonal 2-AM (blue) and 2-PM (red) apparent thermal inertia from TES (×, + symbols) and from layered models of sand over rock (or ground ice) at the Phoenix site (× in Fig. 1). Horizontal dashed line is sand (223 tiu). Curve labels are upper-layer thickness in fractional seasonal skin depth, δ_S (70 cm for sand). Best-fit model (dot-dashed curves) has a sand thickness of ~ 4 cm. Seasonal range is limited by transient CO_2 frost. From Putzig and Mellon [15].

In the erg, Mars Reconnaissance Orbiter High Resolution Imaging Science Experiment (HiRISE) images show bright deposits between individual dune crests (Fig. 3), which may be relatively consolidated and thus have higher thermal inertia than the surrounding dune materials. Also evident are diverging dune slopes, which will experience differential heating both diurnally and seasonally. Since their scales are well below that of TES (~ 3 km), both the horizontal material mixtures and the divergent slopes may have large effects on TES-derived apparent thermal inertia [13]. It will thus be essential to account for any contributions of horizontal heterogeneity when attempting to relate the thermal behavior of the erg to the presence of ground ice beneath a veneer of unconsolidated materials.

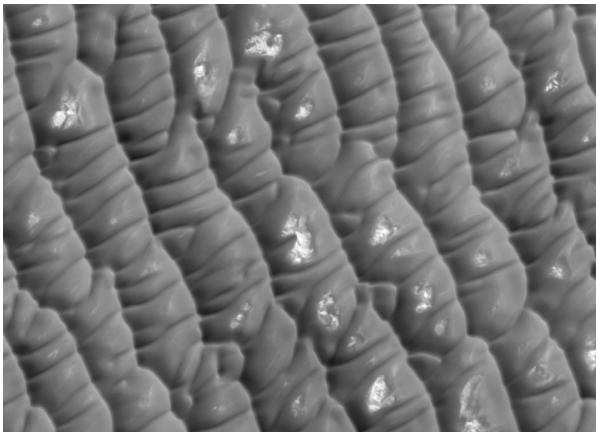

Figure 3. Portion of HiRISE image PSP_001736_2605 (center at 80.19° N, 168.77° W; + in Fig. 1), showing an area in Olympia Undae with bright deposits between dune crests. Illumination is from lower left. Image is 4.6 km wide. NASA/JPL/University of Arizona.

References: [1] Thomas P. et al. (1992) in: *Mars*, Kieffer H. H. et al. (1992) U. AZ Press, Tucson. [2] Clifford S. M. et al. (2000) *Icarus 144*, 210–242. [3] Thomas P. and Weitz C. (1989) *Icarus 81*, 185-215. [4] Sagan C. and Bagnold R. A. (1975) *Icarus 26*, 209-218. [5] El-Baz F. et al. (1979) *JGR 84*, 8205-8221. [6] Breed et al. (1979) *JGR 84*, 8183-8204. [7] Paige D. A et al. (1994) *JGR 99*, 25,959–25,991. [8] Vasavada A. R. et al. (2000) *JGR 105*, 6961–6969. [9] Herkenhoff K. E. and Vasavada A. R. (1999) *JGR 104*, 16,487–16,500. [10] Cutts J. A. et al. (1976) *Science 194*, 1329-1337. [11] Byrne S. and Murray B. C. (2002) *JGR 107*, E6, 5044. [12] Fishbaugh K. E. and Head J. W. III (2005) *Icarus 174*, 444-474. [13] Putzig N. E. and Mellon M. T. (2007) *Icarus 191*, 52-67. [14] Mellon M. T. and Putzig, N. E. (2007) *LPS XXXVIII*, Abstract #2184. [15] Putzig N. E. and Mellon M. T. (2007) *Icarus 191*, 68-94. [16] Smith P. H. et al. (2007) *LPS XXXVIII*, Abstract #1176.

TERRESTRIAL ANALOGUES OF LONGITUDINAL DUNES ON TITAN. J. Radebaugh[1], R. Lorenz[2], C. Spencer[1], and the Cassini Radar Team, [1]Brigham Young University, Department of Geological Sciences, Provo, UT 84602, jani.radebaugh@byu.edu, [2]Johns Hopkins University Applied Physics Laboratory, Laurel, MD 20723.

Introduction: Among the many features indicative of a young surface acted upon by an active atmosphere seen by the Cassini Radar instrument on Saturn's moon Titan are vast fields of dunes [1]. These fields are located mainly at equatorial regions, within ±30°, and nearly encircle the globe [2,3]. Dune materials on this icy moon are organics as suggested by their dark appearance to Radar and V-NIR instruments as well as their spectral signature [4,5]. These materials are likely snowed to the surface as solids out of an atmosphere where they were produced by photochemical processes. Winds of ~1 m/s in Titan's 1.5 bar atmosphere are able to saltate slightly smaller than sand-sized particles (0.25 mm) into dune forms [1,3].

Dunes on Titan are longitudinal in form, and have the appearance of dunes on Earth, enabling valuable comparisons to be drawn. Notably, there are not many Martian or Venusian longitudinal dune fields with which to compare Titan's dunes [6].

Dune Morphology: The Radar-dark, linear-formed dunes on Titan are 1-3 km wide, have a 1-4 km spacing, are up to 100 m high, and are several to hundreds of kilometers long (Fig. 1). These dimensions are similar to those of longitudinal dunes in the Namib and Saharan deserts (Fig. 2) [1,2].

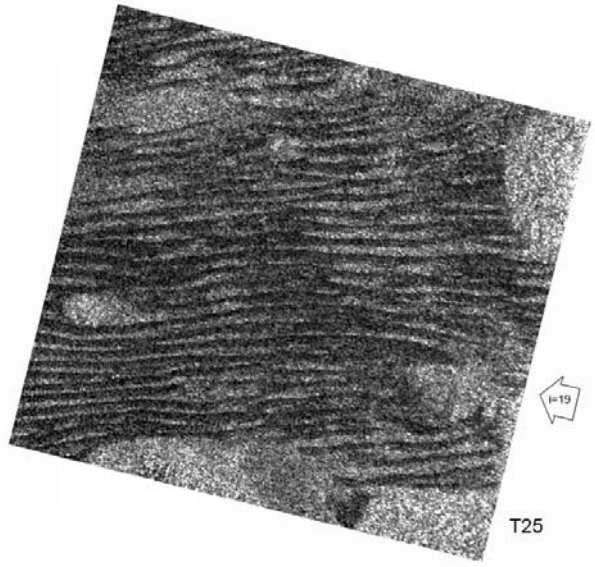

Fig. 1. Longitudinal dunes on Titan, widths ~2 km. Bright objects are probably topographically higher.

Dunes of this type form by a wide range of hypothesized wind directions [7,8,9]. Of the leading possibilities, this work favors the prevailing wind hypothesis, in which sand transportation occurs along the dune axis [10]. In this model, winds blow along one dominant direction with seasonal or minor off-axis winds.

The prevailing wind hypothesis model is, for example, best suited for dunes in the Mauritanian Sahara, where longitudinal dune axes parallel winds that blow from northern Africa out west to sea. Dunes here appear to diverge around topographic obstacles, then resume their orientations on the downwind side. High-resolution images reveal wind streaks that trail behind these obstacles (Fig. 2). Dunes on Titan show similar behavior around topographic obstacles, although image resolution (~170 m) does not enable smaller forms such as wind streaks to be visible. Some large-scale, Radar- and optically-bright features on the purported lee of obstacles have the appearance of being deposited by winds, strengthening the connection of Titan's dune fields to the prevailing wind hypothesis model. Nearly uniformly across Titan, dunes indicate that winds are primarily W-E [2,3].

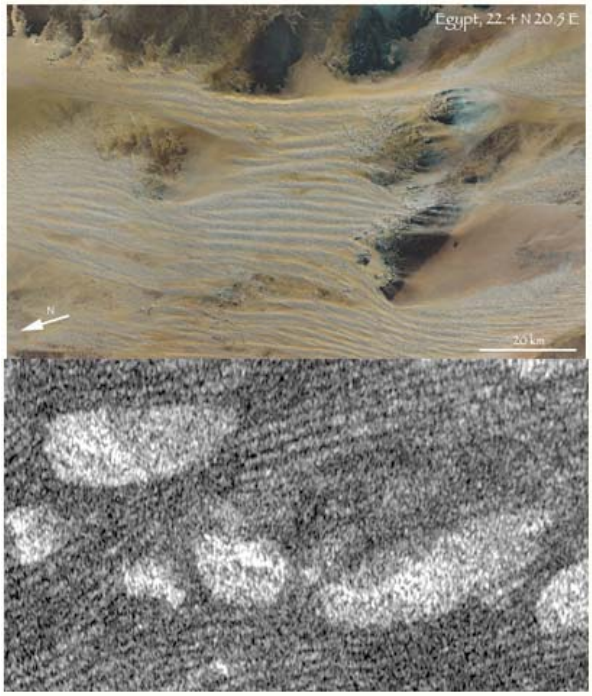

Fig. 2. Longitudinal dunes in Egypt (top) and at the equator of Titan, to scale (bottom – image from T41 flyby, 2/08).

Formation and Longevity of Titan's Dunes: Due to their sizes and location in large deserts, longitudinal

dunes are the most areally extensive dune form on Earth. Yet the formation of this dune type is not well understood, both in terms of wind and sand transportation models. One model for formation involves the elongation of one horn of a barchan dune into a linear dune [11]. This may occur when sand supply has increased in a region, given that barchan dunes often form in regions of low sand supply, while longitudinal dunes are stable in a wider range of sand supply.

Another formation model claims that complete barchan dunes can form chains in the downwind direction that merge to form a single linear dune (Fig. 4) [12]. This scenario may occur again in a condition of increased sand supply. Evidence for both of these models has been seen on Earth and Mars, and may be evident in select regions on Titan.

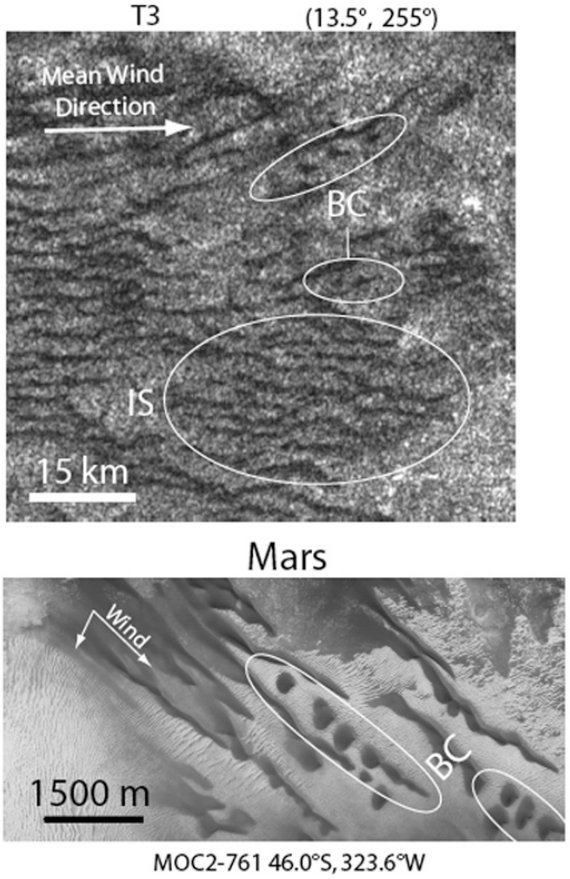

Fig. 4. Barchan convoys on Mars (bottom) and possibly on Titan. IS indicates a region of increased sinuosity, also an indicator of sand supply changes and wind variation.

Since images are only snapshots in time, it is difficult to determine the long-term evolution of a system from isolated data taken closely spaced in time, as often happens with planetary image analysis. It is possible, in fact, that the above models run the other way, if for example sand supply or winds vary from conditions conducive to longitudinal dune persistence. There is some evidence for changes in Titan's dune fields, in cases where longitudinal dunes appear to overly transverse dunes or previously existing longitudinal dunes. But given the vast majority of Titan's dunes are longitudinal, even at the edges of sand seas and at the far northern and southern reaches of dunes, where sand supply appears to be more limited, these features seem to have reached a currently stable existence.

It has been hypothesized that longitudinal dunes are at the most highly progressed end of broad dune evolutionary trends. Some large, terrestrial, longitudinal dune fields are estimated to be as old as 100,000 years [13], while other types of dune fields are typically younger by at least an order of magnitude. This idea may be bolstered by the pervasiveness of longitudinal dunes on Titan, where we expect wind and sand supply patterns are not interrupted by episodes of abrupt climate change, invasion by vegetation, or encroachment by sand-stealing oceans. Processes on Titan appear to be efficient at carrying sand-sized particles to equatorial dune-forming regions, where they are worked by winds into dunes. This is probably ongoing, as there are almost no features that can claim to overlie the dunes, despite evidence of fluids that could conceivably fill channels at polar and equatorial locations [14].

Thus, despite the proposed and observed youth of individual dunes, the dune fields of Titan may be relatively old in Titan's current climate configuration.

References: [1] R. D. Lorenz et al. (2006) The Sand Seas of Titan : Cassini RADAR observations of Longitudinal Dunes, Science, 312, 724-727 [2] J. Radebaugh, Dunes on Titan Observed by Cassini Radar (2008) Icarus, in press. [3] Lorenz, R.D., J. Radebaugh and the Cassini Radar Team (2008) The Sand Seas of Titan: Discovery and Implications for Methane Climatology and Wind Patterns, this conference. [4] Soderblom, L. et al. (2007) PSS 55, 2025-2036. [5] J. Barnes et al. (2008) Spectroscopy, Morphometry, and Photoclinometry of Titan's Dunefields from Cassini/VIMS, Icarus, in press [6] Lee, P. and P.C. Thomas (1995) Longitudinal dunes on Mars: Relation to current wind regimes, JGR 100, 5381-5395. [7] Blandford, W.T. (1877) Geol. Surv. India 10, 10-21. [8] Fryberger, S.G. and G. Dean (1979). Dune forms and wind regime, USGS Prof. Pap. 1052, 137-169. [9] Tsoar, H. (1978). The dynamics of longitudinal dunes, US Army Europ. Res. Off, London. [10] Lancaster, N. (1982) Linear dunes, Prog. Phys. Geog. 6, 476-504. [11] Bagnold, R. 1941. Physics of wind-blown sand and desert dunes, 265 pp. [12] Bourke, M. (2006) A new model for linear dune formation: Merged barchan convoys on Mars. LPS 37, Abst. 2432. [13] Lancaster, N. (1995) The geomorphology of desert dunes, 290 pp. [14] E.R. Stofan et al., The Lakes of Titan (2007) Nature, 441, 61-64.

LONGITUDINAL DUNES ON TITAN : A LABORATORY APPROACH. E. Reffet[1], S. Courrech du Pont[2], P. Hersen[2], S. Douady[2], M. Fulchignoni[1]. [1]LESIA Observatoire de Paris (erwan.reffet@obspm.fr), [2]MSC CNRS-Université Paris 7.

Introduction: Cassini observations of Titan's surface revealed a features-rich body hidden behind its opaque atmosphere. The high spatial resolution (up to 300m/pixel) allows us to study large scale features covering its surface. Moreover, the great diversity of unveiled structures [1] make this planet-like satellite a geological object of interest.

Among these features, linear formations are geomorphologically similar to longitudinal dunes [2,3,4]. These longitudinal dunes observed by Cassini Radar (Fig.1) and Cassini VIMS cover Titan's equatorial regions and represent a large portion of the whole surface. Such constructions indicate a strong interaction between "sand grain"-size particles (typically about 200μm) and the winds close to the surface. As a consequence, the omnipresence of these dunes could help to constrain Titan's winds by understanding their processes of formation.

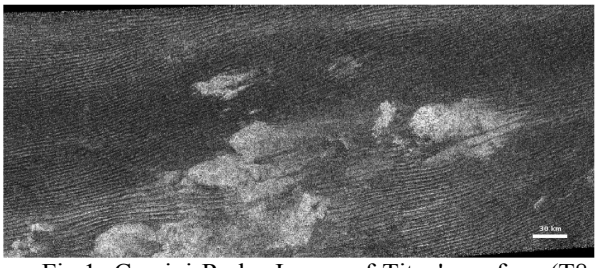

Fig.1: Cassini Radar Image of Titan's surface (T8, 2005). Linear features interpreted as longitudinal dunes appear ubiquitous in Titan's equatorial regions.

Albeit longitudinal dunes are the most commonly encountered type of dune on Earth, they have not been studied in details yet. The large scale of these aeolian features (km-scale on Titan or in the Namib Desert [5]) makes them not directly reproducible under laboratory conditions. We present here an original approach which allows us to reproduce longitudinal dunes in the lab, under controlled conditions. Based on this method, we study the evolution of an homogeneous sand bed under a bimodal wind regime and extend this laboratory work with numerical simulations.

Method: The physics of sand dunes is governed by the characteristic length $L_{Drag}=(\rho_p/\rho_f)*D_{p,}$ where ρ_p and D_p are the density and the diameter of the sand grains used to form the dunes and ρ_f is the density of the fluid surrounding the dunes. This length corresponds to the characteristic distance at the end of which an eroded grain reaches the wind velocity [6]. In order to reproduce large scale aeolian patterns such as longitudinal dunes, we developed an under water experimental setup. The high density of water (in comparison to the atmospheric density on Titan or on Earth) decreases L_{Drag} and therefore reduces the size and time-scale of the whole system. This method has already been used to produce and study cm-scale barchan in a lab experiment [7].

To create the wind, we use a baseplate which can be translated under water. We decided to move the sand bed relatively to the fluid rather than the opposite to minimize the size of the setup. The wind direction is modified by rotating the sand bed using a disk located in the center of the baseplate.

We start our experiments with an homogeneous sand bed. The sand (ceramic grains) is spread on the disk to avoid any privileged direction. The wind conditions consist of a bimodal wind regime, where the wind switches successively between two given directions. The angle between these two directions can be tuned from one experiment to another and we explore the influence of this angle on the evolution of the sand bed.

A numerical model is used to investigate the same initial conditions and wind regimes. This model is macroscopic and derives from the behavior of a fluid flow at the surface of a bump[8].

Experimental and numerical results can be compared and confronted to the observations.

Results: We present here (Fig.2) the different patterns obtained for various angles between the two directions of the bimodal wind regime. We report both the laboratory and numerical results for three characteristic states.

The left hand side pictures correspond to the laboratory experiments and the right hand side to the simulations results. For each picture, the mean wind direction is from the bottom to the top. The arrows indicate the two distinct directions of the bimodal wind regime. The angle between these directions increases from the top to the bottom panel.

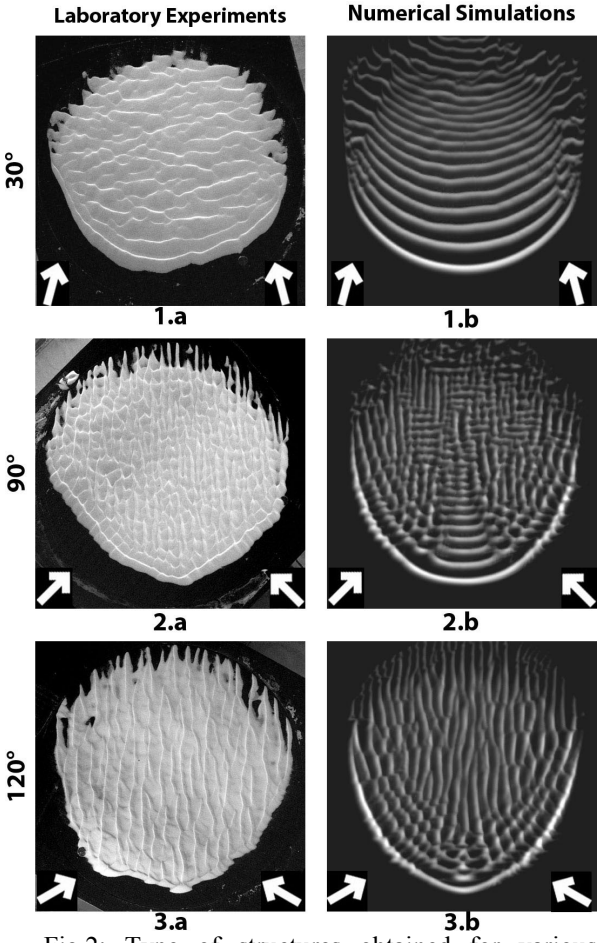

Fig.2: Type of structures obtained for various angles of the bimodal wind regime. For each angle, left picture (a) corresponds to the laboratory experiment (pictures are 30cm wide) and right (b) to the numerical simulation (scaled to be compared to the experiments). Arrows indicate the directions of the 2 winds : (1) 30°, Transverse dunes. (2) 90°, Intermediate pattern. (3) 120°, Longitudinal dunes.

For small angles (Fig.2.1): Dunes perpendicular to the mean wind direction developed on the sand bed. These dunes are usually called transverse dunes.

For intermediate angles (Fig.2.2): Features both perpendicular and parallel to the mean wind direction are formed. Transverse and longitudinal patterns are observed within the same sand bed. These patterns represent the transition from one type of sand bed to the other.

For large angles (Fig.2.3): Structures parallel to the mean wind direction are formed. This type of dunes is commonly called longitudinal dunes. They are morphologically similar to Titan's dunes (Fig.3).

This transition between transverse and longitudinal dunes, when increasing the angle of the bimodal wind regime, corresponds to a separation of the mean wind direction and the principal axis of mass exchange between structures [9].

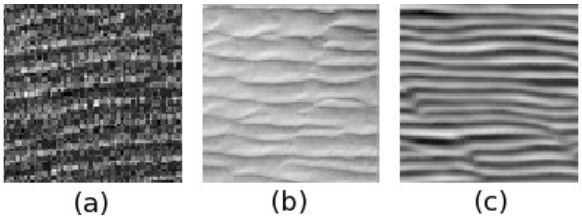

Fig.3: Comparison of longitudinal dunes morphology : (a) Radar image of Titan's surface. (b) Laboratory experiment results. (c) Numerical simulation results. These images are resized to a comparable scale.

Conclusions: We reproduced longitudinal dunes using a bimodal wind regime and under controlled conditions both experimentally and numerically. We also investigated the transition between transverse and longitudinal dunes and the link with the angle between the two wind directions. The presence of longitudinal dunes on Titan's surface as well as on Earth appears to be a good constrain on the local wind regime. Variations of wind direction of more than 90° appear to be required to produce longitudinal dunes. On Titan, the pervasive occurrence of these dunes in the equatorial regions could be an important constrain on Titan's wind model close to the surface[10].

References: [1] Elachi C. et al (2005) *Science, 308, 970-974.* [2] Boubin G. et al. (2005) *37thDPS, Abstract #46.04, 723.* [3] Lorenz R. D. et al. (2006) *Science, 312, 724-727.* [4] Radebaugh et al. (2008) *Icarus, preprint.* [5] Lorenz R. D. et al. (2006) *37th LPSc, Abstract #1249*. [6] Hersen et al. (2002) *PRL, 89*. [7] Hersen et al. (2005) *GeoRL, 32*. [8] Jackson P. S. and Hunt J. C. R. (1975) *QJRMS, 101*. [9] Rubin D. M. and Ikeda H. (1990) Sedimentology, *37, 673-684*. [10] Tokano T. et al (2007) *P&SS, 55*.

GLOBAL SURVEY OF MARTIAN TRANSVERSE AEOLIAN RIDGES. M. R. Salvatore[1], [1]Department of Geography, Penn State University, 302 Walker Building, University Park, PA 16802, salvatorem@psu.edu.

Introduction: Martian transverse aeolian ridges (TARs) are small-scale aeolian bedforms that appear to be either large ripples or small dunes [1]. The distribution and extent of TARs across the Martian surface has only been analyzed in certain regions of the planet [2]. The atmospheric conditions responsible for the formation of these features are largely unknown.

This study analyzed 500 randomly selected images from the Mars Orbiter Camera (MOC) instrument to determine the global distribution of TARs. Climate data obtained using the *MarsWRF* climate model were then analyzed to identify any correlation between TAR characteristics and current climatic conditions.

Global TAR Distribution: Of the 500 random MOC images, 167 (33.4%) of images contained TARs, although only 107 images had clearly identifiable TAR orientations. All of the images containing TARs were between 60ºN and 60ºS with no images containing TARs poleward of these latitudes (Fig. 1, 2). Additionally, no relationship between TAR wavelength (distance between successive ridge crests), orientation (ridge direction), or latitude is apparent.

***MarsWRF* Climate Variable Correlations:** The *MarsWRF* data output includes temperature, wind speed, wind direction, surface pressure, and pressure 30 meters above the surface for 2,304 evenly spaced point locations across Mars [3]. For convenience, the data were divided into 18 latitude bands that were each 10º thick, from 90ºN-80ºN to 80ºS-90ºS.

Surface Temperature (Fig. 3). Temperatures associated with TAR locations are an average 1.33K higher than averages within their respective latitude bands. However, statistically significant relationships between TAR distribution and temperature were not found.

Surface Pressure. Model-predicted surface pressures do not seem to correlate with TAR distribution or characteristics. In this study, TARs were found to exist at a wide range of surface pressures, including Hellas Basin (>10 mb) and the Tharsis Bulge (3-4 mb).

Wind Speed. No clear correlation exists between modern predicted wind speeds and TAR wavelength, orientation, or location.

Wind Direction (Fig. 4). To analyze both wind direction and TAR orientation, wind roses were created using the WRPLOT View software. Again, no correlation seems to exist between the modern predicted climate data and the observed TAR characteristics.

Discussion: Three different possibilities may account for the lack of correlation between the *MarsWRF* climate data and observed TAR characteristics:

Inactive TARs. Recent observations from the Mars Exploration Rovers reveal that TARs consist of coarse-grained material that mantles finer-grained material [4]. Terrestrial granule ripples, similar in composition, were previously suggested as potential Earth analogs for Martian TARs [5, 6]. Such a composition suggests that these features formed during a different climate regime than the one that currently exists. The current Martian climate is likely incapable of initiating and sustaining adequate rates of particle saltation to actively construct and modify TARs.

Sediment Cementation. The current Martian climate may be capable of initiating and sustaining particle saltation. One theory of why TAR migration has not been seen may be due to physical or chemical cementation of the sediment. The presence of seasonal water- or carbon dioxide-frost may effectively eliminate particle saltation. In addition, the presence of salts formed during evaporation events may be stabilizing much of the current visible TARs.

Local Climate. Lack of correlation between global-scale climate data and TAR characteristics may show that local climatic factors and variables drive TAR mobility as opposed to larger-scale phenomena. This possibility suggests that TARs may be young and active features. Although no TAR migration has been documented, orbital observations of TARs have only been available for slightly more than a decade. Because Mars has a much thinner atmosphere than is present on Earth, the term "active" on Mars may refer to small-scale motion over extremely long time periods.

Future Studies: Future studies should be conducted using climate models with higher spatial resolution. This would identify whether the local climate influences TAR wavelength and orientation or whether TARs are stable and immobile features. Additionally, studying TARs using extended ground-based observations would also determine whether microscale migration is occurring.

References: [1] Zimbelman, J. R. and S. Wilson (2002) *LPS XXXIII*, Abstract #1514. [2] Wilson, S. A. and J. R. Zimbelman (2004) *JGR, 109*, doi: 10.1029/2004JE002247. [3] Richardson, M. I. et al. (2007) *JGR, 112*, doi:10.1029/2006JE002825. [4] Sullivan, R. et al. (2007) *Eos Trans. AGU, 88(52)*, Fall Meet. Suppl., Abstract P11A-0254. [5] Zimbelman, J. R. and S. H. Williams (2006) *LPS XXXVII*, Abstract #2047. [6] Zimbelman, J. R. et al. (2007) *LPS XXXVIII*, Abstract #1324.

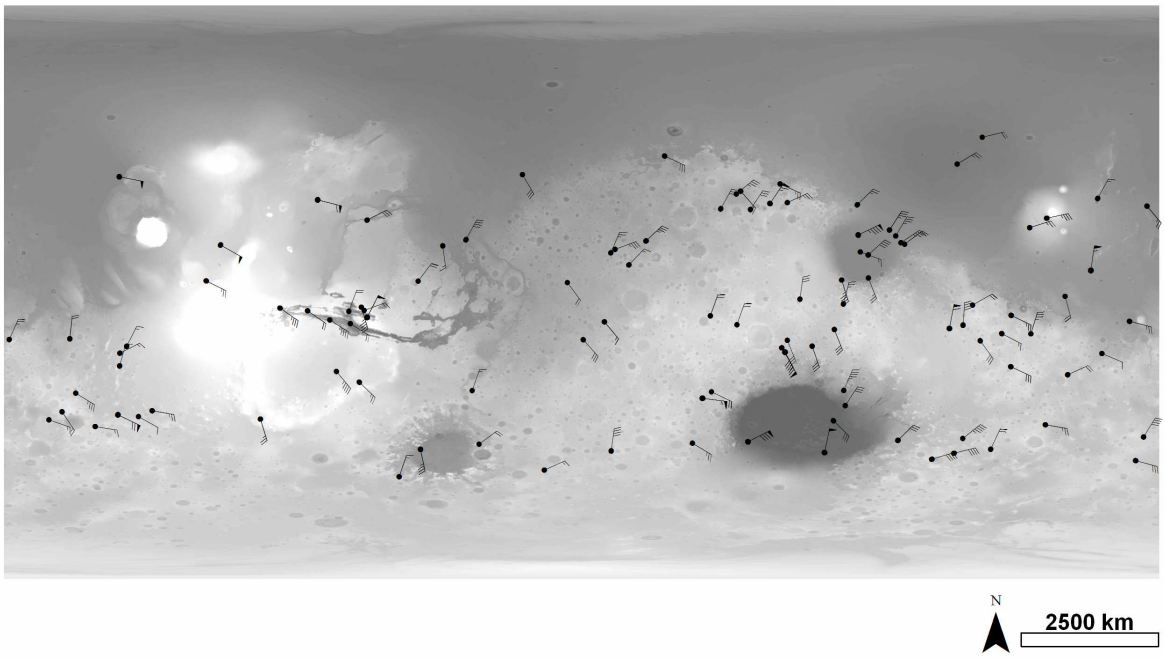

Figure 1: A map of the location of the 107 MOC images containing TARs with identifiable orientations. The wind barbs represent the image locations, their direction represents the TAR orientation, and the tick marks represent wavelength (in meters).

Figure 2: A subset of a MOC image (M0306282) containing TARs. These high resolution subsets were used to determine average ridge wavelength and orientation.

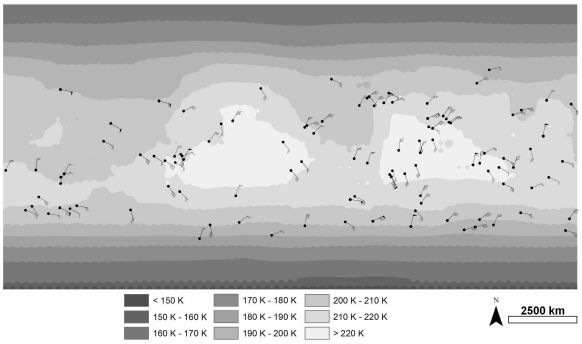

Figure 3: A map of average surface temperature with the locations of MOC images containing TARs.

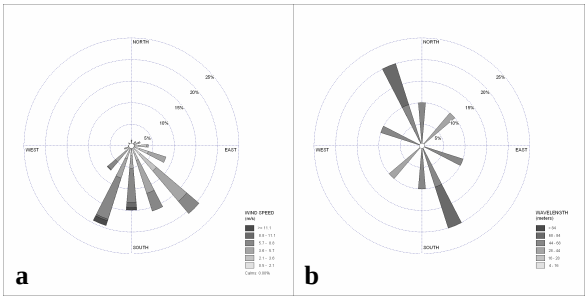

Figure 4: (a) A wind rose showing average Martian wind speed and direction between 0º and 10ºN latitude. (b) A wind rose showing average TAR wavelength and orientation between 0º and 10ºN latitude.

THERMAL REMOTE SENSING OF SAND TRANSPORT SYSTEMS
Scheidt, S., Ramsey, M.S., and Lancaster, N.

The spectral emissivity and kinetic temperature of the land surface can be derived from thermal radiance data (TIR) collected by The Advanced Spaceborne Thermal Emission and Reflection (ASTER) radiometer. The spectral emissivity is used to determine mineral composition for dune fields and sand seas. Kinetic temperature and apparent thermal inertia (ATI) data may also reveal surface properties such as variation in soil moisture and grain size. Gypsum sand transported by westerly winds is continually resupplied to the dune fields in the White Sands National Monument originating from ephemeral playa lakes southwest of the dune field. Wet-dry cycles resupply material by evaporation and mineral formation on the surface. The dune field remains dynamic with dunes moving in the northeastly direction. Over the duration of ASTER's mission, a high-temporal resolution, cloud-free remote sensing data set of day- and night-time has been generated for the area from May 2, 2000 to March 12, 2008. Changes in emissivity, temperature and ATI through time can be used to observe and study the relative timing of the wetting and drying of Lake Lucero, the transport of sand, changes in mineral composition and changes in dune morphology. In addition, ASTER also provides high spatial resolution (15m) visible/near-infrared (VNIR) data and optically-generated digital elevation models (DEM) that can be combined with these thermal data sets. The high temporal ASTER TIR data set may be used as a useful tool for using White Sands as a terrestrial, analogue for aeolian sites on Mars.

INTERCONNECTED ERGS IN EAST THAUMASIA REGION: SEDIMENT TRANSPORT PATHWAYS AND POSSIBLE SOURCE AREAS. S. Silvestro[1] and G. G. Ori[1,2], [1]International Research School of Planetary Sciences, Università d'Annunzio, Pescara, Italy (simone@irsps.unich.it), [2]Ibn Battuta Centre, Unversitè Cadi Ayyad, Marrakech, Morocco.

Introduction: Dark ergs often appear in the Martian highlands as isolated, low-albedo patches inside craters. Dust cover and erosion often mask or remove any trace of previous sediment movement from source to sink areas. Nevertheless, some efforts for identifying such sediment transport pathways at global and regional scale were made by several authors [1] [2] [3]. Investigation of sand deposit and dunes morphology allow us to identify several sand transport pathways that connect different ergs in the eastern part of Thaumasia region.

Studied area: The studied area is located in Aonia Terra, near the western rim of the Argyre impact basin (52° S ; 292.5° E). Several ergs in this region form dark sand seas resting over the ancient cratered unit Noachian in age [4]. The dune fields are connected by sand corridors characterized by the presence of dark sand streaks, barchans, falling and climbing dunes.

Methodology: Ergs were identified in the HRSC images. They have been mapped following the seminal work by McKee [5]. Mapping has been performed using, besides HRSC, THEMIS visible, MOC NA and HIRISE images, which provide the details necessary to identify dune slipfaces. THEMIS infrared mosaics (day and night) were also used to derive the thermal properties of the surface. The dataset were then integrated into a GIS project and projected in a sinusoidal projection (center longitude 292.5°E). Modeled wind (Ames GCM) [6] have been downloaded from the Martian Digital Dunes Database [7] and compared with wind direction deduced from dune slipface orientations.

Ergs description: Six dune fields in Aonia Terra labeled A, B, C, D, E, and F have been identified (Fig.1). Dune morphology reflects one dominant wind direction for most of the ergs. These sand seas are characterized by the presence of barchans and transverse dunes organized in a simple pattern (all dunes

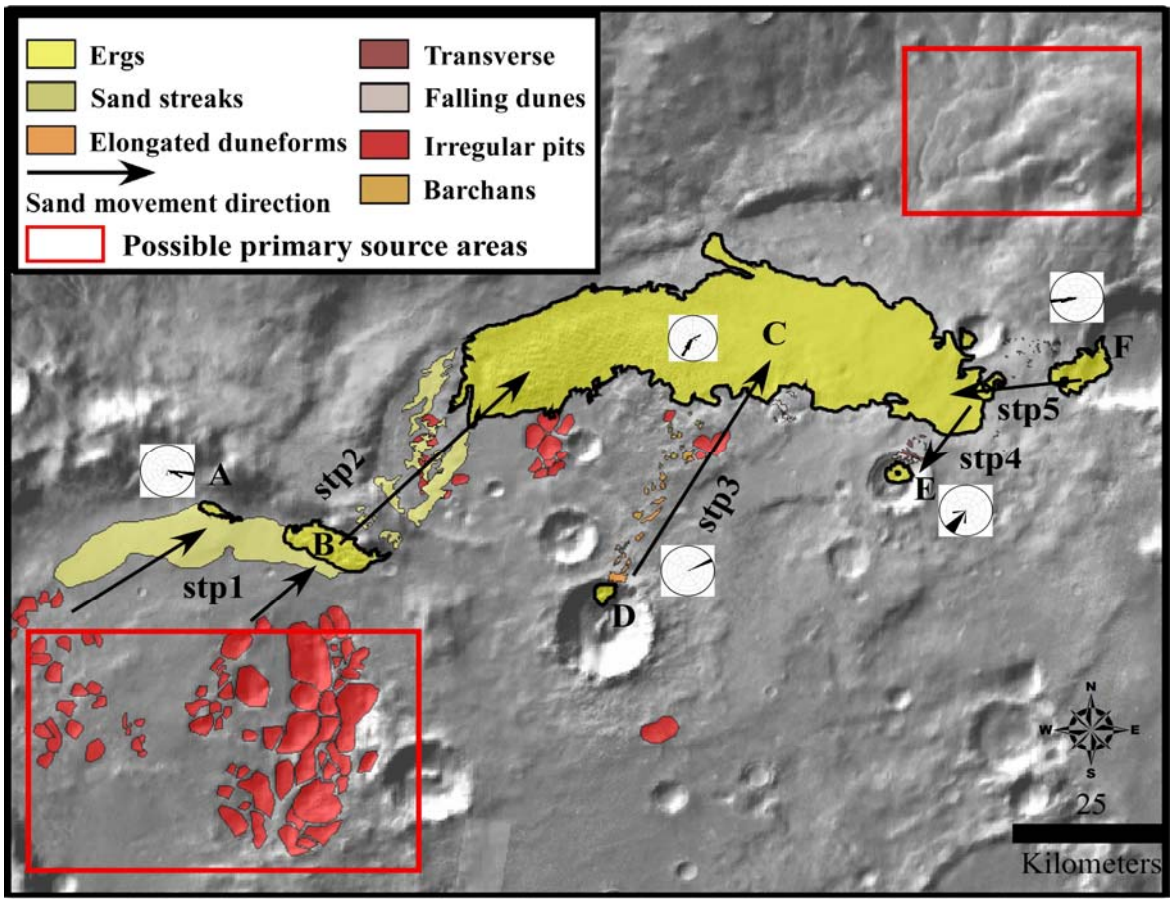

Fig 1, geomorphological map of the studied area, rose diagrams (rapresenting dune slipface orientations in the downwind direction) are created for di ergs A, C, E, F and for the barchans connecting the ergs D and C (stp3).

oriented in the same direction), and locally affected by gullies on their slipfaces [8]. An exception is represented by the Erg C (Fig. 2, see caption for units description), where barchanoid and transverse dunes are arranged in a more complex pattern that reflects a convergence of several winds. Reversing dunes are found in the centre of the erg. The ergs B, D, E and F are all connected to the erg C through different sand transport pathways labeled 2, 3, 4, and 5.

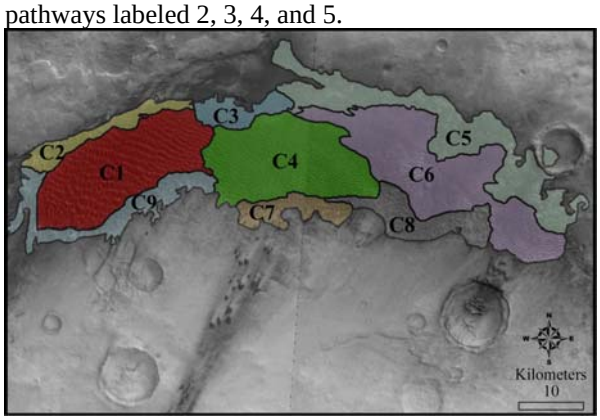

Fig. 2, dunes morphology of the erg C. C1 Barchanoids and transverse, C2 Barchans, C3 Irregular barchans (2 slipface orientations), C4 Transverse reversing ridges, C5 Barchans and domes, C6 Transverse ridges with fork junctions, C7 Barchans (elongation of one horn) C8 Barchans-unknown, C9 Barchans.

Sand transport pathways observations: The regional sediment transport pathways could be divided in 5 parts that we labeled from 1 to 5. The sand transport pathways 2 (stp2) connects the ergs B and C. Trail of dark sand leading away from the erg B (source) feeds the larger erg C (sink) 34 kilometers north (Fig. 3). The stp 3 (about 40 km long) links the ergs D and C in the same way. The material that leaves the erg D is organized in sand streaks and barchans that are probably still migrating towards the erg C. Falling dunes form downwind. The erg C is not only the depositional site of the material transported from the other ergs, but it is itself source of sediment for the erg E, that lies in a younger and smaller crater just few kilometers south. The stp 4 (about 10 km long) that connects the two dune fields is marked by patches of dark sand and transverse dunes which slipfaces are oriented towards southwest. Well developed gullies from the slipfaces of the transverse dunes near the northern crater rim seems to be associated to the downslope movement of the dark material into the crater. The stp 5 (about 12 km long) connects the erg F (source) with the erg C (sink), through dark streaks and barchan dunes.

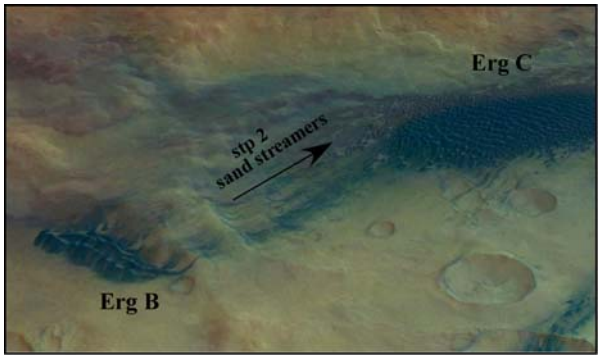

Fig. 3, sand streaks connecting the ergs B and C (stp 2), HRSC color image draped on HRSC derived dtm (100 m).

Possible source areas: While the sediment transport pathways that connect the ergs are well recognizable, the ones that link the sand seas to their relative primary source area are more difficult to identify. Nevertheless, some hypothesis can be done. Several irregular pits are present on the floor of different craters in the studied area and in some case it is possible to detect thin streaks of dark material departing from them. This is the case of stp 1, where these streaks seem to connect the eroded pits to the ergs A and B downwind. This is not the case of the ergs D and F where such streaks are not visible upwind to the dune fields. This could suggest that the material probably comes from the craters themselves. In the case of the erg E the principal source of sand seems to be the erg C upwind. Source areas of the erg C are identified in the ergs B, D and F. Slipface orientations in the northeastern part of the erg reflect winds from N-NE. This suggests that other source zones are possibly located upwind, where several channels cut the ancient highlands materials.

Conclusions: The eastern part of Thaumasia is one of the few areas of Mars where different sand transport pathways connect several ergs regionally. The erg labeled C in this work is in the same time source and sink of dark material and different source areas are identified. Wind directions derived from dune morphology reflect present atmospheric flows obtained by GCM data. Furthermore, slipface structures are present [9], suggesting that such sediment pathways have been recently active or are still active today.

References: [1] Anderson F. S. et al. (1999) *JGR, 104(E8),* 18,991–19,002. [2] Fenton L. K. (2005) *JGR, 110,* E11004. [3] Bourke M. C. (2004) *JGR ,109,* E07005. [4] Scott D. H. and Tanaka K. L. (1986) *USGS map I-1802-A.* [5] McKee E. D. (1978) *USGS Professional Paper no. 1052.* [6] Haberle et al. (2006) *GRL 33,* L19S04. [7] Hayward et al. (2007), *USGS Open File Report 2007-1158.* [8] Di Achille et al. (2008), *this volume* [9] Edgett K. S. and Malin M. C. (2000) *JGR, 105,* 1623-1650.

THE ROLE OF REPTATION IN DUNE SLIPFACE DYNAMICS. Stephen L.F. Sutton[1], C. McKenna Neuman[1] and W. Nickling[2], [1]Dept. of Geog., Trent University, Peterborough, ON, Canada, K9J 7B8, stephensutton@trentu.ca, cmckneuman@trentu.ca, [2]Dept. of Geog., Univeristy of Guelph, Guelph, ON, Canada, N1G 2W1.

Introduction: The sediment dynamics of dune lee slopes has received very little attention when compared with the stoss face. Historically, this interest has focused on the bedding strata or laminations formed through avalanching and grainfall (e.g. [1-3]). However lack of understanding of the process of avalanching, specifically the linkage between the rate of sediment transport over the dune brink with the frequency and magnitude of the event, has hampered the use of laminae in reconstructing dune dynamics from these preserved records.

Two 2-D kinematic dune avalanche models have been developed [4,5], although neither have been field tested. Through their development both avalanche models demonstrated the requirement of an accurate predictive description of the spatial distribution of lee slope grainfall settling (S) for use in determining the changing angle of the slipface slope, and thus the moment of avalanche when the slope reaches its angle of initial yield (θ_i). As the grainfall rate drops off with distance from the crest a "pillow" of sand develops on the upper reach, avalanche initiation will occur when the slope inflection point (the maximum slope of the changing surface) exceeds θ_i. Figure 1 shows an avalanche which initiated mid-slope, and the length of the scarp receding towards the crest shows the extent of this sand "pillow".

Laboratory, field and modeling studies into the grainfall pattern [5-9] have all relied on direct capture of the falling grains and have not examined the redistribution of the grains through reptation, grains rebounding from the bed yet lacking the energy to be considered saltators [10].

Experiments were conducted to investigate the significance of reptation to the pre-avalanche sediment dynamics on dune slipfaces, and its impact on avalanching.

Methods: The experiments were carried out in a Dune Simulation Tunnel (Fig. 1), constructed jointly by the University of Guelph's Wind Erosion Laboratory, and the Desert Research Institute of Nevada. Located in Harley, Ontario, Canada, this tunnel was designed to simulate a small 1.2 m crest height, aspect ratio 0.08 h/L dune for which field observations existed [9], and contained both lee and stoss slopes with a 1:1 scaling.

Measurements of grainfall rates through cup collection, reptation rates with custom reptation traps, and changes in elevation (both through solely grainfall/ reptation, and through grainfall/ reptation/ avalanching) were made using a 3-D laser scanner (Konica-Minolta

Figure 1: Avalanching in the Dune Simulation tunnel. Main avalanche (left) progressing through scarp recession, smaller center avalanches show paralel recession paths and were triggered through excavation by the larger slide.

9i). Reptation pathways were observed at several distances from the dune brink through the use of a laser sheet and recorded with a digital camera.

Results: The evidence indicates that reptation is a significant mode of sediment redistribution on the slipface. Fig. 2 compares the rate of grainfall settling (S) with that of the rate of net deposition or erosion (dQ/dx), where Q is the sediment flux in kg m^{-1} s^{-1}, and x is the distance from crest in m, for the same spatial location. Significantly, reptation sediment delivery rates (dQ/dx > 0) frequently exceed the rate of grainfall by as much as an order of magnitude, especially over the lower slope. Indeed, in only 15% of the observations in Fig. 2 does S account for more than 75% of the total sediment transport for a given location.

Recognizing reptation as a significant mode of sediment transport alters our understanding of dune slipface dynamics. Through redistribution of settled grains further downslope, reptation will alter the rate of change of the slipface angle (θ) as well as the volume of sediment poised to avalanche once θ_I is reached. Previous models [4,5] used solely the settling rate distribution to predict the change in slipface angle and sand volume.

By altering these two parameters reptation becomes an important factor to consider when modeling slipface sediment dynamics, avalanching, and by extension dune grainflow lamane.

References: [1] McKee, E.D., et al. (1971) *Geol. Soc. Am. Bul. 82*, 359-378. [2] Hunter, R. (1977) *Sedimentology, 24(3)*, 361-387. [3] Fryberger, S.G. and C. Schenk (1981) *Sedimentology 28*, 805-821. [4] Allen, J. (1970) *J. Geol. 78*, 326-351. [5] Hunter, R. (1985) *Sedimentology 32(2)*, 409-422. [6] Allen, J. (1968). *J. Sed. Petrol. 38(2)*, 621-633. [7] Anderson, R. (1988) *Sedimentology 35(2)*, 175-188. [8] McDonald, R. and R. Anderson (1995) *Sedimentology 42(1)*, 39-56. [9] Nickling, W. et al (2002) *Sedimentology 49(1)*, 191-209. [10] Mitha, S. et al (1986) *Acta Mech. 63*, 267-278.

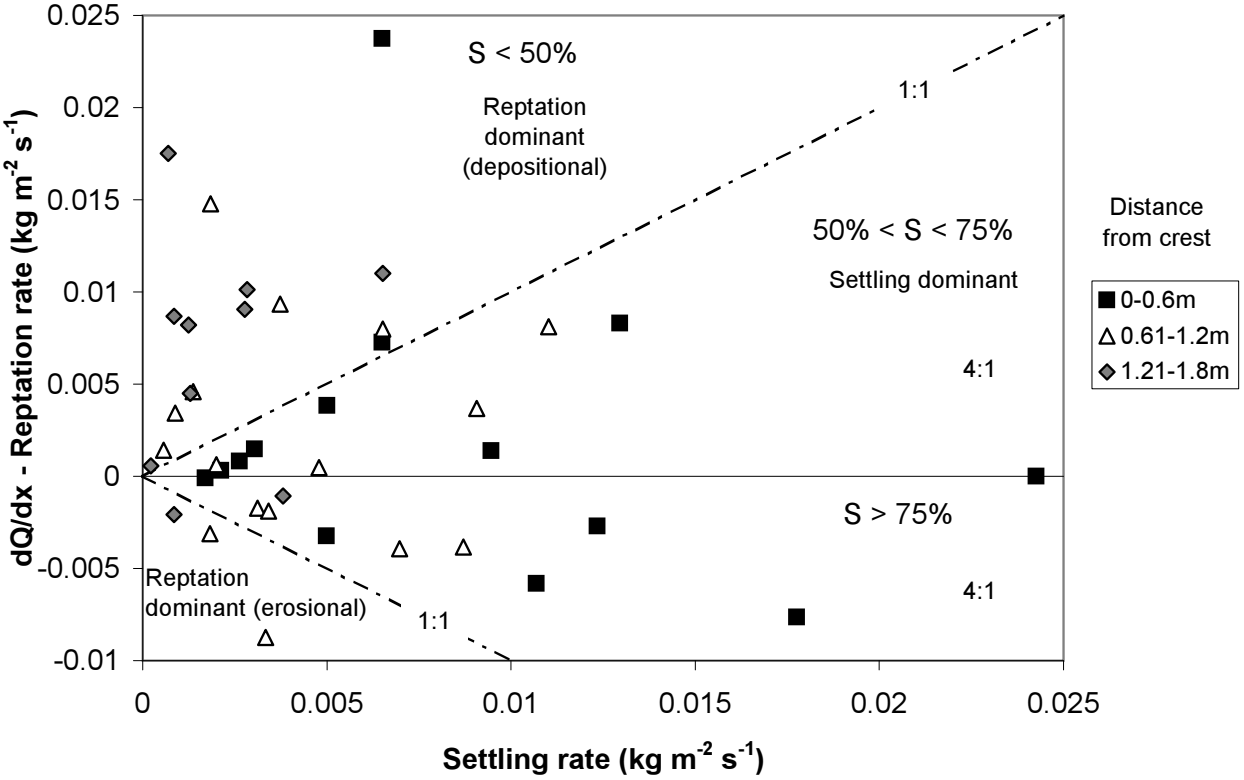

Figure 2: Demonstration of the variability in the importance of reptation compared with grainfall. Delineated are zones where reptation is responsible for the majority of localized sediment dynamics (S<50%), where grainfall exceed reptation by a factor of 4x (S > 75%), and where grainfall is dominant yet repatation accounts for over ¼ of the sediment activity (50% < S > 75%). Reptation tends to dominant for the lower reaches of the dune slipface, and is of less importance higher on the slope where the rate of grainfall is greater.

WHITE SANDS GYPSUM DUNES: A TERRESTRIAL ANALOG TO NORTH POLAR DUNES ON MARS? A. Szynkiewicz[1], L.M. Pratt[1], M. Glamoclija[2], C.H. Moore[1], Esther Singer[1] and D. Bustos[3], ([1]Indiana University Department of Geological Sciences, 1001 East 10th Street, Bloomington, IN 47405-1405, aszynkie@indiana.edu; [2]Geophysical Laboratory, Carnegie Institution of Washington, 5251 Broad Branch Road NW Washington, DC 20015; [3]White Sands National Monument, P.O. Box 1086, Holloman Air Force Base, NM 88330).

Introduction: Many dunes on Earth are indicators of an arid climate where strong aeolian processes cause deposition of well-sorted, fine, sandy material. Although dune *deposition* is primarily associated with arid conditions, the deposition of the source sediments is usually related to water-associated processes.

The White Sands gypsum dunes (WSgd) are the largest known aeolian sulfate-rich deposits on Earth and are an excellent natural laboratory for studying the origins of sulfate dunes. In particular, this communication focuses on the interaction between hydrology and climate that lead to the deposition of the source sediment for the dunes and controls the current dune field morphology.

The WSgd may be a terrestrial analog to the gypsum-rich dunes of Olimpia Undae (OUgd) detected in the north polar region of Mars. The OUgd appear to have undergone complex chemical and physical evolution, possibly involving hydrothermal heating and mobilization of sulfides by fluids, followed by aeolian weathering [1,2,3,4].

The source area for gypsum in the OUgd has not yet been determined but the OUgd are near the north polar cap, a plausible Martian water-source. Also, the proximity of the OUgd to the outwash channels of the Chasma Boreal [2,4] suggests that the gypsum supply might have been controlled by water-involved processes similar to those on Earth.

We have used stable isotope methods at WSgd to determine the source of the original dune sediments, document the involvement of water in their deposition, and to trace the connection of these sediments to the current dune field. We also present examples of aeolian sedimentary features, recognizable on aerial photographs, that show the influence of geochemical processes on the character of the surface morphology as seen "from the air". This study of the WSgd region, at multiple scales, may help in the understanding and recognition of similar processes operating in the OUgd and possibly elsewhere on the surface of Mars.

Geological setting: The WSgd are located in south central New Mexico, in the closed-drainage Tularosa Basin, a graben formed by extensional tectonics in the Rio Grande Rift. The basin is bordered on the east and west by mountain ranges containing Precambrian and Paleozoic rocks. Both the ranges and Tularosa Basin show evidence of tectonic processes within the last 20 ka. The pluvial Lake Otero existed in the northern part of the basin during the late-Pleistocene/Holocene and left gypsiferous evaporative deposits [5]. Regional deflation events have been dated at 7 ka and 4 ka BP [5].

Methods: We sampled a 7 m thick sequence of Holocene age lakebeds from a fault scarp in the southern part of the White Sands National Monument in order to determine the sulfur isotope composition of this probable sediment source for the dunes. Also, gypsum sand was sampled and the sulfur isotope composition determined for samples from 8 transects across the northern, central and southern part of the dune field inside the Monument.

Results and discussion: The current groundwater system at White Sands is dominated by SO_4 ions originated from the dissolution, by meteoric water, of Middle Permian strata with $\delta^{34}S$ values from 10.8 to 12.3 ‰ (all values reported vs. VCDT). However, the range of $\delta^{34}S$ values, from the bottom (11.3 ‰) to the top (13.8 ‰), of the lakebed sequence indicates that an SO_4 ion source with higher $\delta^{34}S$ must have been involved. This source is the Lower Permian strata that has higher $\delta^{34}S$ values (12.5 to 14.4 ‰). Because, in the basin center, the Lower Permian strata are overlain by the Middle Permian approximately 1000 m beneath the surface, the positive excursion of $\delta^{34}S$ values suggests the influx, in the past, of water from deeper parts of the basin into the playa. The change in sulfate source can be tied to climate evolution toward more arid conditions and possibly to tectonic activity that might have increased the release of deeper-seated groundwater through faults extending into the playa surface.

After that time, gypsiferous sediments underwent extensive deflation that led to the formation of the White Sands dune field with parabolic and traverse dunes prevailing on the eastern and western sides, respectively. To explain the evolution of the dune field, we used $\delta^{34}S$ values as a tracer of the gypsum source and compared them to the studied lakebed sequence. The increase of $\delta^{34}S$ values in gypsum sand from the SW towards the NE of the dune field follows the prevailing wind direction (Fig. 1) and suggests that the eastern parabolic dunes were formed from deflation of sediments from the top of the lakebed sequence, and the western traverse dunes were sourced by gypsum coming from older lakebeds that were deflated during a later episode(s). Based on our data, we propose that an approximately 4 m thick sequence of playa sediments was removed from the source region to form the White

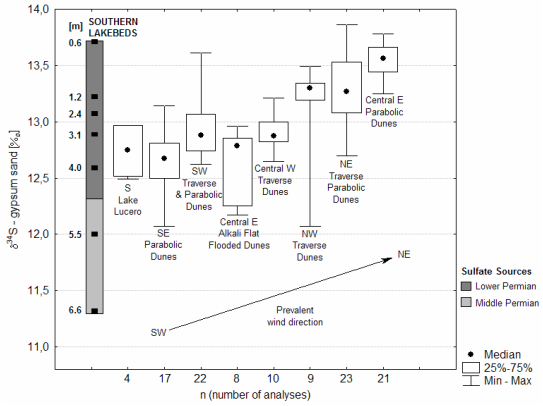

Fig. 1. A box diagram showing the statistical distribution of $\delta^{34}S$ values of gypsum sand in a dune field inside the White Sands National Monument. The left side shows variation of $\delta^{34}S$ values along the sequence of lakebed sediments from the southern part of the Monument. Lighter and darker gray colors indicate the influx of sulfate from dissolution of Middle and Lower Permian strata, respectively.

Sands dunes and that the process was essentially unidirectional.

Today, in the White Sands area, aeolian processes are limited by a relatively high groundwater table [5], advanced dune cementation [6], and re-exposure of an old lacustrine, sulfate-poorer, clay sequence on the playa surface. This indicates that, if the sediment sequence in the playa includes less or non-gypsiferous sediments, the source region may be subject to exhaustion of gypsum. Similarly, the lack of an observed (currently) source area for gypsum at the OUgd, suggests that there were limited amounts of gypsiferous sediments in the north polar region of Mars in the past, or that such gypsiferous sediments have been buried by younger rocks.

Remote sensing is the dominant technique for investigating the Martian surface. Studies of comparable terrestrial geological systems, as analogs, should increase our understanding of geological processes and related morphological features and so help in our interpretation of the geological history of Mars. Aerial photographs of the White Sands area reveal well-developed cross-bedding features related to aeolian transport of sand particles and reveal a long-term record of migration because of advanced cementation (Fig. 2). Large horizontal cross-bedding features are best exposed in the interdune areas and less so in the downwind slopes of dunes. These are stoss slopes of migrating dunes that have been cemented by gypsum and are erosion resistant. In the central parts of interdune areas stoss slopes are progressively buried by

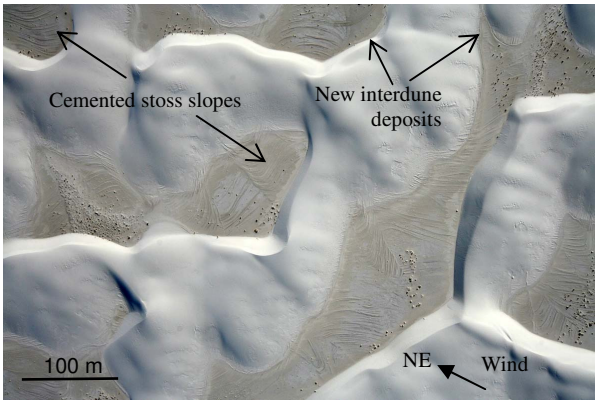

Fig. 2. An aerial photo, taken from an altitude of about 450 m in October of 2007 over the heart of the White Sands dunes and revealing a longer-term record of migration because of advanced cementation of stoss slopes.

wet/damp interdune deposits [7]. After groundwater discharge into interdune areas during the 2006/2007 winter, new interdune gypsum-rich deposits partly covered large cross-bedding features. This process is best visible around interdune areas at the bottom of downwind and slip slopes (Fig. 2).

Conclusions: The $\delta^{34}S$ values in gypsum sand from the WSgd indicate that the dune field was mainly sourced by gypsum precipitated from an old deep groundwater system that discharged into the White Sands area. WSgd formation appears to be linked to a specific time period characterized by a distinct climatic and/or tectonic regime during the Holocene.

The geographical position of OUgd on Mars indicates that a similar sulfate-rich aeolian system might have formed under Martian polar conditions. The spatial distribution of gypsum within OUgd may be connected to melting events in the Martian north polar cap and the OUgd may be indicators of water-involved processes on Mars similar to those observed at WSgd.

Acknowledgments: This study was supported by the NASA Astrobiology Institute team award directed by L.M. Pratt. Sincere thanks are due to Parker Bradley and Kevin Dunshee from a Division of Heron Aerospace Corp. in Alamogordo for obtaining high quality aerial photographs; and to Dave Love for providing new information about the geology of the White Sands area.

References: [1] Fishbaugh K.E. et al. (2007) *JGR, 112, E07002*. [2] Fishbaugh K.E. et al. (2006) *LPSC XXXVII,* Abstract#1642. [3] Tanaka (2006) *Fourth Mars Polar Science Conference,* Abstract#8024. [4] Langevin et al. (2005) Science, 307,1584-1586. [5] Langford R.P. (2003) *Quatern Internat, 104, 31-39*. [6] Schenk C.J. and Fryberger S.G. (1988) *Sediment Geol 55, 109-120*. [7] Kocurek G. et al. (2007) *Sediment Geol 197, 313-331.*

MARS' NORTH CIRCUM-POLAR DUNES: DISTRIBUTION, SOURCES, AND MIGRATION HISTORY.
K. L. Tanaka[1] and R. K. Hayward[1], [1]U. S. Geological Survey, 2255 N. Gemini Dr., Flagstaff, AZ 86001 (ktanaka@usgs.gov, rhayward@usgs.gov).

Introduction: North polar dunes were previously mapped using Viking image data, showing their distribution, morphology, and inferences of sand supply and migration direction [1]. Transverse dunes occur where sand is abundant and summer winds are strong, including Hyperboreae Undae within Chasma Boreale and Olympia Undae across lower Olympia Planum (Fig. 1). The latter occur in a warm zone between areas of residual summer ice in upper Olympia Planum and in the Scandia region, where cyclones develop having counter-clockwise rotation and eastward drift [1]. Recent work based on higher-resolution images has added to this picture. Particularly noteworthy is the recognition of dark, variably-bedded materials from which dark sand is being eroded [2-3].

In this study, we use available post-Viking datasets to map the distribution of the north circum-polar dunes in greater detail, creating a Geographical Information Systems (GIS) geospatial database of dune fields and comparing this information and previous work with recent mapping of dune sources [3]. Based on this comparison, we develop a scenario for the recent migration history of the circum-polar sands.

Dune field and wind-direction mapping: The dune fields in the north polar region are outlined using Thermal Emission Imaging System (THEMIS) infrared images [4] and the Viking image mosaic. The Viking-based north polar geologic map at 1:15,000,000 scale [5] was also consulted, using an updated version that is georeferenced to the more accurately-located Mars Orbiter Laser Altimeter data [6]. Refinements to the dune field mapping and wind-direction measurements are based on THEMIS visible (VIS) [4], Mars Orbiter Camera narrow angle (MOC NA) [7], and Mars Reconnaissance Orbiter (MRO) Context Camera (CTX) [8] images. We also subdivided dune fields based on the dune density, using a relative density parameter defined as the ratio of mean dune length vs. dune crest separation (Fig. 1).

Dune-based wind-direction azimuth measurements were made using MOC NA, THEMIS VIS, and CTX images in instances where image quality permitted sufficient resolution of wind directions based on dune morphology (which entails inspection of slipface orientations). To further simplify our method, we only use the dunes that formed under a unidirectional wind regime (i.e., barchan, barchanoid and transverse), as multi-directional wind regimes often create morphologies that require detailed study to decipher. We then group and average spatially-clustered azimuths, resulting in inferred, local prevailing wind orientations for the latest period of major dune modification. The averaged azimuths are subdivided by color according to the number of measurements averaged (Fig. 1).

Dune mapping results: The overall distribution of circum-polar dune fields matches well with results of Tsoar et al. [1]. The fields entirely ring the north pole in the plains encircling Planum Boreum and upper Olympia Planum, mostly between 70° and 85°N, with a couple gaps a couple tens of kilometers wide over a horizontal range of ~4800 km. Also, a few dense dune fields emerge from depressions in flank areas of Planum Boreum and course southwestward where they meet with a "circum-polar ring"—a collection of dunes that encircles Planum Boreum that is mostly within 100 to 300 km of its periphery. Its farthest southern extent is ~600 km south of Chasma Boreale, which is the deepest part of the northern plains of Mars (<-5000 m elevation). Locally, the circum-polar dune fields embay scattered, high-standing crater rims and ejecta blankets as well as irregular knobs, ridges, and rises in the Scandia region. The densest dune fields appear to be made up of transverse dunes trains that collectively form broad platforms tens to ~200 m thick. These include Olympia, Hyperboreae, Siton, and Abalos Undae (Fig. 1).

The wind-direction measurements appear to be largely consistent with those measured by Tsoar et al. [1], confirming their four wind belts but with some modifications. The off-plateau belt includes the dense dune fields that migrate mostly southwestward from re-entrants in polar deposits (including Tenuis, Boreum, and Olympia Cavi). The fields extend down broad valleys carved into polar deposits; the sandy Planum Boreum cavi unit mapped by [3] (red lines and dots in Fig. 1) appears to be the primary source of these dune fields. The Olympia Undae defines a second wind belt that chiefly has migrated east to west, consistent with both dune orientations [1] and the dispersion of gypsum detection in OMEGA spectral data [9]. Tanaka et al. [3], in agreement with [2], suggested that the cavi unit also underlies most of eastern Olympia Undae and perhaps the western half as well, thus material underlying Olympia Undae may be the primary source of the dune sand (exposure of the cavi unit in Olympia Cavi also contributed to Olympia Undae). East of Olympia Undae a third wind belt is defined by mostly intermediate density dune fields that extend to the prime meridian. These fields are augmented by off-plateau sand migration at Abalos Undae and Hyperboreae and Siton Undae; the latter field is the southernmost high-density dune field and indicates effective transport and deposition of sand from its ap-

parent western and northern sources. The final wind belt surrounds about 60% of Planum Boreum, extending from Scandia to the prime meridian. It includes intermediate- and low-density dune fields, which occur preferentially in lows of Scandia and surrounding the low plateaus of Olympia Mensae. In places west of Olympia Undae on its northern flank, some west-trending wind directions occur, but most others point east to northeast. We think that the belt's most likely sources are sands of Olympia Undae and Cavi, based on its overall westward decrease in dune density. The eastward and northeastward wind trends may reflect recent activity that realigned dune orientations but that did not cause substantial dune-field movement. Finally, the separation between Planum Boreum and most dune fields indicates that off-planum katabatic winds keep the sands pushed away from the planum; the dark surfaces in these areas may be loose sand or exposed bedrock.

If these interpretations are largely correct, north polar dunes preserve a history of largely traceable migration from their source outcrops. Most other possible sources, such as other older plains and polar materials [3], may be largely buried by young mantle materials [e.g., 10] and thus protected from erosion. An exception may be the gypsum in Olympia Undae, which might be scoured from underlying, plains-forming bedrock [3, 11]. Further investigation of wind directions of lower-order or contradictory to the overall pattern may reveal excursions in wind patterns.

References: [1] Tsoar H. et al. (1979) *J. Geophys. Res. 84,* 8167. [2] Byrne S. and Murray B. (2002) *J. Geophys. Res., 107,* E6. [3] Tanaka K.L. et al. (2008) *Icarus, in press.* [9] Langevin Y. et al. (2005) *Science 307,* 1584. [4] Christensen P.R. et al. (2008) *THEMIS Public Data Releases*, http://themis-data.asu.edu. [5] Tanaka K.L. and Scott D.H. and Tanaka, K.L. (1987) *USGS Map I-1802-C*. [6] Skinner J.A. Jr. et al. (2006) *LPSC XXXVII*, Abs. #2331. [7] Malin M.C. et al. (2008) *Mars Orbiter Camera Image Gallery,* http://www.msss.com. [8] Malin M.C. et al. (2007) *J. Geophys. Res., 112*, E055S04. [10] Mustard J. et al. (2001) *Nature 412,* 411. [11] Tanaka K.L. (2006) *4th Mars Polar Sci. Conf.,* Abs. #8024.

Figure. 1. *North polar region of Mars showing distribution of dune fields of low to high relative density (white, ~0.01-0.1; gray, 0.1-0.6; black, >0.8). Wind-direction vectors (arrows) inferred from averaged dune orientations (averaged from <10 (yellow), 10-19 (orange), and ≥20 (red) measurements). Red lines and dots are exposures of the Planum Boreum cavi unit, a main source of dune sand [3] (MOLA color shaded relief base, 5° grid, polar stereographic projection; prime meridian at bottom).*

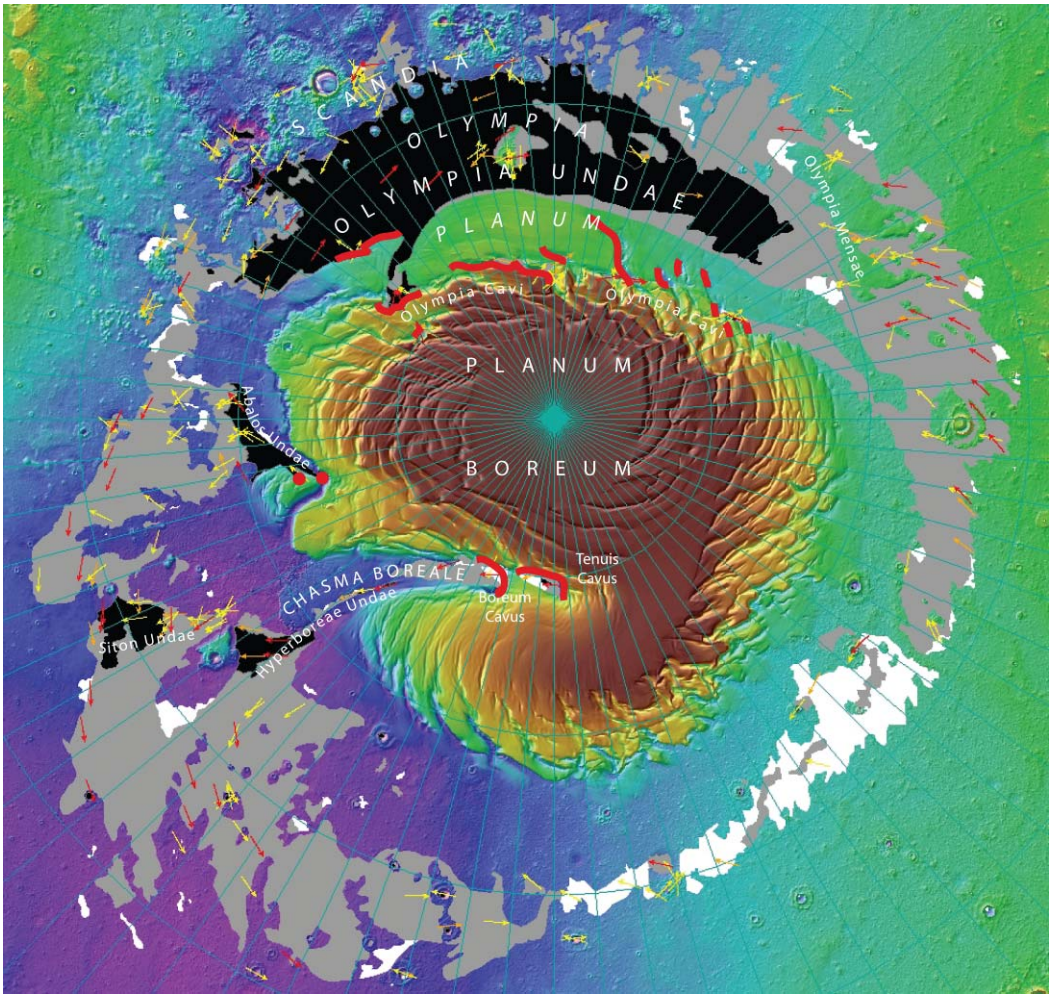

MARS: DARK INTRA-CRATER DUNES ON A REGIONAL SCALE Tirsch, D.[1] and R. Jaumann[1], [1]Institute of Planetary Research, German Aerospace Center (DLR), 12489 Berlin, Germany; daniela.tirsch@dlr.de.

Introduction: Aeolian sand dunes are the topic of numerous scientific studies on Mars. For example, [1] provide a quantitative view of the geographic distribution of dune fields and calculated several necessary properties such as aerial extend, volume, and slip face orientation in a global scale. Local dune field analyses were made by several workers [e.g. 2, 3] who analyzed selected dune fields for grain size, dune-forming winds, volume, sediment sources, and sedimentary history in a local scale. Our analysis is situated in the middle of these two scale types. We focus on dark material occurrences on Martian crater floors by a global selection of 70 impact craters and take a special interest on the intra-crater dark dunes and dune fields. We try to bridge the gap between global and small-scale analysis by investigating local dune field properties and bring them into a global context.

Morphology: The dark material on the selected crater floors can be found in various different deposition types. These can be single dunes, multiple dunes coadunated to huge complex dune fields, but also thin sand sheets. The dune morphology is very diverse (Fig 1): Barchan, barchanoid, and transverse dunes are the most common dune types, but also star dunes, linear dunes and dome dunes can be found on Mars [e.g. 1, 4-7]. The global view of dune type distribution shows that it follows no specific geographically driven aspects but depends on local topography, wind regime, and sediment supply. Figure 2(a) shows that barchan and barchanoid dunes can be found in most of the analyzed localities. Transverse, linear, and star dunes occur more seldom and are preferably situated in huge complex dune fields of the southern cratered terrain. Note that these latter dune types coexist with barchan or barchanoid dunes in most cases. Sand sheets are deposited where the sediment supply is too low for the deposition of aeolian bed forms such as it is in the Thaumasia region and the northern lowlands.

Wind regimes: In most cases, the dune shape is a good indicator for the formative wind regime. For example, barchan dunes develop in unidirectional winds, while linear dunes or seif dunes develop in bidirectional wind regimes [8]. This information is useful for answering the question if the dunes are influenced be current winds or if they were built by paleo wind regimens. In general, if the dune slipface deduced wind directions coincide with current winds, it could be an indicator for recent aeolian dune forming processes [9]. Thus, we compared the morphology deduced wind directions with modeled yearly maximum winds from the Mars Climate Database

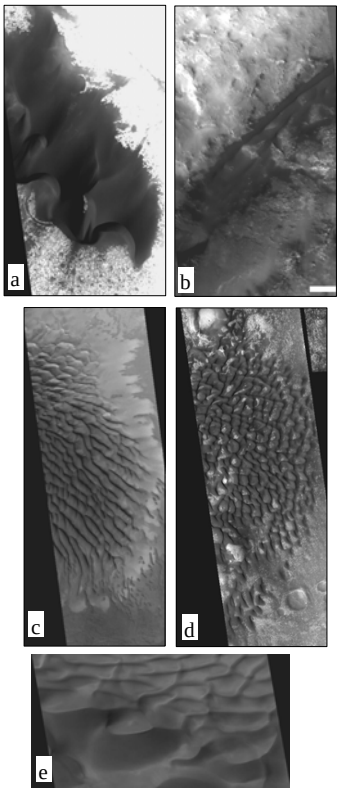

Fig. 1: (a) Barchan dunes in a small crater in Arabia Terra (subset of MGS/MOC image E2200514); (b) Linear dune in Dawes crater (subset of MGS/MOC image 1101900); (c) Transverse dunes in Lyot crater (subset of MGS/MOC image M1800073); (d) Barchanoid dunes in Moreux crater (subset of MGS/MOC image E0100550); (e) Star dunes in a small crater near Argyre Planitia (subset of MGS/MOC image R1501756).

(MCD) [10, 11] for every crater location. The results are shown in figure 2(b), providing a global overview of places where the slipface deduced wind directions coincide with current winds and where not. The maximum wind speeds modeled in the 3.7°/5.6° latitude/longitude grid for 10m above the surface are around 19 s/m. However, [12] established the minimum friction threshold velocity needed to lift sand sized particles on Mars to be 2.2 m/s. This friction velocity corresponds to wind speeds higher than 45 m/s [13]. Thus, the modeled yearly maximum wind speeds are not high enough to initiate saltation. This indicates that unconsolidated dune sands could only be influenced by much stronger winds, at most occurring during dust storm events. These infrequent basic conditions for particle motion (and thus for dune movement) is consistent with several observations that a proportion of Martian dunes seem to be immobile (at

least seasonally) [e.g. 5, 14, 15], and is also consistent with small number of observations of moving dunes [e.g. 3, 7]. Finally, it is not possible to make assumptions about the current wind influence on dunes by the comparison with these yearly maximum wind speed data.

Mineralogy: Analyses of OMEGA near infrared spectra reveal a mafic composition for all the examined dark materials (fig. 3). A detailed description of this analysis is given in [16, 17]. Figure 2(c) provides an overview of the global distribution of the mineralogy of the studied dark material occurrences. Pyroxene is the predominant mineral, while olivine absorptions were only found in 13 of the 70 localities. These unoxidized mafics point to a mechanical weathering of the material without aqueous alteration. However, absorption features pointing to the presence of hydrated minerals (likely phyllosilicates) gives evidence for a chemical alteration of the material in some places. These localities cluster in Arabia Terra. Except of the hydrated minerals, there is no obvious correlation between the geographical location and the mineralogical composition of the mark material. This leads to the conclusion that all the dark materials in Martian craters are in the whole of the same composition and thus might have the same origin.

Acknowledgements: We want to thank François Forget and Ehouarn Millour from the Laboratoire de Météorologie Dynamique du CNRS, IPSL, Paris, for kindly providing the MCD wind data. Furthermore, we thank François Poulet form Institut d'Astrophysique Spatiale, CNRS Université Paris-Sud, France, for developing and kindly providing the technique for the spectral analysis of OMEGA data and the helpful discussions of the results.

References: [1] Hayward, R.K. (2007), *JGR*, *112*, E11007, doi:10:1029/2007JE002943. [2] Fenton, L.K. and J.L. Bandfield (2003), *JGR*, *108* (E12), 5129, doi:10.1029/2002JE002051. [3] Fenton, L.K. (2005), *LPSC XXXVI*, Abstract #2169. [4] Breed, C.S. (1977), *Icarus*, *30*, 326-340. [5] Breed, C. S. et al. (1979), *JGR*, *84*, 8183-8204. [6] Bourke, M. (2004), *LPSC XXXV*, Abstract #1453. [7] Bourke, M. et al. (2007), *Geomorphology*, *94* (1-2), 247-255. [8] Bagnold, R.A. (1954): *The physics of blown sand and desert dunes*, 4 ed., Dover Publications, inc., Mineola, New York. [9] Greeley, R. and A. Skypeck (1993), *JGR*, 98 (E2), 3183-3196. [10] Lewis, S.R. et al. (1999), *JGR*, *104* (E10), 24,177-124,194. [11] Forget, F. et al. (1999), *JGR*, *104* (E10), 24,155-124,175. [12] Greeley, R. et al. (1980), *JGR*, 7(2), 121-124. [13] Sullivan, R. et al. (2005), *Nature*, 436, 58-61. [14] Schatz, V. et al. (2006), *JGR*, 111 E04006, doi:10.1029/2005JE002514. [15] Tirsch, D. et al. (2007), *LPSC XXXVIII*, Abstract #1596. [16] Tirsch, D. et al. (2008), *LPSC XXXIX*, Abstract #1693. [17] Poulet, F. et al. (2007), *JGR*, 112, doi:10.1029/2006JE002840.

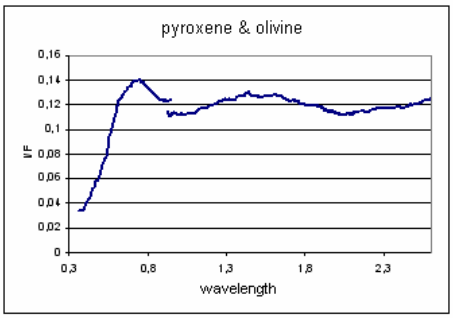

Fig. 3: Typical OMEGA reflectance spectrum of dark material showing pyroxene and olivine absorption features (ORB0295_5).

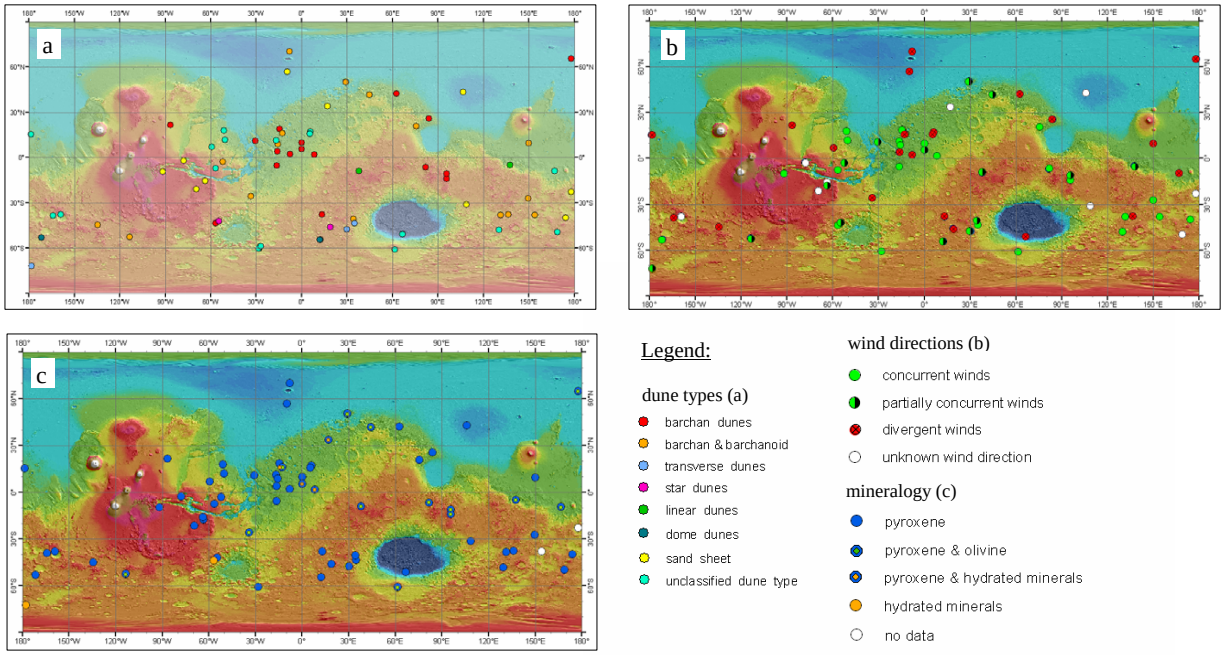

Fig 2: Global consideration of (a) dune types, (b) wind direction comparison, and (c) mineralogy of dark material in the studied craters.

THERMAL INERTIA CHARACTERIZATION OF OLYMPIA UNDAE. T. N. Titus, United States Geological Survey, 2255 North Gemini Dr., Flagstaff, AZ 86004 (ttitus@usgs.gov)

Introduction: With the detection of a widespread water ice table in the Mars polar regions [1,2] and the impending landing of the Phoenix Polar Lander, it is important to understand the thermal inertia and hydration states of both the north polar ice table and the top layer of soil that covers the H_2O ice table (hereafter referred to as ice table).

The presence of hydrated minerals, most likely gypsum, has been identified within part of Olympia Undae by the Mars Express (MEX) near-infrared imaging spectrometer OMEGA [3]. The Mars Reconnaissance Orbiter (MRO) Compact Reconnaissance Imaging Spectrometer for Mars (CRISM) has also mapped out these features [4].

During the site-selection process for the Phoenix Polar Lander, several studies estimated the depth to the ice table at the proposed landing site to be ~1 to ~10 cm [5]. In one of these studies, Bandfield [6] used multiple Mars Odyssey Thermal Emission Imaging System (THEMIS) observations to estimate depths to the ice table at high spatial resolution (~100 m); this study found large variation of ice table depths at the 100 m scale.

Feldman et al. [7] have used both the Mars Odyssey Neutron Spectrometer (NS) and the Mars Global Surveyor (MGS) Thermal Emission Spectrometer (TES) observations to further constrain the ice composition distribution of Olympia Undae.

In this study, we use MGS TES temperature observations immediately following the springtime disappearance of seasonal CO_2 to estimate the depth to the ice table and the thermal inertia of both the soil and ice table within the Olympia Undae and the region of Vastitas Borealis south of Olympia Undae. The methodology used in this study is similar to that used by Feldman et al. [7], except we include temperatures from both the day and night, as well as temperatures from the season immediately following the disappearance of CO_2 ice. Feldman et al. [7] excluded the temperatures from both the daytime and the earlier seasons to minimize systematic errors caused by variations in surface and atmospheric conditions, such as dust opacity and albedo. However, by including these additional observations, we can estimate the underlying ice table thermal inertia.

KRC Model and TES Data: We used the MGS TES thermal bolometer brightness temperatures and solar albedo observations to constrain the depth of the soil overburden covering the ice table. We use a thermal model originally written by Hugh Kieffer, KRC [8], to fit the rise in both the 2AM and 2PM brightness temperatures following sublimation of seasonal CO_2 frost. This approach has proven successful in detecting both the presence of exposed H_2O ice and estimating the overburden for buried H_2O ice [9].

Several thermal models are generated for a range of soil depth, soil thermal inertia, and ice table thermal inertia values. We then use a least-squares best-fit approach to match the brightness temperatures with the model that provides an estimate of both the depth and thermal inertia of the soil and the thermal inertia of the ice table.

Results: Estimates of the depth and composition of the soil and ice table derived from the diurnal and seasonal temperature trends are generally consistent with prior thermal and high-energy (neutrons and gamma rays) studies [10, 11, 12].

Thermal Edge of the Ice Table: Based on the results from the analysis of Phoenix Region B [12], the thermal edge of the ice table is approximately where the lower layer thermal inertia drops below 600 $Jm^{-2}K^{-1}s^{-1/2}$. Based on this criterion, the thermal edge of the ice table is ~67ºN latitude for the longitude range 140ºE-220ºE. Fig. 1c shows this effect for the longitude range 180ºE-220ºE.

Thermal Properties of Olympia Undae. The thermal inertia of the top layers of Olympia Undae appears to be similar to that of lower latitudes within Vastitas Borealis which is ~200 $Jm^{-2}K^{-1}s^{-1/2}$. The depth of this top layer is also similar to lower latitudes of Vastitas Borealis with a depth of ~5-7mm. The difference between Olympia Undae at the lower latitudes (65N-70N) is the underlying layer, which has a thermal inertia consistent with ice. Near the same location that the NS observes a drop in Water Equivalent Hydrogen (WEH), the lower layer thermal inertia drops from ~1600 $Jm^{-2}K^{-1}s^{-1/2}$ to ~1100 $Jm^{-2}K^{-1}s^{-1/2}$, suggesting a significant drop in water ice content.

Future Work: The highest thermal inertia used for thermal models used in this study was ~1600 $Jm^{-2}K^{-1}s^{-1/2}$. Since pure CO_2 ice has a thermal inertia of ~2000 $Jm^{-2}K^{-1}s^{-1/2}$, additional analysis must be conducted using higher thermal inertia values for the ice table.

References: [1] Boynton, W.V. et al. (2002) Sci., 297, 5578. [2] Feldman et al. (2002) Sci., 297, 5578. [3] Langevin et al. (2005) Sci., 307, 1584. [4] Roach et al. (2007) LPSC XXXVIII, Abstract #1970. [5] Mellon et al. (2008) submitted [6] Bandfield, 2007 [7] Feldman et al. (2008) Icarus, in press. [8] Kieffer, H.H. (1977) JGR, 82, 4249-4291. [9] Titus, T. et al. (2003),

Sci, 299, 1048-1051. [10] Titus et al. (2005) AGU Fall Meeting, Abstract #P31A-0197 [11] Titus et al. (2006) LPSC XXXVII, Abstract #2161 [12] Titus et al. (2007) LPSC XXXVIII, Abstract #1338.

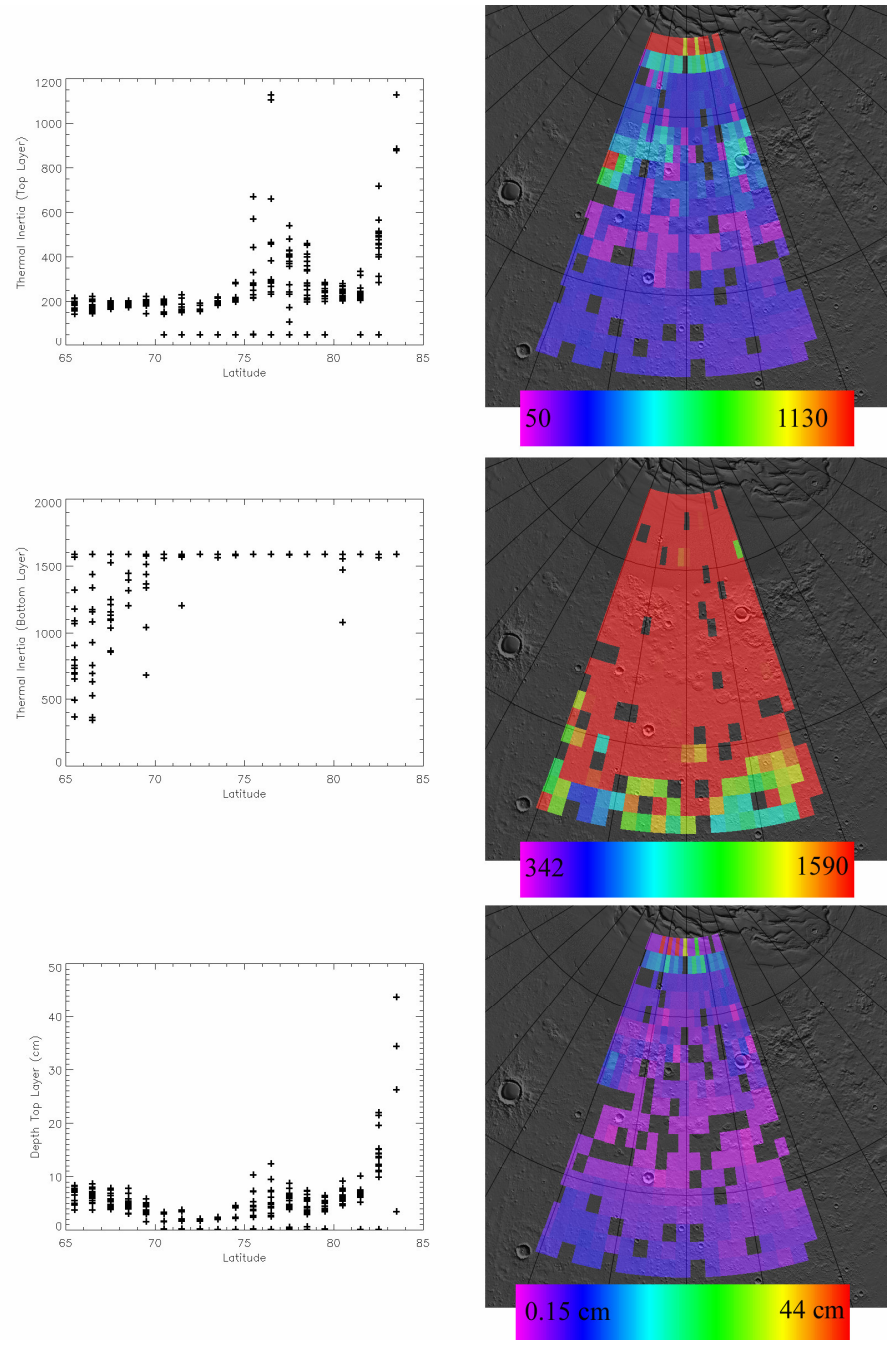

Figure 1: Results of Thermal Model Fits to 1°(Lat) x 2°(Lon) for the eastern part of Olympia Undae extending south into Vastitas Borealis. The maps are centered at longitude 200°E and extend from 180°E to 220°E, and from 65°N to 84°N. (A) Plot of top layer thermal inertia vs. latitude. (B) Regional distribution of the top layer thermal inertia. The majority of the top surface layer is between 150 $Jm^{-2}K^{-1}s^{-1/2}$ and 200 $Jm^{-2}K^{-1}s^{-1/2}$. (C) Plot of the bottom layer thermal inertia vs. latitude. (D) Regional distribution of the bottom layer thermal inertia. Red colors indicate a thermal inertia value ~ 1600 SI units. Because 1600 SI units was the highest thermal inertia used for the ice table, these thermal inertia values could actually be higher (E) Plot of the thickness of the top layer (cm) vs. latitude. (F) Regional distribution of the top layer thickness.

LINEAR DUNES ON EARTH AND MARS - SIMILARITY AND DISSIMILARITY. H. Tsoar, Department of Geography and Environmental Development, Ben Gurion University of the Negev, Beer Sheva 84105, Israel, e-mail: tsoar@bgu.ac.il.

Linear dunes on Earth: There is more than one sand dune type characterized by a linear or a longitudinal pattern. These linear dunes fall into two type categories, characterized by a simple longitudinal pattern corresponding to vegetated and un-vegetated surfaces. While the former are known as vegetated linear dunes (VLDs), the latter are better named seif (sword in Arabic, because of the sharp crest). All linear dunes possess one common characteristic of elongation that differentiates these from transverse and barchan dunes where the whole body of the dune advances. Another dune type that resembles seif dune is lee dune (also known as sand shadow [1]). Lee dunes have linear shape with a sharp-edged crest and are formed from sand that accumulates at the lee side of obstacles such as boulders, cliffs, shrubs or bushes.

Seif dunes are common in the driest deserts, where vegetation cannot survive, such as the Namib or the Sahara. A typical characteristic of the seif dune is the sinuosity of the crest. From its primary formation, seif dune is affected by wind flows coming obliquely from both sides of its slopes, meeting the dune at an acute angle of attack and separating over the crest-line. Each wind flow is diverted at the lee slope to blow parallel the crest-line in a down dune direction. Deposition occurs where the dune meanders and the angle of wind attack becomes consequently less acute and the wind's magnitude over the lee slope gradually drops.

VLDs have a different shape with a rounded crest. They are sparsely or densely covered by vegetation. VLDs may run in parallel for scores of kilometers and are known to cover vast areas of the deserts of Australia and the Kalahari in South Africa [2, 3]. Vegetated linear dunes extend parallel to the dominant wind direction and can be formed in areas with unidirectional winds. An exclusive attribute of vegetated-linear dunes is the tendency for two adjacent dunes to converge and continue as a single ridge. Convergence is in the form of a Y-junction (tuning fork) commonly open to the formative wind. Some descriptions of linear dunes on planets emphasize the Y-junctions [4, 5].

It is not so clear whether VLD is a seif dune that stabilized because of climate change or a distinct dune type. Some argue that when vegetation cover is reduced or eliminated, VLDs may evolve towards seif dunes [6], while others claim that straight VLDs can only form in the presence of vegetation cover [7].

Linear dunes on mars: As was mentioned above, seif dunes on Earth are wiggling like a river meanders. This form is essential for the dune's elongation mechanism [8]. Seif dunes elongate approximately in the direction of the resultant of the two main wind directions. Meandering linear dunes are rare on Mars. On the other hand, rectilinear dunes that have sharp crest line, similar to that of a seif, are more common on Mars where they are always intermingling with barchan dunes (an indication of unidirectional winds; Fig. 1). These linear dunes on Mars are not compatible with the known seif dunes of Earth because of the shape and dynamical differences, although some researchers have referred to the Martian rectilinear dunes as seif [9,10].

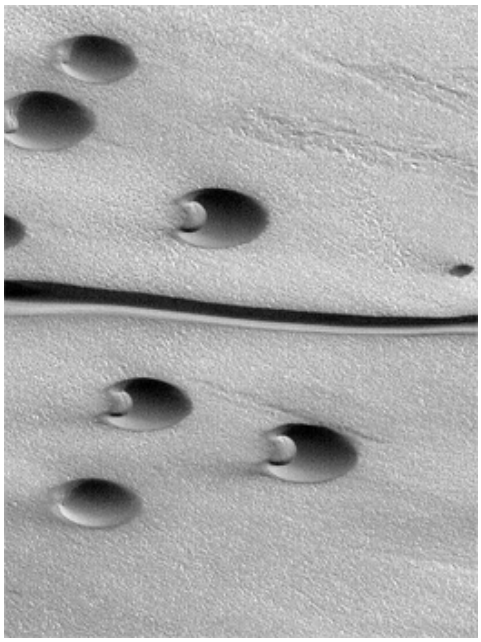

Figure 1. Barchan dunes and a single rectilinear dune in the Martian North Polar Region at 84.4°N 26.4°W. Picture is 1.5 km wide. Mars Global Surveyor - Mars Orbiter Camera image (NASA/JPL/Malin Space Science Systems).

Hypothesis and discussion: We assume that the differences in the shape of linear dunes on Earth and Mars stem from the phenomenon of induration of the dunes (crust formation) on Mars and especially in the Martian North Polar Region. Crusts may form as water vapor diffuses into and out of the fine-grained materials on the planet's surface. Salts would be deposited as intergranular cement. Because these bedforms occur mostly in the polar region, the cementing agent

could be ice instead of salts; indeed, the dunes spend more than half each Martian year beneath a covering of seasonal frost, mostly frozen carbon dioxide. Elliptical shaped barchans that were indurated on Mars [11] form an obstacle to the wind. Once a barchan is stabilized by induration or crust, it functions as an obstacle to the wind. If sand is transported from the upwind direction, short lee dune that has a linear shape with a sharp-edged crest is formed from sand accumulation at the lee side of obstacles. This linear lee dune stabilizes quickly by ice (water or carbon dioxide) or mineral crust and continues to lengthen and to form a long linear dune that aligns parallel to the wind. Melting of the ice will set up a straight linear dune, with loose sand, parallel to the dominant wind. Such a dune shape is not stable and tends to disintegrate into a string of small barchans.

Field observations on terrestrial deserts show that when vegetation is removed from VLD, the bare linear dune disintegrates into small barchans. Simulation also shows that linear dune, aligning parallel to the wind direction, is unstable and deforms until it takes the shape of a string of barchans, which are the stable shape under unidirectional winds.

References: [1] Bagnold R. A. (1941) *The physics of blown sand and desert dunes*, Methuen, London. [2] Wasson R. J. et al. (1983) *Z. Geomorph. Supp. Bd. 45*, 117-151. [3] Wiggs G. F. S. et al. (1996) *Earth Surf. Proc. Landf. 21*, 19-34. [4] Lee P. et al. (1993) *Bull. Am. Astron. Soc. 25*, 1038. [5] Lorenz R. D. et al. (2006) *Science 312*, 724-727. [6] Lancaster N. (1995) *Geomorphology of desert dunes*, Routledge, London. [7] Tsoar H. (1989) *Prog. Phys. Geog. 13*, 507-528. [8] Tsoar H. (1983) *Sedimentology 30*, 567-578. [9] Edgett K. S. and Malin M. C. (2000) *LPS XXXI* Abstract #1070. [10] Malin M. C. and Edgett K. S. (2001) *J. Geophys. Res.-Planets 106*, 23429-23570. [11] Schatz V. et al. (2006) *J. Geophys. Res.-Planets 111*, Art. No. E04006 APR 04028 02006.

COMPARATIVE STUDY OF HIGHER-ORDER NEIGHBOUR STATISTICS AND DUNE FIELD SELF ORGANIZATION FOR THE HYPERBOREAE UNDAE AND OLYMPIA UNDAE ERGS, MARS. A. J. Wheeler[1] and M. A. Bishop[1,2], [1]School of Natural and Built Environments, University of South Australia, SA 5095, Australia (andrew.wheeler@postgrads.unisa.edu.au), [2]Planetary Science Institute, 1700 East Fort Lowell Road, Tucson, AZ 85719, USA (bishop@psi.edu).

Introduction: Ordered neighbor analysis has shown that dune geography for high-latitude dune fields on Mars is not a random process, but one that identifies with a geomorphic system that has evolved towards a pattern of uniformity across a variety of spatial scales [1]. Wilkins and Ford [2] have suggested also that eolian systems reflect, within different spatial regions of the field, the sum of changes that result in the spatially variable states of dune field organization. Therefore, if barchanoid form of Martian circumpolar dunes, represents a geomorphic system approaching a high degree of self-organization, as exemplified from Hyperboreae Undae, then such a state may be considered to have been numerically characterized by a nearest neighbor index that approaches a dimensionless value of $R \sim 1.42$, and by higher order neighbors that show a tendency towards randomness. Such dimensionless values may be regarded as geographical signatures of crescentic dune self-organization.

HiRISE imagery of portions of dunefields between Olympia Undae and Siton Undae (~ 120° of longitude east from Hyperboreae Undae) presents an opportunity to compare ordered neighbor analyses between north polar ergs and refine the geographical signatures of circumpolar crescentic dune self-organization.

Methodology: Nearest neighbor (NN) or 1st-order statistics identify a particular pattern (clustered, random, dispersed) at the local scale, while higher order statistics are capable of detecting heterogeneous processes at regional or global scales [3]. It has been shown that spatial statistical analysis using Mars Orbiter Camera (MOC) data within a GIS offers quantitative methods from which an understanding of Martian dune geography can be surmised [1].

Some 2800 data points, selected from nine MOC images of Hyperboreae Undae dunefields, were reduced to a set of six-index values, the dimensionless statistic *R*. From these, several major findings were determined for the spatial characterization of dunes associated with the Hyperboreae Undae erg at the Martian north pole and served as benchmarks for understanding the techniques, results and interpretations of point pattern analysis and the distribution of simple and compound crescentic dunes for an extra-terrestrial landscape.

A portion of a dunefield marginal to Olympia Undae, is seen in HiRISE image PSP_001660_2570 (Figure 1). From this, 1216 data points consisting of dome, barchan and barchanoid dunes in simple, compound and complex morphologies, were reduced to a set of six *R* values. Further intra-field analyses were performed on discrete dune forms (barchanoid, barchans and dome).

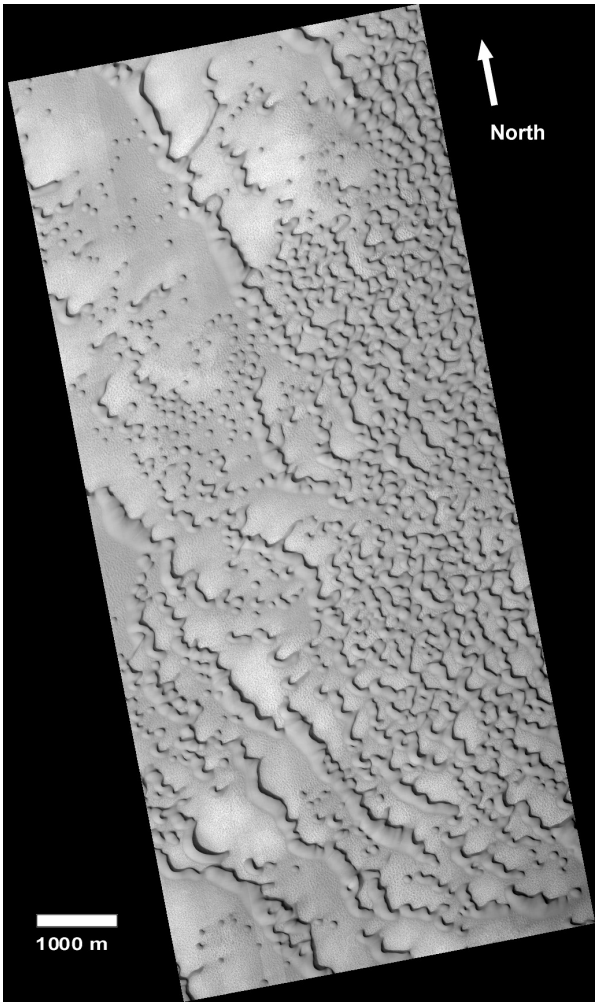

Figure1: Crescentic dunes of the North Polar region, Mars. HiRISE image PSP_001660_2570 centered at 109.6°E 76.7°N.

(The authors acknowledge the use of the HiRISE image processed by HiRISE Operations Centre and available at http://hiroc.lpl.arizona.edu/images/PSP/index.html).

Results and Discussion: The NN statistics show that the pattern for crescentic dunes is one of statistically significant dispersion, R = 1.12, with higher order neighbors successively tending towards spatial randomness (Table 1).

Ordered Neighbor	*R-statistic*	Z_R	*Pattern*
1st	1.12	6.64	Dispersed
2nd	1.06	5.44	Dispersed
3rd	1.04	5.13	Dispersed
4th	1.04	5.34	Dispersed
5th	1.03	5.02	Dispersed
6th	1.03	5.28	Dispersed

Table 1: Ordered neighbor statistics for 1216 crescentic dunes, Olympia Undae (Area of dune sample = 88.32 km²; spatial resolution of PSP_001660_2570 = 0.50m/pixel)

This is consistant also with results obtained from the Hyperboreae Undae (Figure 2). The values for the pattern of dispersion are among the lowest recorded for dunefields on the northern plains at this time. This is particularly true for the nearest neighbor (Figure 2). For Hyperboreae Undae, Bishop [1] has implied that locations exhibiting intermingled duneforms have demonstrated lower *R*-indices. Domes, barchans, barchan-seif, short barchanoid 'chains' and barchanoid ridges are all identified in relatively large numbers in this dunefield. This suggests that morphological diversity correlates with self-organization and maturity of the eolian system. Image PSP_001660_2570 is located marginal to the Olympia Undae erg where nascent barchans (transitional domes) and barchans are in the process of organizing into barchanoid 'chains' and ridges.

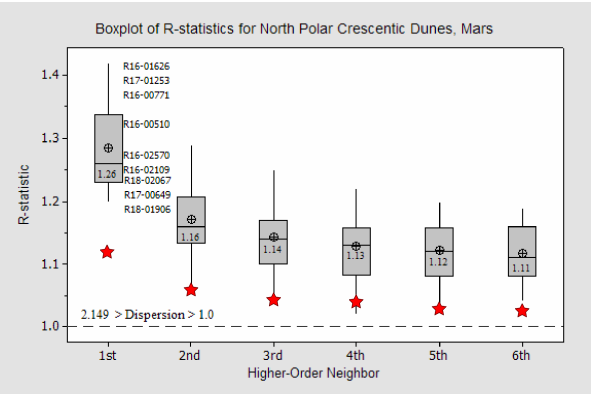

Figure 2: A boxplot of the distribution of the *R*-statistic for the nearest neighbor and higher order neighbors for crescentic dunes of Hyperboreae Undae. 'Star' symbols represent the *R*-statistic for crescentic dunes marginal to Olympia Undae.

Summary: Spatial statistical analysis, as a means to investigate Martian dune geography, has determined a number of major findings for the spatial characterization of dunes associated with Hyperboreae Undae on the Martian north polar plains. A comparative study at a dunefield marginal to Olympia Undae, was undertaken to test these findings.

Firstly, the nearest neighbor *R*-statistic, regardless of crescentic dune morphology, expresses the most significant degree of dispersion relative to the *R*-statistic of all other higher ordered neighbors and is consistent between ergs. Secondly, crescentic dunes, regardless of morphology, have a tendency towards increasing spatial randomness as the distance between neighbors increases (i.e. at higher order neighbors). Thirdly, crescentic dune fields comprising barchanoid morphology exhibit the highest *R*-statistics relative to fields comprised of interspersed domes, barchan, barchanseif, and short barchanoid 'chains' and is consistent between ergs. Dunefields marginal to the ergs, where morphological diversity is greatest, exhibit the lowest *R*-statisitcs relative to dispersion and tend towards random organization.

Further comparative studies at both the margins and interior of other regions (for example; Siton Undae, Nili Patera and southern intracrater and intercrater dunefields) alongside terrestrial sites will better clarify the relationship between spatial patterns, self-organization and the state of geographical maturity of dunescapes.

References: [1] Bishop M.A. (2007) *Icarus 191* 151-157. [2] Wilkins D.E. and Ford R.L. (2007) *Geomorphology 83* 48-57. [3] Wong W. S. and Lee J. *Statistical Analysis of Geographic Information with ArcView GIS® and ArcGIS® (2005)* John Wiley & Sons, Inc., New Jersey. pp 246-248.

Aeolian Megaripples as a Self-Organization Phenomenon: Mathematical Modeling, Field Studies and Implicatuins to Martian Megaripples . H. Yizhaq [1], Ori Isenberg[2], Rimon Wenkrat[2] and Haim Tsoar[2], [1] Solar Energy and Environmental Physics, BIDR, Ben-Gurion University, Midreshet Ben-Gurion, Israel (yiyeh@bgu.ac.il), [2] The Department of Geography and Environmental Development, Ben-Gurion University, Beer Sheva, Israel (orisenberg@gmail.com, rimon@bgu.ac.il, tsoar@bgu.ac.il).

Introduction: Aeolian sand ripples are a common feature on sandy deserts and beaches. Standard aeolian ripples have wavelengths of a 10-15 centimeters and amplitudes of few millimeters. Megaripples, which are much larger ripples, are composed of a mixture of coarse and fine grains. They are characterized by a bi-modal distribution of particle sizes, which is necessary for their formation. Megaripples are bigger in size than regular ripples.

Interestingly enough, aeolian processes are extremely important for understanding the geology of Mars [1]. Images from the Mars Global Surveyor clearly portray dust storms, dust devil traces, dunes and megaripples. Large ripple-like bedforms have been observed in numerous locations on the planet [2]. Various applications of sand ripple studies on Earth and Mars were recently reviewed by Rubin [1]. We present here results from a fieldwork of one and a half year conducted at Nahal Kasuy's mega-ripples field located in the southern Negev Desert, Israel. The Aeolian megaripples in Nahal Kasuy have mean wavelength of about 70 cm (Fig. 1). Regular sand ripples superposed on mega-ripples, are formed by weaker winds of a different directions. We also present a simple mathematical model which is based on Anderson's model [3]. The model with the field experiments show that the basic mechanism responsible for megaripples formation is the same as for normal ripples i.e spatial change in reptation flux. The large wavelength is due to the coarsening process. The large wavelength of megaripples reflects longer time which the patterns have been developing through interactions between smaller ripples. The megaripple system exhibits a self-organization behavior, where ordered spatio-temporal structures spontaneously emerge [4].

Field results: We present here preliminary results from our fieldwork on mega-ripples formation from a flat surface. Mean diameters of coarse and fine grains are 0.7 mm and 0.18 mm, respecteively. The time evolution of the megaripples, starting from a flat surface, was monitored. Megaripples grow due to coarsening mechanism. They start their development as regular ripples that subsequently coarsen via coalescence with other ripples. The smaller, faster-moving ripples overtake larger, slower-moving ripples, resulting in increased size and spacing (Fig. 1). The final state is analyzed by a new technique we developed, using a digital elevation model (DEM) constructed from stereo digital photographs. We also present data on the wind power (DP=drift potential) during the fieldwork and grain-size analysis of samples taken from the mega-ripple crest and trough. The grain-size characteristics are used to prove that due to the low wind power at Nahal Kasuy, only the fine particles saltate. The megaripples evolution at Nahal kasui is slow (more than one year) due to the low value of DP (50 in 2007).

Figure 1. The plot which we had flattened on January 2007, on March 15 (a) and Februray 1st 2008 (b) . The ripples wavelength is about 15 cm in (a) (the ruler's length is 1 m) and increases to 40 cm in (b) .

Mathematical model: Here we adopt the view of ripple formation that was formalized by Anderson [3]. According to this interpretation, the only role of saltatin grains is to bring energy to the system, extracting it from the wind that blows above the sand surface which is consist of fine and coarse particles. In this view, ripple formation is entirely due to spatial chages in the reptation flux of coarse and fine particles. We build a

one dimensional heuristic model of sand transport based on the Exner equation [5]:

$$(1-\lambda_p)\rho_p \frac{\partial h}{\partial t} = -\frac{\partial Q}{\partial x}, \qquad (1)$$

where $h(x,t)$ is the local height of the sand surface at point x and time t, ρ_p is the porosity of the bed, and $Q(x,t)$ is the sand flux which include both saltation and reptation flux. Here, we assume that saltation flux can be taken as constant and we do not consider it in the Exner equation. Thus, in Eq. 1 we take into account only reptation flux of fine and coarse particles, Q_{rf} and Q_{rc} repectively. The repatation flux at a certain point and time, is obtained by the sum on all the grains that are passing by that point at that time. The grains have a probability distribution of repatation lengths. Following Anderson [3] we derive the explict expressin for reptation flux on a flat surface:

$$Q^0_{rf} = m_f n_{rf} \int_{-\infty}^{\infty} d\alpha\, p_f(\alpha) \int_{x-\alpha}^{x} N_{im}(x')dx' \qquad (2)$$

$$Q^0_{rc} = m_c n_{rc} \int_{-\infty}^{\infty} d\alpha\, p_c(\alpha) \int_{x-\alpha}^{x} N_{im}(x')dx,$$

where the subscript f denotes fine grains and c stands for coarse particles. m_f, m_c are the mass of each particle, n_{rf} and n_{cr} are the average numbers of reptating grains ejected by the impact of one saltating grain, and p_f, p_c are the probability distributions of reptating grains, taken as exponential. Because saltation flux is uniform, and the fixed angle ϕ at which the grains descend back to the ground is assumed to be constant, the number density of impacting grains change only because of varations in bed slope. Baesd on geometrical considerations, we obtain,

$$N_{im}(x) = N^0_{im} \frac{1+h_x \cot\phi}{\sqrt{1+h_x^2}}, \qquad (3)$$

where h_x is the local slope and N^0_{im} is the number density of impacting grains on a flat surface. We further modify Eq. (2) to take into account correction of the reptation length on inclined plane [5]. This correction leads to a mean repatation length that is shorter on the windward slope and longer on the leeward slope of the bedform. The full model can be written as:

$$h_t = -Q_0 \partial_x \left[(1-\mu_f) Q^0_{rf} + \delta(1-\mu_c) Q^0_{rc} \right] \qquad (4)$$

where the parameters μ_f and μ_c heuristically includes the correction to reptation flux discussed above, $Q_0 = m_f N^0_{im} \cot\phi / \rho_b (1-\lambda_p)$ and $\delta = m_c / m_f = (D_c / D_f)^3$. According to Bagnold [6] a saltation grain can sustain a forward movement of a coarse grain with a diameter 3-7 times larger than its own diameter thus, $27 \le \delta \le 343$.

Fig.2 shows numerical solutions of the model equations (Eqs. 2-4). The smaller, faster-moving ripples overtake larger, slower-moving ripples, resulting in increased size and spacing. Merging can be viewed as a selection process leading to the production of bedforms with similar-sized ripples

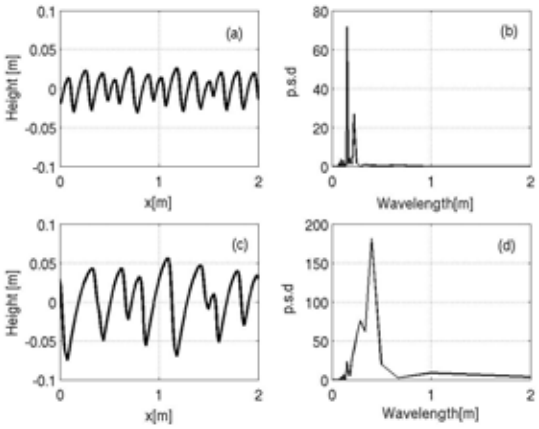

Figure 2. Numerical soutions of the model equation at intial times (a) 0.5 minute, (c) 3 minutes and the corresponding power spectrum density (subplots b and d). After two minutes the average wavelength increased from 15.38 to 40 cm. The mean reptation lengths of the coarse and fine grains were 5 cm and 1.5 cm respectively.

Disscusion: Field experiments conducted at Nahal Kasuy dunes field located at the southeren Negev in Israel, show that megaripples start as normal ripples and grow due to rapid coarsening process. Their evolution is a function of DP (drift potential) and the wind direction variability. Storms can inject new defects to the system by breaking existing megaripples crest and change their dirction. The mathematical model we developed can be used to describe Martian megaripples once the diameter ratio between coarse and fine particles and the number density of impact grains and the average repataion lengths are known.

References: [1] Rubin, D.M., (2006). *Eos.*, 87, 30, 293-297. [2] Jerolmack, D.J. (2006) *JGR*, 111, E12502. [3] Anderson, R. S. (1987) *Sedimentology*, 34, 943-956. [4] Anderson, R. S. (1990) *Earth-Science Reviews*, 29, 77-96. [5] Yizhaq et al, (2004) *Physica D*, 195, 207-228. [6] Bagnold, R.A., 1941. *The Physics of Blown Sand and Desert Dunes*. Methuen, London.

PLANETARY DUNE FIELDS: EXAMPLES OF PERFORMANCE UNDER PRESSURE. J. R. Zimbelman, CEPS/NASM MRC 315, Smithsonian Institution, Washington, DC 20013-7012; zimbelmanj@si.edu.

Introduction: Aeolian studies focus on deposits and processes observed at the interface between a wind-driven atmosphere and a surface of particulate materials, possibly including large blocks or bedrock. Robotic exploration of the solar system has expanded the range of environments in which aeolian deposits have been documented. This report focuses on dune fields observed on several planetary surfaces, following a sequence from lowest to highest atmospheric pressure (Table 1).

Table 1: Properties of planetary environments [from 1]

	Venus	Earth	Mars	Titan
g (m/s^2)	8.88	9.81	3.73	1.36
p (mb)	90000	1013	7	1600
Comp. (%)	CO_2, N_2	N_2, O_2	CO_2, N_2	N_2, CH_4
	(96, 3.5)	(77, 21)	(95, 2.7)	(90, 10)
T_{surf} (°C)	480	22	-23	-200

Mars: Dune fields were first observed on Mars in Mariner 9 images [2]; subsequent spacecraft provided information on the diversity and distribution of dunes across the planet [e.g. 3-5]. Other than the north circumpolar dune field [6], most dune fields on Mars occur on the floors of large impact craters (Fig. 1) [3, 4].

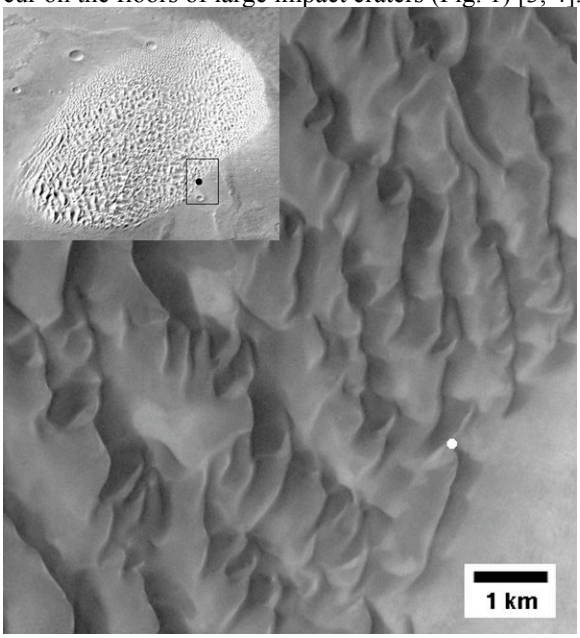

Figure 1. Dune field in Proctor crater, Mars, 47.8°S, 30.7°E. THEMIS V16837003, 17 m/p (ASU). Inset: THEMIS mosaic [7]. Dots show location of Figure 2.

For example, the Proctor dune field has been the subject of detailed mapping and monitoring [8], now supplemented by coverage from HiRISE (Fig. 2). Martian dunes display a variety of forms, from barchans to transverse ridges [3], but there is a lack of longitudinal dunes [9]. MER observations indicate both basaltic sand and dust aggregates on aeolian bedforms [5, 10].

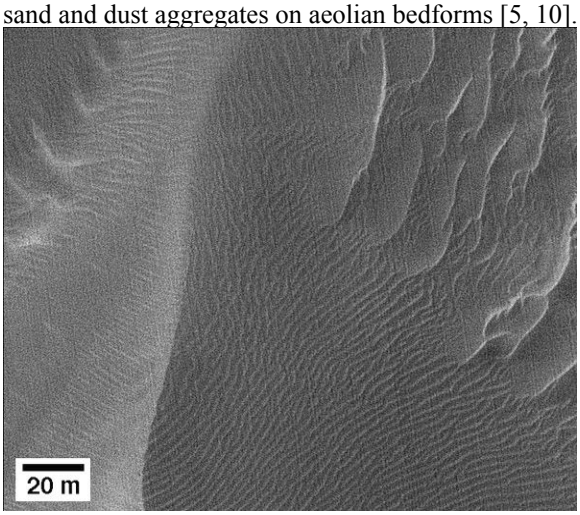

Figure 2. HiRISE view of Proctor dunes and ripples (see Fig. 1). PSP_002455_1320, 25 cm/p (U of A).

Earth: Spacecraft sensors documented dune fields across the planet [e.g., 11] at scales comparable to recent data from Mars (compare Figs. 1 and 3). The vast

Figure 3. Kelso dune field, California, 34.901°N, 115.727°W. ASTER data, acquired on 10/17/00, 15 m/p [12].

array of dune forms found on Earth [e.g., 1, 11, 13] have not yet been observed on other planets, but the physics of particulate movement by the wind established on Earth [14] is readily applicable to other planetary environments [1].

Titan: The RADAR experiment on the Cassini spacecraft is mapping swaths across haze-shrouded Titan; primarily in equatorial areas, large fields of longitudinal dunes are common (Fig. 4, [15]). Radar data

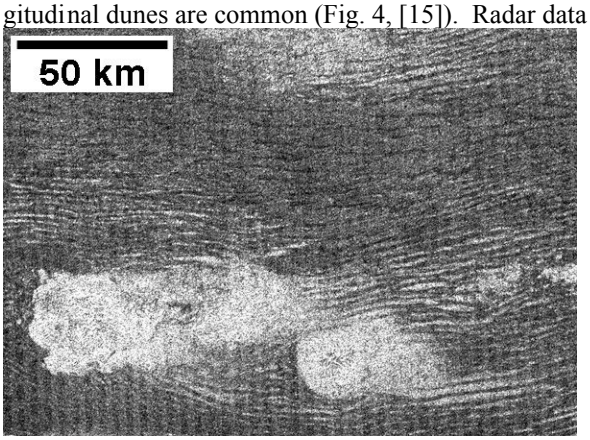

Figure 4. Longitudinal dune field on Titan, 8°N, 44°W. Cassini SAR, ~500 m/p, PIA087380 [15].

show the dunes on Titan have a spacing of 1 to 3 km, lengths of many tens of km, and heights of 100 to 150 m, likely comprised of sand-sized particles consisting of hydrocarbon materials or methane ice coated by hydrocarbons [16]. Thus far, dunes other than those in the longitudinal dune fields are uncommon.

Venus: The Magellan mission used a Synthetic Aperture Radar (SAR) experiment to map >98% of Venus, revealing the presence of >6000 aeolian features across the planet [17]. While wind streaks represent the most common aeolian feature on Venus [18], two prominent fields of dunes were identified: the Aglaonice dune field (Menat Undae, 25°S, 340°E) covering ~1300 km^2, and the Fortuna-Meshkenet dune field (Al-Uzza Undae, 67°N, 91°E) covering ~17,100 km^2 [17-19] (Fig. 5). The dunes in the Fortuna-Meshkenet field consist of arcuate ridges 0.5 to ~10 km in length, oriented transverse to wind streaks in the immediate area, with widths of 0.2 to 0.5 km and an average spacing of 0.5 km (Fig. 5) [17]. The dunes appear to have slopes <25° based on SAR images obtained during separate mapping cycles with different look orientation; several other regions in the southern hemisphere of the planet may have 'microdunes' whose presence is inferred because they are spaced properly for Bragg scattering and/or they have near-normal dune faces that produce subpixel reflections [20].

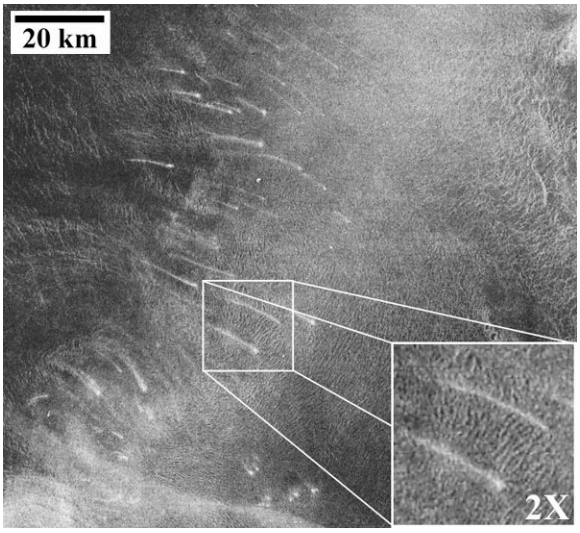

Figure 5. Fortuna-Meshkenet dune field on Venus, 67°N, 91°E. Magellan SAR, ~100 m/p, from NASA F-Map 66N084.

Discussion: The vast differences in atmospheric pressure represented by the above features do not seem to have a strong effect on sand-sized particles that have collected into dunes and dune fields. This is likely a result of the fact that while the threshold friction speed ranges widely for the environments from Mars to Venus, the particle size most easily moved by the wind ranges only from 75 to 180 microns within this broad pressure regime [1].

References: [1] Greeley R. and Iversen J. D. (1985) *Wind as a geological process on Earth, Mars, Venus, and Titan*, Cambridge U Pr. [2] McCauley J. F. (1973) *JGR, 78*, 4123-4137. [3] Greeley R. et al. (1992) *Mars* (H. H. Kieffer et al. Eds.), U of Ariz. Pr., 730-766. [4] Fenton L. K. et al. (2007) LPS XXXVIII, Abs. #1486. [5] Greeley R. et al. (2006) *JGR*, *111*, E02S09, doi: 10.1029/2005JE002491. [6] Tsoar H. R. et al. (1979) *JGR, 84*, 8167-8180. [7] marsoweb.nas.nasa.gov/HiRISE. [8] Fenton L. K. (2005) *JGR*, 110, E06005, doi: 10.1029/2004JE002309. [9] Malin M. C. and Edgett K. S. (2001) *JGR,* 106, E10, 23,429-23,570. [10] Sullivan R. et al. (2008) LPS XXIX, Abs. 2092. [11] Breed C. S. et al. (1979) *USGS Prof. Paper 1052*, 305-397. [12] ivis.eps.pitt.edu/data/Mojave. [13] Lancaster N. (1995) *Geomorphology of Desert Dunes*, Routeledge, London. [14] Bagnold R. (1941) *Physics of Wind-blown Sand and Desert Dunes*, Methuen, London. [15] photojournal.jpl.nasa.gov. [16] Lorentz R. D. et al. (2006) *Science, 312*, 724-727, doi: 10.1126/science.1123257. [17] Greeley R. et al. (1997) *Venus II* (S. W. Bougher et al., Eds.), U of Ariz. Pr., 547-589. [18] Greeley R. et al. (1995) *Icarus, 115*, 399-420. [19] Greeley R. et al. (1992) *JGR, 97*, 13319-13345. [20] Weitz C. M. et al. (1994) *Icarus, 112*, 282-295.

TRANSVERSE AEOLIAN RIDGES ON MARS: RESULTS OBTAINED FROM ANALYSIS OF HiRISE IMAGES. J. R. Zimbelman, CEPS/NASM MRC 315, Smithsonian Institution, Washington, D.C. 20013-7012; zimbelmanj@si.edu.

Introduction: Sand-sized particles have played a significant role in the geologic history of Mars, particularly with regard to the numerous sand-related landforms that are prevalent across the planet at a variety of scales [e.g., 1-4]. Recent data support an evaluation of the role played by graunules and impact creep in the formation of aeolian transverse landforms with wavelengths <100 m [5-7], features given the general name 'Transverse Aeolian Ridges' (TARs) to allow for both dune and ripple processes during their formation [8, 9]. Mars Orbiter Camera (MOC) Narrow Angle (NA) images first clearly revealed the wide distribution of transverse bedforms with wavelengths of ~20 to 80 m [2]; a survey of MOC NA images from pole to pole in the longitudinal band of 180° to 240° E showed that TARs were pervasive equatorward of 60° latitude in both hemispheres [9], but MOC data remained inconclusive as to whether the smallest TARs (wavelengths <50 m) were large ripples or small dunes [5]. New images obtained by the High Resolution Imaging Science Experiment (HiRISE) [10] provide important information about aeolian features on Mars [11, 12]. Here inferences about TARs obtained from portions of HiRISE images are compared to field measurements for dunes and ripples from the western US [13].

Ius Chasma: The first full-resolution HiRISE image released to the public (TRA_000823_1720) revealed an abundance of TARs at wavelength scales ranging from ~5 m to >80 m, imaged at 25 cm/pixel resolution. This HiRISE image shows not only complex interactions of the crests of TARs, but also crenulation of TAR crests, along with the presence of a distinct class of smaller landforms (wavelengths <20 m) in the troughs between, and superposed on, the large TARs (Fig. 1). The smaller features are oriented perpendicular to the crests of the large TARs, suggesting that they are the result of wind flow along the large TARs; this observation is consistent with HiRISE observations from across the planet that reveal two or even three orders of aeolian bedforms, each apparently influenced by their larger neighbors [12]. The spatial resolution of the HiRISE image provides the first clue to the shape of TAR bedforms through simplified photoclinometry (Fig. 2) [6]; the symmetric shape is more consistent with the shape of granule coated ripples than with the profiles of either sand ripples or linear sand dunes, with the exception of reversing dunes (which have shapes very similar to that of Fig. 2) [7].

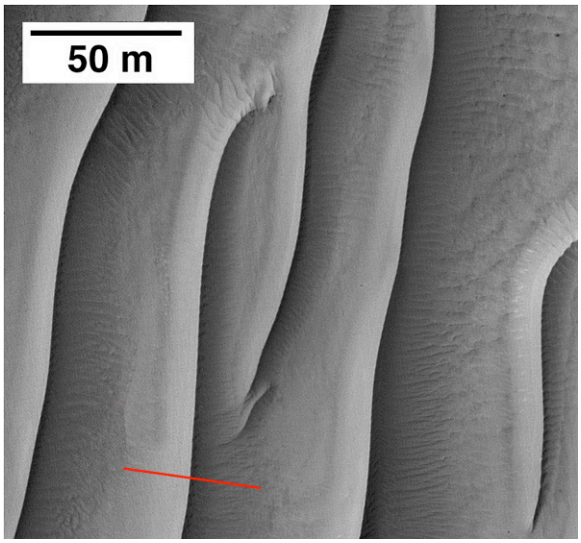

Figure 1. TARs on the floor of Ius Chasma. From HiRISE image TRA_000823_1720, 7.8°S, 279.5°E. Line shows location of profile in Figure 2.

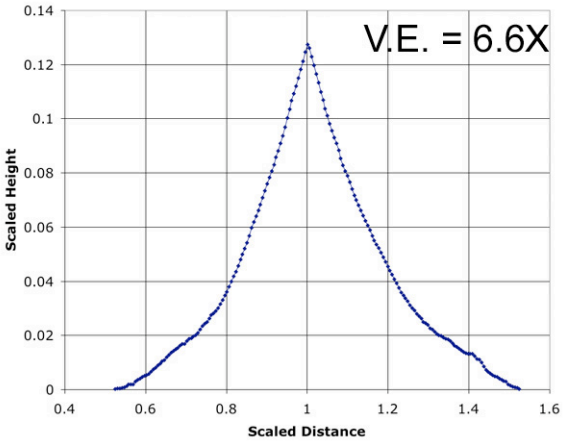

Figure 2. Profile of TAR shown in Fig. 1. Both height and width are scaled to the 45 m width of the feature.

Gamboa Crater: HiRISE image PSP_002721_2210, of the interior of Gamboa impact crater, reveals information about the interaction between what are obviously sand accumulations and a 'reticulate' [12] arrangement of smaller bedforms surrounding the sand patches (Fig. 3). The distribution of various types of aeolian bedforms were mapped across the floor of Gamboa crater, identifying classes of both broad, low-albedo features lacking slip faces and narrow, relatively linear, medium-to-high albedo features more typical of TARs seen in MOC NA images [14]. Photo-

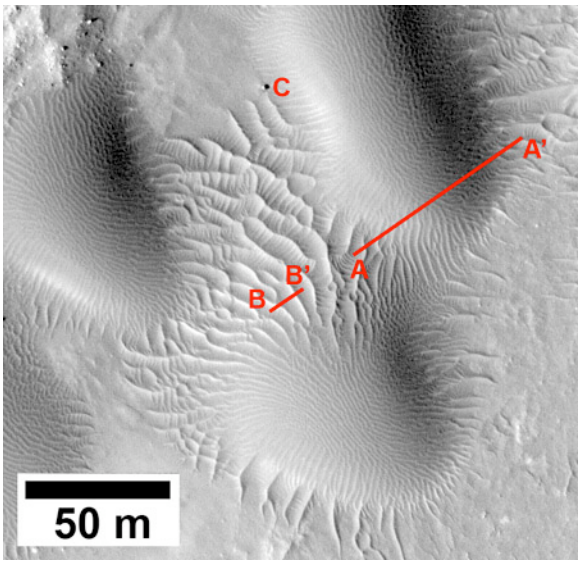

Figure 3. Dunes and ripples on the floor of Gamboa crater. A-A' and B-B' are locations of profiles shown in Fig. 4. Shadow length indicates that the block at C is 0.8 m tall. From HiRISE image PSP_002721_2210, 40.8°N, 315.7° E.

clinometry provides valuable information about the profile shapes of both the dark dune patches and the bright TARs (Fig. 4); the dark sand patches (Fig. 4, top) are comparable to incipient dunes that have not yet collected sufficient sand to develop a slip face, while the smaller ridged features (Fig. 4, bottom) are identical to granule-coated sand-cored ripples [14].

Other HiRISE images: The TARs just described are distinct from duneforms in HiRISE images targeted on dune fields (e.g., Proctor, PSP_004077_1325; Rabe, PSP_003325_1355; Herschel, PSP_002728_1645; Nili Patera, PSP_004339_1890). TARs inside a crater in Terra Sirenum (PSP_001684_1410) show unusual crest truncations and branching, apparent layering in between the TAR bedforms, and extremely narrow terminations of some TARs, all of which suggest that these TARs perhaps are being eroded.

Conclusions: Broad, low-albedo features are most likely sand dunes, even where they lack slip face development. Medium to large TARs (generally wavelengths 40 to 100 m) are most likely reversing sand dunes. Small TARs (wavelengths <20 m) are most likely either granule-coated ripples or very small dunes (although such dunes would be substantially different from the dark sand patches and dunes with slip faces).

Acknowledgements: This work was supported by grant NNG04GN88G from the NASA Mars Data Analysis Program.

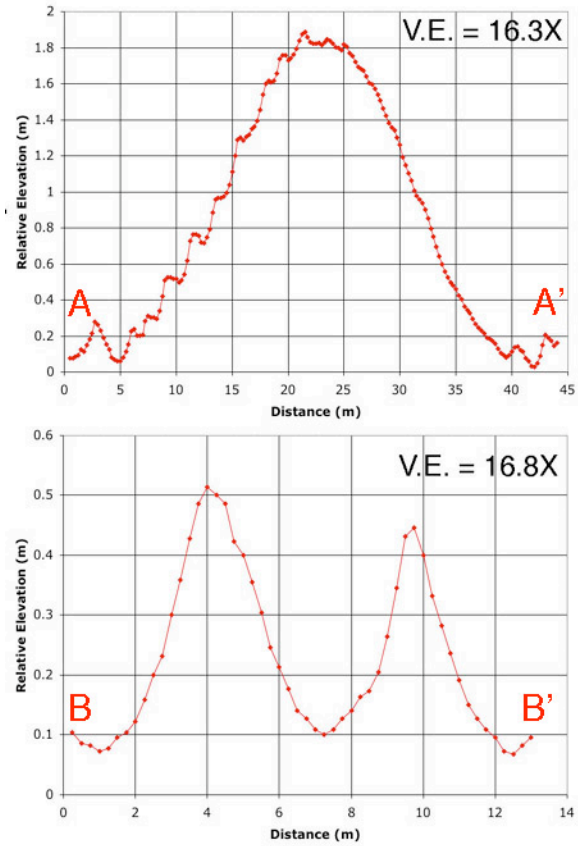

Figure 4. Relief for profile locations shown in Fig. 3; note differing scales. The top profile is comparable to incipient sand dunes (lacking a slip face) on Earth, and the bottom profiles are nearly identical to granule ripples in the western US [14].

References: [1] Greeley R. et al. (1992) *Mars*, U of A Pr., 730-766. [2] Malin M. C.and Edgett K. S. (2001) *JGR, 106*, 23429-23570. [3] Greeley R. et al. (2004) *Science, 305*, 810-821. [4] Sullivan R. et al. (2005) *Nature, 436*, doi: 10.1038/nature03641. [5] Zimbelman J. R. and Williams S. H. (2006) *LPS XXXVII*, Abstract #2047. [6] Zimbelman J. R. and Williams S. H. (2007) *7th Int. Mars Conf.*, Abstract #3047. [7] Zimbelman J. R. and Williams S. H. (2007) *GSA Abs. Prog., 39(6)*, Abstract 218-5. [8] Bourke M. C. et al. (2003) *LPS XXXIV*, Abstract #2090. [9] Wilson S. A. and Zimbelman J. R. (2004) *JGR, 109*, E10003, doi: 10.1029/2004JE002247. [10] McEwen A. S. et al. (2007) *JGR, 112*, E05S02, doi: 10.1029/JE002605. [11] Bridges N. T. et al. (2007) *LPSC XXXVIII*, Abstract #2098. [12] Bridges N. T. et al. (2007) *GRL, 34(23)*, doi: 10.1029/2007GL031445. [13] Zimbelman J. R. and Williams S. H. (2007) *Geology of Mars*, Cambr. Un. Pr., 232-264. [14] Telling J. W. et al. (2007) *Eos Trans. AGU, 88(52)*, Abstract P13A-1038.

Notes

Notes